A posteriori error analysis of a mixed finite element method for the coupled Brinkman–Forchheimer and double-diffusion equations*

Sergio Caucao† Gabriel N. Gatica‡ Ricardo Oyarzúa§ Paulo Zúñiga¶

Abstract

In this paper we consider a partially augmented fully-mixed variational formulation that has been recently proposed for the coupling of the stationary Brinkman–Forchheimer and double-diffusion equations, and develop an *a posteriori* error analysis for the 2D and 3D versions of the associated mixed finite element scheme. Indeed, we derive two reliable and efficient residual-based *a posteriori* error estimators for this problem on arbitrary (convex or non-convex) polygonal and polyhedral regions. The reliability of the proposed estimators draws mainly upon the uniform ellipticity and inf-sup condition of the forms involved, a suitable assumption on the data, stable Helmholtz decompositions in Hilbert and Banach frameworks, and the local approximation properties of the Clément and Raviart–Thomas operators. In turn, inverse inequalities, the localization technique based on bubble functions, and known results from previous works, are the main tools yielding the efficiency estimate. Finally, several numerical examples confirming the theoretical properties of the estimators and illustrating the performance of the associated adaptive algorithms, are reported. In particular, the case of flow through a 3D porous media with channel networks is considered.

Key words: Brinkman–Forchheimer equations, double-diffusion equations, stress-velocity formulation, mixed finite element methods, *a posteriori* error analysis

Mathematics subject classifications (2000): 65N30, 65N12, 65N15, 35Q79, 80A20, 76R05, 76D07

1 Introduction

We have recently introduced in [8] a partially augmented-mixed finite element method for the problem of steady double-diffusive convection in a fluid-saturated porous medium described by the coupling of the stationary Brinkman–Forchheimer and double-diffusion equations in $\mathrm{R}^d, d \in \{2, 3\}$. In there, the fluid pseudostress tensor, and the pseudoheat and pseudodiffusive vectors are introduced as further unknowns of the system (besides the velocity, temperature and concentration fields), thus yielding a

*This research was partially supported by ANID-Chile through the projects ACE 210010, Centro de Modelamiento Matemático (FB210005), Anillo of Computational Mathematics for Desalination Processes (ACT210087), and Fondecyt projects 1200666 and 11220393; by Centro de Investigación en Ingeniería Matemática (CI^{2}MA), Universidad de Concepción; and by Universidad del Bío-Bío through VRIP-UBB project 2120173 GI/C.

†Departamento de Matemática y Física Aplicadas, Universidad Católica de la Santísima Concepción, Casilla 297, Concepción, Chile, email: scaucao@ucsc.cl.

‡CI^{2}MA and Departamento de Ingeniería Matemática, Universidad de Concepción, Casilla 160-C, Concepción, Chile, email: ggatica@ci2ma.udec.cl.

§GIMNAP-Departamento de Matemática, Universidad del Bío-Bío, Casilla 5-C, Concepción, Chile, and CI^{2}MA, Universidad de Concepción, Casilla 160-C, Concepción, Chile, email: royarzua@ubiobio.cl.

¶Department of Applied Mathematics, University of Waterloo, Waterloo, ON N2L 3G1 Canada, email: paulo.zuniga@uwaterloo.ca.

fully-mixed formulation. Furthermore, since the nonlinear term in the Brinkman–Forchheimer equation requires the velocity to live in H^1 instead of L^2 as usual, the approach in [8] follows similarly to [13], [14] and [27], so that the variational formulation is augmented with suitable Galerkin type terms, which forces both the temperature and concentration scalar fields to live in L^4. As a consequence, the aforementioned pseudoheat and pseudodiffusive vectors live in a suitable H(div)-type Banach space. The resulting augmented scheme is written equivalently as a fixed point equation, and the well-known Schauder and Banach theorems, combined with the Lax–Milgram and Banach–Nečas–Babuška theorems, are utilized to address the solvability of the continuous problem. As for the associated Galerkin scheme, whose solvability is established similarly to the continuous case by using the Brouwer and Banach fixed-point theorems, we use Raviart–Thomas spaces of order $k \geq 0$ to approximate the pseudostress tensor, and the pseudoheat and pseudodiffusive vectors, whereas continuous piecewise polynomials of degree $\leq k+1$ are employed for the velocity, and piecewise polynomials of degree $\leq k$ for the temperature and concentration fields. Optimal *a priori* error estimates were also derived in [8].

On the other hand, it is well known that under the eventual presence of singularities or high gradients of some components of the solution, most of the standard Galerkin procedures such as finite element and mixed finite element methods inevitably lose accuracy, and hence one usually tries to recover it by applying an adaptive algorithm based on *a posteriori* error estimates. In particular, this powerful tool has been applied to quasi-Newtonian fluid flows obeying the power law, which include the Brinkman–Forchheimer model, and among the respective references we first mention [19], where the authors propose and analyze an *a posteriori* error estimator, defined via a non-linear projection of the residues of the variational equations, for a three-field model of a generalized Stokes problem. In turn, a fully local residual-based *a posteriori* error estimator for the mixed formulation of the p-Laplacian problem in a polygonal domain, is derived in [16]. In this case, the authors study the reliability of the estimator defining two residues and then bounding the norm of the errors in terms of the norms of these residues. Later on, *a posteriori* error analyses for the aforementioned Brinkman–Darcy–Forchheimer model in velocity-pressure formulation have been developed in [31]. In fact, two types of error indicators related to the discretization and to the linearization of the problem are established there. Furthermore, the first *a posteriori* error analysis of the primal-mixed finite element method for the Navier–Stokes/Darcy–Forchheimer coupled problem was developed in [9]. More precisely, usual techniques employed within the Hilbertian framework are extended in [9] to the case of Banach spaces by deriving a reliable and efficient *a posteriori* error estimator for the mixed finite element method introduced in [6]. The above includes corresponding local estimates and new Helmholtz decompositions for the reliability, as well as respective inverse inequalities and local estimates of bubble functions for the efficiency. We refer to [4] for a recent *a posteriori* error analysis of a momentum conservative Banach space-based mixed finite element method for the Navier–Stokes problem. Standard arguments relying on duality techniques, a suitable Helmholtz decomposition in a Banach framework and classical approximation properties, are combined there with corresponding small data assumptions to derive the reliability of the estimators. Finally, we also refer to some works devoted to the *a posteriori* error analysis of Hilbert spaces-based variational formulations of nonlinear and coupled problems, particularly Navier–Stokes, Boussinesq, Oldroyd–Stokes, and related flow-transport coupling models (see, e.g. [23], [25], [17], [28], [10], [14], [27], [15], and [7]).

According to the above discussion, and in order to complement the study started in [8] for the coupling of the Brinkman–Forchheimer and double-diffusion equations, in the present paper we combine the *a posteriori* error analysis techniques developed in [7], [14], [26], and [28] for augmented-mixed formulations in Hilbert spaces, with the ones recently obtained in [9], [4], [11], and [24] for Banach spaces-based mixed formulations, and develop two reliable and efficient residual-based *a posteriori*

error estimators in 2D and 3D for the partially augmented-mixed finite element method from [8]. More precisely, in each case we derive a global quantity Θ that is expressed in terms of calculable local indicators Θ_T defined on each element T of a given triangulation $\mathcal{T}$. This information can be afterwards used to localize sources of error and construct an algorithm to efficiently adapt the mesh. In this way, the estimator Θ is said to be efficient (resp. reliable) if there exists a positive constant $C_{\rm eff}$ (resp. $C_{\rm rel}$), independent of the meshsizes, such that

$$C_{\rm eff}\,\Theta \,+\, \text{h.o.t.} \;\leq\; \|\text{error}\| \;\leq\; C_{\rm rel}\,\Theta \,+\, \text{h.o.t.}\,,$$

where h.o.t. is a generic expression denoting one or several terms of higher order. We observe that, up to our knowledge, the present work provides the first *a posteriori* error analyses of mixed finite element methods for the coupling of the stationary Brinkman–Forchheimer and double-diffusion equations.

This paper is organized as follows. The remainder of this section introduces some standard notations and functional spaces. In Section 2 we recall from [8] the model problem and its continuous and discrete augmented fully-mixed variational formulations. Next, in Section 3 we provide some preliminary results to be employed in the derivation and analysis of our *a posteriori* error estimator. The core of the present work is given by Section 4, where we develop the *a posteriori* error analysis. In Section 4.1 we employ the uniform ellipticity and inf-sup condition of the bilinear forms involved, suitable Helmholtz decompositions in Hilbert and Banach frameworks, the local approximation properties of the Clément and Raviart–Thomas operators, and known estimates from [4] and [26], to derive a reliable residual-based *a posteriori* error estimator. Then, inverse inequalities, and the localization technique based on element-bubble and edge-bubble functions are utilized in Section 4.2 to prove the efficiency of the estimator. A second (also reliable and efficient) residual-based *a posteriori* error estimator is introduced and studied in Section 5, where the Helmholtz decomposition in a Hilbert framework is not employed in the corresponding proof of reliability. Finally, numerical results confirming the reliability and efficiency of the *a posteriori* error estimators, and showing the good performance of the associated adaptive algorithms, are presented in Section 6.

1.1 Preliminary notations

Let $\Omega \subset \mathrm{R}^d, d \in \{2,3\}$, denote a bounded domain with polyhedral boundary Γ, and denote by $\mathbf{n}$ the outward unit normal vector on Γ. Standard notation will be adopted for Lebesgue spaces $\mathrm{L}^p(\Omega)$ and Sobolev spaces $\mathrm{W}^{s,p}(\Omega)$, with $s \in \mathrm{R}$ and $p > 1$, whose corresponding norms, either for the scalar, vector, or tensor case, are denoted by $\|\cdot\|_{0,p;\Omega}$ and $\|\cdot\|_{s,p;\Omega}$, respectively. In particular, when $p = 2$, $\mathrm{W}^{s,2}(\Omega)$ is also denoted by $\mathrm{H}^s(\Omega)$, and the writing of its norm and seminorm are simplified to $\|\cdot\|_{s,\Omega}$ and $|\cdot|_{s,\Omega}$, respectively. By $\mathbf{M}$ and $\mathbb{M}$ we will denote the corresponding vector and tensor counterparts of the generic scalar functional space M, and $\|\cdot\|$, with no subscripts, will stand for the natural norm of either an element or an operator in any product functional space. In turn, for any vector field $\mathbf{v} = (v_i)_{i=1,d}$, we let $\nabla\mathbf{v}$ and $\mathrm{div}(\mathbf{v})$ be its gradient and divergence, respectively. Furthermore, given tensor fields $\boldsymbol{\tau} = (\tau_{ij})_{i,j=1,d}$ and $\boldsymbol{\zeta} = (\zeta_{ij})_{i,j=1,d}$, we let $\mathbf{div}(\boldsymbol{\tau})$ be the divergence operator div acting along the rows of $\boldsymbol{\tau}$, and define the transpose, the trace, and the deviatoric tensor of $\boldsymbol{\tau}$, as well as the tensor inner product between $\boldsymbol{\tau}$ and $\boldsymbol{\zeta}$, respectively, as

$$\boldsymbol{\tau}^{\mathrm{t}} := (\tau_{ji})_{i,j=1,d}, \quad \mathrm{tr}(\boldsymbol{\tau}) := \sum_{i=1}^{d} \tau_{ii}, \quad \boldsymbol{\tau}^{\mathrm{d}} := \boldsymbol{\tau} - \frac{1}{d}\,\mathrm{tr}(\boldsymbol{\tau})\,\mathbb{I}, \quad \text{and} \quad \boldsymbol{\tau} : \boldsymbol{\zeta} := \sum_{i,j=1}^{d} \tau_{ij}\,\zeta_{ij},$$

where $\mathbb{I}$ is the identity matrix in $\mathrm{R}^{d\times d}$. In what follows, when no confusion arises, $|\cdot|$ will denote the Euclidean norm in R^d or $\mathrm{R}^{d\times d}$. Additionally, given $p > 1$, we define the following tensor and vector

functional spaces (see [8, Section 2.2] for details):

$$\mathbb{H}_0(\mathbf{div};\Omega) := \Big\{ \boldsymbol{\tau} \in \mathbb{H}(\mathbf{div};\Omega) : \quad \int_\Omega \mathrm{tr}(\boldsymbol{\tau}) = 0 \Big\} \tag{1.1}$$

and

$$\mathbf{H}(\mathrm{div}_p;\Omega) := \Big\{ \boldsymbol{\eta} \in \mathbf{L}^2(\Omega) : \quad \mathrm{div}(\boldsymbol{\eta}) \in \mathrm{L}^p(\Omega) \Big\}, \tag{1.2}$$

endowed with the norms

$$\|\boldsymbol{\tau}\|^2_{\mathbf{div};\Omega} := \|\boldsymbol{\tau}\|^2_{0,\Omega} + \|\mathbf{div}(\boldsymbol{\tau})\|^2_{0,\Omega} \quad \text{and} \quad \|\boldsymbol{\eta}\|_{\mathrm{div}_p;\Omega} := \|\boldsymbol{\eta}\|_{0,\Omega} + \|\mathrm{div}(\boldsymbol{\eta})\|_{0,p;\Omega},$$

respectively. In addition, $\mathrm{H}^{1/2}(\Gamma)$ is the space of traces of functions of $\mathrm{H}^1(\Omega)$ and $\mathrm{H}^{-1/2}(\Gamma)$ denotes its dual. Also, by $\langle \cdot, \cdot \rangle_\Gamma$ we will denote the corresponding product of duality between $\mathrm{H}^{-1/2}(\Gamma)$ (resp. $\mathbf{H}^{-1/2}(\Gamma)$) and $\mathrm{H}^{1/2}(\Gamma)$ (resp. $\mathbf{H}^{1/2}(\Gamma)$).

2 The model problem and its variational formulation

In this section we recall from [8] the model problem of interest, its fully-mixed variational formulation, the associated Galerkin scheme, and the main results concerning the corresponding solvability analyses.

2.1 The coupling of the Brinkman–Forchheimer and double-diffusion equations

In what follows we consider the model introduced in [29] (see also [8]), which is given by a steady double-diffusive convection system in a fluid saturated porous medium. More precisely, we focus on solving the coupling of the incompressible Brinkman–Forchheimer and double-diffusion equations, which reduces to finding a velocity field $\mathbf{u}$, a pressure field p, a temperature field ϕ_1 and a concentration field ϕ_2, the latter two defining a vector $\boldsymbol{\phi} := (\phi_1, \phi_2)$, such that

$$\begin{array}{rcll} -\nu\,\Delta\mathbf{u} + \mathbf{K}^{-1}\mathbf{u} + \mathtt{F}\,|\mathbf{u}|\mathbf{u} + \nabla p &=& \mathbf{f}(\boldsymbol{\phi}) & \text{in } \Omega, \\ \mathrm{div}(\mathbf{u}) &=& 0 & \text{in } \Omega, \\ -\mathrm{div}(\mathbf{Q}_1\,\nabla\phi_1) + \mathtt{R}_1\,\mathbf{u}\cdot\nabla\phi_1 &=& 0 & \text{in } \Omega, \\ -\mathrm{div}(\mathbf{Q}_2\,\nabla\phi_2) + \mathtt{R}_2\,\mathbf{u}\cdot\nabla\phi_2 &=& 0 & \text{in } \Omega, \\ \mathbf{u} = \mathbf{u}_\mathrm{D}, \quad \phi_1 = \phi_{1,\mathrm{D}}, \quad \text{and} \quad \phi_2 &=& \phi_{2,\mathrm{D}} & \text{on } \Gamma, \\ \int_\Omega p &=& 0, & \end{array} \tag{2.1}$$

with parameters $\nu := \mathtt{D}_a\,\widetilde{\mu}/\mu$ and $\mathtt{F} := \vartheta\,\mathtt{D}_a\,\mathtt{R}_1$, where $\mathtt{D}_a$ stands for the Darcy number, $\widetilde{\mu}$ the viscosity, μ the effective viscosity, $\mathtt{R}_1$ the thermal Rayleigh number, $\mathtt{R}_2$ the solute Rayleigh number, and ϑ is a real number that can be calculated experimentally. In addition, the Dirichlet boundary data is given by $\mathbf{u}_\mathrm{D} \in \mathbf{H}^{1/2}(\Gamma)$, $\phi_{1,\mathrm{D}} \in \mathrm{H}^{1/2}(\Gamma)$ and $\phi_{2,\mathrm{D}} \in \mathrm{H}^{1/2}(\Gamma)$. Owing to the incompressibility of the fluid and the Dirichlet boundary condition for $\mathbf{u}$, the datum $\mathbf{u}_\mathrm{D}$ must satisfy the compatibility condition

$$\int_\Gamma \mathbf{u}_\mathrm{D}\cdot\mathbf{n} = 0. \tag{2.2}$$

In turn, the external force $\mathbf{f}$ is defined by

$$\mathbf{f}(\boldsymbol{\phi}) := -(\phi_1 - \phi_{1,\mathtt{r}})\,\mathbf{g} + \frac{1}{\varrho}\,(\phi_2 - \phi_{2,\mathtt{r}})\,\mathbf{g},$$

with $\mathbf{g}$ representing the potential type gravitational acceleration, $\phi_{1,\mathtt{r}}$ the reference temperature, $\phi_{2,\mathtt{r}}$ the reference concentration of a solute, both of them in $\mathrm{L}^4(\Omega)$, and ϱ is another parameter experimentally valued that can be assumed to be greater than 1 (see [29, Section 2] for details). In turn, the permeability, thermal diffusion and concentration diffusion tensors are denoted, respectively, by $\mathbf{K}, \mathbf{Q}_1$ and $\mathbf{Q}_2$, all them lying in $\mathbb{L}^\infty(\Omega)$. Moreover, $\mathbf{K}$ and the inverses of $\mathbf{Q}_1$ and $\mathbf{Q}_2$, are uniformly positive definite tensors, which means that there exist positive constants $C_{\mathbf{K}}$, $C_{\mathbf{Q}_1}$, and $C_{\mathbf{Q}_2}$, such that

$$\mathbf{v}\cdot\mathbf{K}(\mathbf{x})\mathbf{v} \geq C_{\mathbf{K}}\,|\mathbf{v}|^2 \quad \text{and} \quad \mathbf{v}\cdot\mathbf{Q}_j^{-1}(\mathbf{x})\mathbf{v} \geq C_{\mathbf{Q}_j}\,|\mathbf{v}|^2 \quad \forall\,\mathbf{v}\in\mathrm{R}^n,\,\forall\,\mathbf{x}\in\Omega, \quad j\in\{1,2\}. \tag{2.3}$$

Next, in order to derive a fully-mixed formulation for (2.1), in which the Dirichlet boundary conditions become natural ones, we now proceed as in [8], and introduce the pseudostress tensor, and the pseudoheat and pseudodiffusive vectors as further unknowns, that is

$$\boldsymbol{\sigma} := \nu\,\nabla\mathbf{u} - p\,\mathbb{I}, \quad \boldsymbol{\rho}_1 := \mathbf{Q}_1\,\nabla\phi_1 - \mathtt{R}_1\,\phi_1\,\mathbf{u}, \quad \boldsymbol{\rho}_2 := \mathbf{Q}_2\,\nabla\phi_2 - \mathtt{R}_2\,\phi_2\,\mathbf{u} \quad \text{in} \quad \Omega. \tag{2.4}$$

In this way, applying the trace operator to $\boldsymbol{\sigma}$ and utilizing the incompressibility condition $\mathrm{div}(\mathbf{u}) = 0$ in Ω, one arrives at

$$p = -\frac{1}{d}\,\mathrm{tr}(\boldsymbol{\sigma}) \quad \text{in} \quad \Omega. \tag{2.5}$$

Hence, replacing (2.5) back into the first equation of (2.4), we find that our model problem (2.1) can be rewritten, equivalently, as follows: Find $(\boldsymbol{\sigma},\mathbf{u})$ and $(\boldsymbol{\rho}_j,\phi_j)$, $j\in\{1,2\}$, in suitable spaces to be indicated below, such that

$$\begin{array}{rcll}
\dfrac{1}{\nu}\,\boldsymbol{\sigma}^{\mathrm{d}} & = & \nabla\mathbf{u} & \text{in } \Omega,\\
-\mathbf{div}(\boldsymbol{\sigma}) + \mathbf{K}^{-1}\mathbf{u} + \mathtt{F}\,|\mathbf{u}|\mathbf{u} & = & \mathbf{f}(\boldsymbol{\phi}) & \text{in } \Omega,\\
\mathbf{Q}_j^{-1}\boldsymbol{\rho}_j + \mathtt{R}_j\,\mathbf{Q}_j^{-1}\phi_j\,\mathbf{u} & = & \nabla\phi_j & \text{in } \Omega,\\
-\mathrm{div}(\boldsymbol{\rho}_j) & = & 0 & \text{in } \Omega,\\
\mathbf{u} = \mathbf{u}_{\mathrm{D}} \quad \text{and} \quad \boldsymbol{\phi} & = & \boldsymbol{\phi}_{\mathrm{D}} & \text{on } \Gamma,\\
\displaystyle\int_\Omega \mathrm{tr}(\boldsymbol{\sigma}) & = & 0, &
\end{array} \tag{2.6}$$

where the Dirichlet datum for $\boldsymbol{\phi}$ is certainly given by $\boldsymbol{\phi}_{\mathrm{D}} := (\phi_{1,\mathrm{D}},\phi_{2,\mathrm{D}})$. At this point we stress that, as suggested by (2.5), p is eliminated from the present formulation and computed afterwards in terms of $\boldsymbol{\sigma}$ by using that identity. This fact justifies the last equation in (2.6), which ensures that the resulting p satisfies $\int_\Omega p = 0$.

2.2 The fully-mixed variational formulation

We begin by recalling from [8, Section 2.2] the augmented fully-mixed variational formulation for the coupling of the Brinkman–Forchheimer and double-diffusion equations (cf. (2.6)), which reads: Find $(\boldsymbol{\sigma},\mathbf{u})\in\mathbb{H}_0(\mathbf{div};\Omega)\times\mathbf{H}^1(\Omega)$ and $(\boldsymbol{\rho}_j,\phi_j)\in\mathbf{H}(\mathrm{div}_{4/3};\Omega)\times\mathrm{L}^4(\Omega)$, $j\in\{1,2\}$, such that

$$\begin{array}{rcl}
A((\boldsymbol{\sigma},\mathbf{u}),(\boldsymbol{\tau},\mathbf{v})) + B_{\mathbf{u}}((\boldsymbol{\sigma},\mathbf{u}),(\boldsymbol{\tau},\mathbf{v})) & = & F_{\mathrm{D}}(\boldsymbol{\tau},\mathbf{v}) + F_{\boldsymbol{\phi}}(\boldsymbol{\tau},\mathbf{v}),\\
a_j(\boldsymbol{\rho}_j,\boldsymbol{\eta}_j) + b(\boldsymbol{\eta}_j,\phi_j) + c_j(\mathbf{u};\phi_j,\boldsymbol{\eta}_j) & = & G_j(\boldsymbol{\eta}_j),\\
b(\boldsymbol{\rho}_j,\psi_j) & = & 0,
\end{array} \tag{2.7}$$

for all $(\boldsymbol{\tau},\mathbf{v})\in\mathbb{H}_0(\mathbf{div};\Omega)\times\mathbf{H}^1(\Omega)$ and for all $(\boldsymbol{\eta}_j,\psi_j)\in\mathbf{H}(\mathrm{div}_{4/3};\Omega)\times\mathrm{L}^4(\Omega)$, where, given $\mathbf{w}\in\mathbf{H}^1(\Omega)$, $A, B_{\mathbf{w}}, a_j, b$, and $c_j(\mathbf{w};\cdot,\cdot)$ are the forms defined, respectively, as

$$A((\boldsymbol{\sigma},\mathbf{u}),(\boldsymbol{\tau},\mathbf{v})) := \frac{1}{\nu}\int_\Omega \boldsymbol{\sigma}^{\mathrm{d}}:\boldsymbol{\tau}^{\mathrm{d}}+\int_\Omega \mathbf{K}\mathbf{div}(\boldsymbol{\sigma})\cdot\mathbf{div}(\boldsymbol{\tau})+\kappa_1\int_\Omega\Big(\nabla\mathbf{u}-\frac{1}{\nu}\boldsymbol{\sigma}^{\mathrm{d}}\Big):\nabla\mathbf{v}+\kappa_2\int_\Gamma \mathbf{u}\cdot\mathbf{v}, \tag{2.8}$$

$$B_{\mathbf{w}}((\boldsymbol{\sigma},\mathbf{u}),(\boldsymbol{\tau},\mathbf{v})) := -\mathtt{F}\int_\Omega \mathbf{K}\,|\mathbf{w}|\mathbf{u}\cdot\mathbf{div}(\boldsymbol{\tau}), \tag{2.9}$$

and

$$a_j(\boldsymbol{\rho}_j,\boldsymbol{\eta}_j) := \int_\Omega \mathbf{Q}_j^{-1}\,\boldsymbol{\rho}_j\cdot\boldsymbol{\eta}_j, \quad b(\boldsymbol{\eta}_j,\psi_j) := \int_\Omega \psi_j\,\mathrm{div}(\boldsymbol{\eta}_j), \tag{2.10}$$

$$c_j(\mathbf{w};\psi_j,\boldsymbol{\eta}_j) := \mathtt{R}_j\int_\Omega \mathbf{Q}_j^{-1}\,\psi_j\,\mathbf{w}\cdot\boldsymbol{\eta}_j, \tag{2.11}$$

for all $(\boldsymbol{\sigma},\mathbf{u}),(\boldsymbol{\tau},\mathbf{v})\in\mathbb{H}_0(\mathbf{div};\Omega)\times\mathbf{H}^1(\Omega)$ and for all $(\boldsymbol{\rho}_j,\phi_j),(\boldsymbol{\eta}_j,\psi_j)\in\mathbf{H}(\mathrm{div}_{4/3};\Omega)\times\mathrm{L}^4(\Omega)$. In turn, given $\boldsymbol{\varphi}:=(\varphi_1,\varphi_2)\in\mathbf{L}^4(\Omega)$, $F_{\mathrm{D}}, F_{\boldsymbol{\varphi}}$, and G_j are the bounded linear functionals defined by

$$F_{\mathrm{D}}(\boldsymbol{\tau},\mathbf{v}) := \langle\boldsymbol{\tau}\mathbf{n},\mathbf{u}_{\mathrm{D}}\rangle_\Gamma+\kappa_2\int_\Gamma \mathbf{u}_{\mathrm{D}}\cdot\mathbf{v}, \quad F_{\boldsymbol{\varphi}}(\boldsymbol{\tau},\mathbf{v}) := -\int_\Omega \mathbf{K}\,\mathbf{f}(\boldsymbol{\varphi})\cdot\mathbf{div}(\boldsymbol{\tau}), \tag{2.12}$$

for all $(\boldsymbol{\tau},\mathbf{v})\in\mathbb{H}_0(\mathbf{div};\Omega)\times\mathbf{H}^1(\Omega)$ and

$$G_j(\boldsymbol{\eta}_j) := \big\langle\boldsymbol{\eta}_j\cdot\mathbf{n},\phi_{j,\mathrm{D}}\big\rangle_\Gamma, \tag{2.13}$$

for all $\boldsymbol{\eta}_j\in\mathbf{H}(\mathrm{div}_{4/3};\Omega)$. Notice that κ_1 and κ_2 are positive parameters that can be taken as (see [8, Lemma 3.2 and eq. (3.36)] for details):

$$\kappa_1=\nu \quad\text{and}\quad \kappa_2=\frac{\nu}{2}. \tag{2.14}$$

These particular values will be used later on for the computational implementation of the Galerkin scheme associated with (2.7). Next, we recall from [8] that $\mathbf{u}\in\mathbf{W}_r:=\big\{\mathbf{w}\in\mathbf{H}^1(\Omega):\ \|\mathbf{w}\|_{1,\Omega}\le r\big\}$, where $r\in(0,r_0)$, with $r_0:=\min\{r_1,r_2\}$ and

$$r_1:=\frac{\alpha_A}{2\,\mathtt{F}\,\|\mathbf{K}\|_\infty\,\|\mathbf{i}_4\|^2}, \quad r_2:=\min\{r_2^1,r_2^2\}, \quad r_2^j:=\frac{\gamma_j}{2\,\mathtt{R}_j\,\|\mathbf{Q}_j^{-1}\|_\infty\,\|\mathbf{i}_4\|}, \tag{2.15}$$

where $\mathbf{i}_4$ is the injection of $\mathbf{H}^1(\Omega)$ into $\mathbf{L}^4(\Omega)$, whereas α_A and γ_j are positive constants establishing ellipticity and a global inf-sup condition, respectively, of A and the bilinear form $\mathcal{A}_j$ that arises after adding the left hand sides of the last two equations of (2.7), but excluding c_j (cf. [8, eqns. (3.23) and (3.28)]). According to [8, eq. (3.25)], and using the fact that $\mathbf{u}\in\mathbf{W}_r$, we have that the bilinear form $A+B_{\mathbf{u}}$ is uniformly elliptic on $\mathbb{H}_{\mathtt{BF}}:=\mathbb{H}_0(\mathbf{div};\Omega)\times\mathbf{H}^1(\Omega)$ with positive constant $\alpha_A/2$ independent of h. This implies that

$$\sup_{\mathbf{0}\neq(\boldsymbol{\tau},\mathbf{v})\in\mathbb{H}_{\mathtt{BF}}}\frac{(A+B_{\mathbf{u}})((\boldsymbol{\zeta},\mathbf{z}),(\boldsymbol{\tau},\mathbf{v}))}{\|(\boldsymbol{\tau},\mathbf{v})\|}\ \ge\ \frac{\alpha_A}{2}\,\|(\boldsymbol{\zeta},\mathbf{z})\|, \tag{2.16}$$

for all $(\boldsymbol{\zeta},\mathbf{z})\in\mathbb{H}_{\mathtt{BF}}$. In turn, we recall from [8, eq. (3.33)] the following inf-sup condition

$$\sup_{\mathbf{0}\neq(\boldsymbol{\eta}_j,\psi_j)\in\mathbf{H}_{\mathtt{D}}}\frac{a_j(\boldsymbol{\chi}_j,\boldsymbol{\eta}_j)+b(\boldsymbol{\eta}_j,\varphi_j)+b(\boldsymbol{\chi}_j,\psi_j)+c_j(\mathbf{u};\varphi_j,\boldsymbol{\eta}_j)}{\|(\boldsymbol{\eta}_j,\psi_j)\|}\ \ge\ \frac{\gamma_j}{2}\,\|(\boldsymbol{\chi}_j,\varphi_j)\|, \tag{2.17}$$

for all $(\boldsymbol{\chi}_j, \varphi_j) \in \mathbf{H}_{\mathtt{D}} := \mathbf{H}(\mathrm{div}_{4/3};\Omega) \times \mathrm{L}^4(\Omega)$. Further details yielding the solvability of (2.7) were developed in [8, Theorem 3.9]. In particular, we recall for later use the following *a priori* estimates

$$\|(\boldsymbol{\sigma}, \mathbf{u})\| \, \leq \, c_{\mathbf{T}} \left\{ \|\mathbf{u}_{\mathrm{D}}\|_{0,\Gamma} + \|\mathbf{u}_{\mathrm{D}}\|_{1/2,\Gamma} + \|\mathbf{g}\|_{0,4;\Omega} \left(\|\boldsymbol{\phi}_{\mathrm{D}}\|_{1/2,\Gamma} + \|\boldsymbol{\phi}_{\mathbf{r}}\|_{0,4;\Omega} \right) \right\} \tag{2.18}$$

and

$$\sum_{j=1}^{2} \|(\boldsymbol{\rho}_j, \phi_j)\| \, \leq \, c_{\widetilde{\mathbf{S}}} \, \|\boldsymbol{\phi}_{\mathrm{D}}\|_{1/2,\Gamma} \, , \tag{2.19}$$

where $c_{\mathbf{T}} := c_{\mathbf{S}} \max\left\{1, c_{\widetilde{\mathbf{S}}}\right\}$, and $c_{\mathbf{S}}$ and $c_{\widetilde{\mathbf{S}}}$ are positive constants defined in [8, eqns. (3.21) and (3.29)].

2.3 The fully-mixed finite element method

We denote by $\mathcal{T}_h$ a regular partition of $\overline{\Omega}$ made up of triangles T (when $d = 2$) or tetrahedral T (when $d = 3$) of diameter h_T, and meshsize $h := \max\left\{h_T : T \in \mathcal{T}_h\right\}$. In addition, for each $T \in \mathcal{T}_h$, we let $\mathbf{RT}_k(T)$ be the local Raviart–Thomas space of order $k \geq 0$, i.e.,

$$\mathbf{RT}_k(T) \, := \, \mathbf{P}_k(T) \oplus \mathrm{P}_k(T) \, \mathbf{x},$$

where $\mathrm{P}_k(T)$ is the space of polynomials defined on T of degree $\leq k$, $\mathbf{P}_k(T)$ stands for its vector version (as indicated in Section 1.1), and $\mathbf{x} := (x_1, \ldots, x_d)^{\mathrm{t}}$ is a generic vector of R^d. Next, we recall from [8, Section 4.3] the finite element spaces

$$\begin{aligned}
\mathbb{H}_h^{\boldsymbol{\sigma}} &:= \left\{ \boldsymbol{\tau}_h \in \mathbb{H}_0(\mathbf{div};\Omega) : \quad \mathbf{c}^t \boldsymbol{\tau}_h|_T \in \mathbf{RT}_k(T) \quad \forall \, \mathbf{c} \in \mathrm{R}^d, \quad \forall \, T \in \mathcal{T}_h \right\}, \\
\mathbf{H}_h^{\mathbf{u}} &:= \left\{ \mathbf{v}_h \in \mathbf{C}(\overline{\Omega}) : \quad \mathbf{v}_h|_T \in \mathbf{P}_{k+1}(T) \quad \forall \, T \in \mathcal{T}_h \right\}, \\
\mathbf{H}_h^{\boldsymbol{\rho}} &:= \left\{ \boldsymbol{\eta}_h \in \mathbf{H}(\mathrm{div}_{4/3};\Omega) : \quad \boldsymbol{\eta}_h|_T \in \mathbf{RT}_k(T) \quad \forall \, T \in \mathcal{T}_h \right\}, \\
\mathrm{H}_h^{\phi} &:= \left\{ \psi_h \in \mathrm{L}^4(\Omega) : \quad \psi_h|_T \in \mathrm{P}_k(T) \quad \forall \, T \in \mathcal{T}_h \right\},
\end{aligned} \tag{2.20}$$

and set $\boldsymbol{\phi}_h := (\phi_{1,h}, \phi_{2,h}) \in \mathbf{H}_h^{\phi} := \mathrm{H}_h^{\phi} \times \mathrm{H}_h^{\phi}$. Then the Galerkin scheme associated with (2.7) reads: Find $(\boldsymbol{\sigma}_h, \mathbf{u}_h) \in \mathbb{H}_h^{\boldsymbol{\sigma}} \times \mathbf{H}_h^{\mathbf{u}}$ and $(\boldsymbol{\rho}_{j,h}, \phi_{j,h}) \in \mathbf{H}_h^{\boldsymbol{\rho}} \times \mathrm{H}_h^{\phi}$, $j \in \{1, 2\}$, such that

$$\begin{aligned}
A((\boldsymbol{\sigma}_h, \mathbf{u}_h), (\boldsymbol{\tau}_h, \mathbf{v}_h)) + B_{\mathbf{u}_h}((\boldsymbol{\sigma}_h, \mathbf{u}_h), (\boldsymbol{\tau}_h, \mathbf{v}_h)) &= F_{\mathrm{D}}(\boldsymbol{\tau}_h, \mathbf{v}_h) + F_{\boldsymbol{\phi}_h}(\boldsymbol{\tau}_h, \mathbf{v}_h), \\
a_j(\boldsymbol{\rho}_{j,h}, \boldsymbol{\eta}_{j,h}) + b(\boldsymbol{\eta}_{j,h}, \phi_{j,h}) + c_j(\mathbf{u}_h; \phi_{j,h}, \boldsymbol{\eta}_{j,h}) &= G_j(\boldsymbol{\eta}_{j,h}), \\
b(\boldsymbol{\rho}_{j,h}, \psi_{j,h}) &= 0,
\end{aligned} \tag{2.21}$$

for all $(\boldsymbol{\tau}_h, \mathbf{v}_h) \in \mathbb{H}_h^{\boldsymbol{\sigma}} \times \mathbf{H}_h^{\mathbf{u}}$ and $(\boldsymbol{\eta}_{j,h}, \psi_{j,h}) \in \mathbf{H}_h^{\boldsymbol{\rho}} \times \mathrm{H}_h^{\phi}$. The solvability analysis and *a priori* error bounds for (2.21) are established in [8, Theorems 4.7, 5.4 and 5.6]. In particular, we recall the *a priori* estimates

$$\|(\boldsymbol{\sigma}_h, \mathbf{u}_h)\| \, \leq \, c_{\mathbf{T}_h} \left\{ \|\mathbf{u}_{\mathrm{D}}\|_{0,\Gamma} + \|\mathbf{u}_{\mathrm{D}}\|_{1/2,\Gamma} + \|\mathbf{g}\|_{0,4;\Omega} \left(\|\boldsymbol{\phi}_{\mathrm{D}}\|_{1/2,\Gamma} + \|\boldsymbol{\phi}_{\mathbf{r}}\|_{0,4;\Omega} \right) \right\} \tag{2.22}$$

and

$$\sum_{j=1}^{2} \|(\boldsymbol{\rho}_{j,h}, \phi_{j,h})\| \, \leq \, c_{\widetilde{\mathbf{S}}_h} \, \|\boldsymbol{\phi}_{\mathrm{D}}\|_{1/2,\Gamma} \, , \tag{2.23}$$

where $c_{\mathbf{T}_h} := c_{\mathbf{S}} \max\left\{1, c_{\widetilde{\mathbf{S}}_h}\right\}$ and $c_{\widetilde{\mathbf{S}}_h}$ is a positive constant, independent of h, defined in [8, eq. (4.15)].

3 Preliminaries for the a posteriori error analysis

We start by introducing a few useful notations for describing local information on elements and edges or faces depending on wether $d = 2$ or $d = 3$, respectively. Let $\mathcal{E}_h$ be the set of edges or faces of $\mathcal{T}_h$, whose corresponding diameters are denoted by h_e, and define

$$\mathcal{E}_h(\Omega) := \big\{ e \in \mathcal{E}_h : \quad e \subseteq \Omega \big\} \quad \text{and} \quad \mathcal{E}_h(\Gamma) := \big\{ e \in \mathcal{E}_h : \quad e \subseteq \Gamma \big\} .$$

For each $T \in \mathcal{T}_h$, we let $\mathcal{E}_{h,T}$ be the set of edges or faces of T, and denote

$$\mathcal{E}_{h,T}(\Omega) = \big\{ e \subseteq \partial T : \quad e \in \mathcal{E}_h(\Omega) \big\} \quad \text{and} \quad \mathcal{E}_{h,T}(\Gamma) = \big\{ e \subseteq \partial T : \quad e \in \mathcal{E}_h(\Gamma) \big\} .$$

We also define the unit normal vector $\mathbf{n}_e$ on each edge or face by

$$\mathbf{n}_e := (n_1, \ldots, n_d)^{\mathrm{t}} \quad \forall\, e \in \mathcal{E}_h .$$

Hence, when $d = 2$ we can define the tangential vector $\mathbf{s}_e$ by

$$\mathbf{s}_e := (-n_2, n_1)^{\mathrm{t}} \quad \forall\, e \in \mathcal{E}_h .$$

However, when no confusion arises, we will simply write $\mathbf{n}$ and $\mathbf{s}$ instead of $\mathbf{n}_e$ and $\mathbf{s}_e$, respectively.

The usual jump operator $[\![\cdot]\!]$ across internal edges or faces is defined for piecewise continuous matrix, vector, or scalar-valued functions $\boldsymbol{\zeta}$, by

$$[\![\boldsymbol{\zeta}]\!] = (\boldsymbol{\zeta}|_{T_+})|_e - (\boldsymbol{\zeta}|_{T_-})|_e \quad \text{with} \quad e = \partial T_+ \cap \partial T_- ,$$

where T_+ and T_- are the elements of $\mathcal{T}_h$ having e as a common edge or face. Finally, for sufficiently smooth scalar ψ, vector $\mathbf{v} := (v_1, \ldots, v_d)^{\mathrm{t}}$, and tensor fields $\boldsymbol{\tau} := (\tau_{ij})_{i,j=1,d}$, we let

$$\mathrm{curl}(\psi) := \Big(-\frac{\partial \psi}{\partial x_2} , \frac{\partial \psi}{\partial x_1} \Big)^{\mathrm{t}}, \quad \mathbf{curl}(\mathbf{v}) := \begin{pmatrix} \mathrm{curl}(v_1)^{\mathrm{t}} \\ \mathrm{curl}(v_2)^{\mathrm{t}} \end{pmatrix} \quad \text{for } d = 2,$$

$$\underline{\mathrm{curl}}(\mathbf{v}) := \begin{cases} \dfrac{\partial v_2}{\partial x_1} - \dfrac{\partial v_1}{\partial x_2} & , \text{ for } d = 2, \\ \nabla \times \mathbf{v} & , \text{ for } d = 3, \end{cases} \qquad \underline{\mathbf{curl}}(\boldsymbol{\tau}) = \begin{cases} \begin{pmatrix} \underline{\mathrm{curl}}(\boldsymbol{\tau}_1) \\ \underline{\mathrm{curl}}(\boldsymbol{\tau}_2) \end{pmatrix} & , \text{ for } d = 2, \\ \begin{pmatrix} \underline{\mathrm{curl}}(\boldsymbol{\tau}_1) \\ \underline{\mathrm{curl}}(\boldsymbol{\tau}_2) \\ \underline{\mathrm{curl}}(\boldsymbol{\tau}_3) \end{pmatrix} & , \text{ for } d = 3, \end{cases}$$

$$\boldsymbol{\gamma}_*(\mathbf{v}) = \begin{cases} \mathbf{v} \cdot \mathbf{s} & , \text{ for } d = 2, \\ \mathbf{v} \times \mathbf{n} & , \text{ for } d = 3, \end{cases} \quad \text{and} \quad \underline{\boldsymbol{\gamma}}_*(\boldsymbol{\tau}) = \begin{cases} \boldsymbol{\tau}\mathbf{s} & , \text{ for } d = 2, \\ \begin{pmatrix} \boldsymbol{\tau}_1 \times \mathbf{n} \\ \boldsymbol{\tau}_2 \times \mathbf{n} \\ \boldsymbol{\tau}_3 \times \mathbf{n} \end{pmatrix} & , \text{ for } d = 3, \end{cases}$$

where $\boldsymbol{\tau}_i$ is the i-th row of $\boldsymbol{\tau}$ and the derivatives involved are taken in the distributional sense.

Now, let $\Pi_h^k : \mathbf{H}^1(\Omega) \to \mathbf{H}_h^{\boldsymbol{\rho}}$ (cf. (2.20)) be the Raviart–Thomas interpolation operator, which is characterized by the following identities

$$\int_e (\Pi_h^k(\mathbf{v}) \cdot \mathbf{n})\, q = \int_e (\mathbf{v} \cdot \mathbf{n})\, q \quad \forall\, \text{edge/face } e \in \mathcal{E}_h, \quad \forall\, q \in \mathrm{P}_k(e) \quad \text{when } k \geq 0 , \tag{3.1}$$

and

$$\int_T \Pi_h^k(\mathbf{v}) \cdot \mathbf{q} = \int_T \mathbf{v} \cdot \mathbf{q} \quad \forall\, T \in \mathcal{T}_h, \quad \forall\, \mathbf{q} \in \mathbf{P}_{k-1}(K) \quad \text{when } k \geq 1 , \tag{3.2}$$

for all $\mathbf{v} \in \mathbf{H}^1(\Omega)$. As a consequence of (3.1) and (3.2), it is easy to show that (see [20, Lemma 3.7])

$$\mathrm{div}(\Pi_h^k(\mathbf{v})) = \mathcal{P}_h^k(\mathrm{div}(\mathbf{v})),$$

where $\mathcal{P}_h^k$ is the $\mathrm{L}^2(\Omega)$-orthogonal projector onto the picewise polynomials of degree $\leq k$ on Ω. A tensor version of Π_h^k, say $\mathbf{\Pi}_h^k : \mathbb{H}^1(\Omega) \to \mathbb{H}_h^{\boldsymbol{\sigma}}$, which is defined row-wise by Π_h^k, and a vector version of $\mathcal{P}_h^k$, say $\boldsymbol{\mathcal{P}}_h^k$, which is the $\mathbf{L}^2(\Omega)$-orthogonal projector onto the piecewise polynomial vectors of degree $\leq k$, might also be required. The local approximation properties of Π_h^k (and hence of $\mathbf{\Pi}_h^k$) are established in what follows. For the corresponding proofs we refer to [20, Lemma 3.16] and [4, Lemma 4.2] (see also [3]).

Lemma 3.1 *Let $p > 1$. Then, there exist positive constants c_1, c_2, independent of h, such that for all $\mathbf{v} \in \mathbf{H}^1(\Omega)$ there hold*

$$\|\mathbf{v} - \Pi_h^k(\mathbf{v})\|_{0,T} \leq c_1\, h_T\, \|\mathbf{v}\|_{1,T} \quad \forall\, T \in \mathcal{T}_h,$$

and

$$\|\mathbf{v}\cdot\mathbf{n} - \Pi_h^k(\mathbf{v})\cdot\mathbf{n}\|_{0,p;e} \leq c_2\, h_e^{1-1/p}\, \|\mathbf{v}\|_{1,p;T_e} \quad \forall\, e \in \mathcal{E}_h,$$

where T_e is a triangle of $\mathcal{T}_h$ containing the edge e on its boundary.

In turn, let $I_h : \mathrm{H}^1(\Omega) \to \mathrm{H}_h^1(\Omega)$ be the Clément interpolation operator, where

$$\mathrm{H}_h^1(\Omega) := \Big\{ v \in \mathcal{C}(\overline{\Omega}) :\ v|_T \in \mathrm{P}_1(T) \quad \forall\, T \in \mathcal{T}_h \Big\}.$$

The local approximation properties of this operator are established in the following lemma (see [12]).

Lemma 3.2 *There exist positive constants c_3, c_4, independent of h, such that for all $v \in \mathrm{H}^1(\Omega)$ there holds*

$$\|v - I_h(v)\|_{0,T} \leq c_3\, h_T\, \|v\|_{1,\Delta(T)} \quad \forall\, T \in \mathcal{T}_h,$$

and

$$\|v - I_h(v)\|_{0,e} \leq c_4\, h_e^{1/2}\, \|v\|_{1,\Delta(e)} \quad \forall\, e \in \mathcal{E}_h,$$

where

$$\Delta(T) := \cup \Big\{ T' \in \mathcal{T}_h :\ T' \cap T \neq \emptyset \Big\} \quad \textit{and} \quad \Delta(e) := \cup \Big\{ T' \in \mathcal{T}_h :\ T' \cap e \neq \emptyset \Big\}.$$

In what follows, a vector version of I_h, say $\mathbf{I}_h : \mathbf{H}^1(\Omega) \to \mathbf{H}_h^1(\Omega)$, which is defined component-wise by I_h, will be needed as well. For the forthcoming analysis we will also utilize a couple of results providing stable Helmholtz decompositions for $\mathbb{H}_0(\mathbf{div};\Omega)$ and $\mathbf{H}(\mathrm{div}_p;\Omega)$ (cf. (1.1), (1.2)). More precisely, we have the following lemmas.

Lemma 3.3 *For each $\boldsymbol{\tau} \in \mathbb{H}(\mathbf{div};\Omega)$ there exist*

a) $\mathbf{z} \in \mathbf{H}^2(\Omega)$ and $\boldsymbol{\chi} \in \mathbf{H}^1(\Omega)$ such that $\boldsymbol{\tau} = \nabla\mathbf{z} + \mathbf{curl}(\boldsymbol{\chi})$ when $d = 2$,

b) $\mathbf{z} \in \mathbf{H}^2(\Omega)$ and $\boldsymbol{\chi} \in \mathbb{H}^1(\Omega)$ such that $\boldsymbol{\tau} = \nabla\mathbf{z} + \underline{\mathbf{curl}}(\boldsymbol{\chi})$ when $d = 3$.

In addition, in both cases,

$$\|\mathbf{z}\|_{2;\Omega} + \|\boldsymbol{\chi}\|_{1,\Omega} \leq C_{Hel}\, \|\boldsymbol{\tau}\|_{\mathbf{div};\Omega},$$

where C_{Hel} is a positive constant independent of all the foregoing variables.

Proof. For the proof of *a*) and *b*) we refer to [28, Lemma 3.7] and [21, Theorem 3.1], respectively. We omit further details. □

Lemma 3.4 *Let $1 < p \leq 2$ when $d = 2$ and $6/5 \leq p \leq 2$ when $d = 3$. Then, for each $\boldsymbol{\eta} \in \mathbf{H}(\mathrm{div}_p;\Omega)$ there exist*

a) $\boldsymbol{\xi} \in \mathbf{W}^{1,p}(\Omega)$ and $w \in \mathrm{H}^1(\Omega)$ such that $\boldsymbol{\eta} = \boldsymbol{\xi} + \mathrm{curl}(w)$ when $d = 2$,

b) $\boldsymbol{\xi} \in \mathbf{W}^{1,p}(\Omega)$ and $\mathbf{w} \in \mathbf{H}^1(\Omega)$ such that $\boldsymbol{\eta} = \boldsymbol{\xi} + \underline{\mathrm{curl}}(\mathbf{w})$ when $d = 3$.

In addition, we have that

$$\|\boldsymbol{\xi}\|_{1,p;\Omega} + \|w\|_{1,\Omega} \leq C_{Hel}\,\|\boldsymbol{\eta}\|_{\mathrm{div}_p;\Omega} \quad \textit{and} \quad \|\boldsymbol{\xi}\|_{1,p;\Omega} + \|\mathbf{w}\|_{1,\Omega} \leq C_{Hel}\,\|\boldsymbol{\eta}\|_{\mathrm{div}_p;\Omega},$$

for $d = 2$ and $d = 3$, respectively, where C_{Hel} is a positive constant independent of all the foregoing variables.

Proof. See [4, Lemma 4.4]. □

4 First residual-based a posteriori error estimator

In this section we derive a reliable and efficient residual based *a posteriori* error estimator for the Galerkin scheme (2.21). To this end, in what follows we assume the hypotheses from [8, Theorems 3.9 and 4.7], which guarantee the existence of unique solutions $(\boldsymbol{\sigma}, \mathbf{u}, \boldsymbol{\rho}_j, \phi_j) \in \mathbb{H}_0(\mathbf{div};\Omega) \times \mathbf{H}^1(\Omega) \times \mathbf{H}(\mathrm{div}_{4/3};\Omega) \times \mathrm{L}^4(\Omega)$ and $(\boldsymbol{\sigma}_h, \mathbf{u}_h, \boldsymbol{\rho}_{j,h}, \phi_{j,h}) \in \mathbb{H}_h^{\boldsymbol{\sigma}} \times \mathbf{H}_h^{\mathbf{u}} \times \mathbf{H}_h^{\boldsymbol{\rho}} \times \mathrm{H}_h^{\phi}$, $j \in \{1,2\}$ of the continuous and discrete problems (2.7) and (2.21), respectively. Then, the first global *a posteriori* error estimator is defined by:

$$\Theta_1 := \left\{ \sum_{T \in \mathcal{T}_h} \left(\Theta^2_{\mathtt{BF},T} + \sum_{j=1}^{2} \Theta^2_{\mathtt{D},j,T} \right) \right\}^{1/2} + \left\{ \sum_{T \in \mathcal{T}_h} \sum_{j=1}^{2} \|\mathrm{div}(\boldsymbol{\rho}_{j,h})\|^{4/3}_{0,4/3;T} \right\}^{3/4}, \tag{4.1}$$

where, for each $T \in \mathcal{T}_h$, the local error indicators $\Theta^2_{\mathtt{BF},T}$ and $\Theta^2_{\mathtt{D},j,T}$ are defined as follows:

$$\begin{aligned} \Theta^2_{\mathtt{BF},T} :=\ & \left\| \mathbf{f}(\boldsymbol{\phi}_h) + \mathbf{div}(\boldsymbol{\sigma}_h) - \mathbf{K}^{-1}\mathbf{u}_h - \mathtt{F}\,|\mathbf{u}_h|\mathbf{u}_h \right\|^2_{0,T} + \left\| \nabla \mathbf{u}_h - \frac{1}{\nu}\,\boldsymbol{\sigma}_h^{\mathrm{d}} \right\|^2_{0,T} \\ & + h_T^2 \left\| \underline{\mathbf{curl}} \left(\frac{1}{\nu}\,\boldsymbol{\sigma}_h^{\mathrm{d}} \right) \right\|^2_{0,T} + \sum_{e \in \mathcal{E}_{h,T}(\Omega)} h_e \left\| \left[\!\left[\underline{\boldsymbol{\gamma}}_* \left(\frac{1}{\nu}\,\boldsymbol{\sigma}_h^{\mathrm{d}} \right) \right]\!\right] \right\|^2_{0,e} \\ & + \sum_{e \in \mathcal{E}_{h,T}(\Gamma)} \|\mathbf{u}_{\mathrm{D}} - \mathbf{u}_h\|^2_{0,e} + \sum_{e \in \mathcal{E}_{h,T}(\Gamma)} h_e \left\| \underline{\boldsymbol{\gamma}}_* \left(\frac{1}{\nu}\,\boldsymbol{\sigma}_h^{\mathrm{d}} - \nabla \mathbf{u}_{\mathrm{D}} \right) \right\|^2_{0,e} \end{aligned} \tag{4.2}$$

and

$$\begin{aligned} \Theta^2_{\mathtt{D},j,T} :=\ & h_T^{2-d/2} \left\| \nabla \phi_{j,h} - \mathbf{Q}_j^{-1} \left(\boldsymbol{\rho}_{j,h} + \mathtt{R}_j \phi_{j,h} \mathbf{u}_h \right) \right\|^2_{0,T} + h_T^2 \left\| \underline{\mathrm{curl}} \left(\mathbf{Q}_j^{-1} \left(\boldsymbol{\rho}_{j,h} + \mathtt{R}_j \phi_{j,h} \mathbf{u}_h \right) \right) \right\|^2_{0,T} \\ & + \sum_{e \in \mathcal{E}_{h,T}(\Omega)} h_e \left\| \left[\!\left[\boldsymbol{\gamma}_* \left(\mathbf{Q}_j^{-1} \left(\boldsymbol{\rho}_{j,h} + \mathtt{R}_j \phi_{j,h} \mathbf{u}_h \right) \right) \right]\!\right] \right\|^2_{0,e} + \sum_{e \in \mathcal{E}_{h,T}(\Gamma)} h_e^{1/2} \|\phi_{j,\mathrm{D}} - \phi_{j,h}\|^2_{0,4;e} \\ & + \sum_{e \in \mathcal{E}_{h,T}(\Gamma)} h_e \left\| \boldsymbol{\gamma}_* \left(\mathbf{Q}_j^{-1} \left(\boldsymbol{\rho}_{j,h} + \mathtt{R}_j \phi_{j,h} \mathbf{u}_h \right) - \nabla \phi_{j,\mathrm{D}} \right) \right\|^2_{0,e}. \end{aligned} \tag{4.3}$$

Notice that the last term of $\Theta^2_{\mathtt{BF},T}$ requires $\underline{\boldsymbol{\gamma}}_*(\nabla \mathbf{u}_{\mathrm{D}})\big|_e \in \mathrm{L}^2(e)$ for all $e \in \mathcal{E}_h(\Gamma)$, which is overcome below (cf. Lemma 4.4) by simply assuming that $\mathbf{u}_{\mathrm{D}} \in \mathbf{H}^1(\Gamma)$. Similarly, the last two terms of $\Theta^2_{\mathtt{D},j,T}$ are well defined if we assume that $\phi_{j,\mathrm{D}} \in \mathrm{H}^1(\Gamma) \cap \mathrm{L}^4(\Gamma)$ for each $j \in \{1,2\}$.

The main goal of the present section is to establish, under suitable assumptions, the existence of positive constants C_{eff} and C_{rel}, independent of the meshsizes and the continuous and discrete solutions, such that

$$C_{\mathrm{eff}}\,\Theta_1 + \text{h.o.t.} \,\leq\, \|(\boldsymbol{\sigma},\mathbf{u}) - (\boldsymbol{\sigma}_h,\mathbf{u}_h)\| + \sum_{j=1}^{2} \|(\boldsymbol{\rho}_j,\phi_j) - (\boldsymbol{\rho}_{j,h},\phi_{j,h})\| \,\leq\, C_{\mathrm{rel}}\,\Theta_1\,, \tag{4.4}$$

where h.o.t. is a generic expression denoting one or several terms of higher order. The upper and lower bounds in (4.4), which are known as the reliability and efficiency of Θ_1, are derived below in Sections 4.1 and 4.2, respectively.

4.1 Reliability of the a posteriori error estimator

The main result of this section is stated in the following theorem.

Theorem 4.1 *Assume that the data $\mathbf{u}_{\mathrm{D}}$, $\boldsymbol{\phi}_{\mathrm{D}}$ and $\boldsymbol{\phi}_{\mathtt{r}}$ satisfy*

$$\frac{c_{\mathbf{T}_h}}{r_0}\left\{\|\mathbf{u}_{\mathrm{D}}\|_{0,\Gamma} + \|\mathbf{u}_{\mathrm{D}}\|_{1/2,\Gamma} + \|\mathbf{g}\|_{0,4;\Omega}\left(2\,\|\boldsymbol{\phi}_{\mathrm{D}}\|_{1/2,\Gamma} + \|\boldsymbol{\phi}_{\mathtt{r}}\|_{0,4;\Omega}\right)\right\} \,\leq\, \frac{1}{2}\,, \tag{4.5}$$

with $r_0 := \min\{r_1, r_2\}$, and r_1, r_2 are defined in (2.15). Then, there exists a positive constant C_{rel}, independent of h, such that

$$\|(\boldsymbol{\sigma},\mathbf{u}) - (\boldsymbol{\sigma}_h,\mathbf{u}_h)\| + \sum_{j=1}^{2} \|(\boldsymbol{\rho}_j,\phi_j) - (\boldsymbol{\rho}_{j,h},\phi_{j,h})\| \,\leq\, C_{\mathrm{rel}}\,\Theta_1\,. \tag{4.6}$$

We begin the derivation of (4.6) with a preliminary lemma, for which we first recall that

$$\mathbb{H}_{\mathtt{BF}} := \mathbb{H}_0(\mathbf{div};\Omega) \times \mathbf{H}^1(\Omega) \quad \text{and} \quad \mathbf{H}_{\mathtt{D}} := \mathbf{H}(\mathrm{div}_{4/3};\Omega) \times \mathrm{L}^4(\Omega)\,.$$

Lemma 4.2 *Assume that the data $\mathbf{u}_{\mathrm{D}}$, $\boldsymbol{\phi}_{\mathrm{D}}$ and $\boldsymbol{\phi}_{\mathtt{r}}$ satisfy (4.5). Then, there exists a positive constant C, independent of h, such that*

$$\begin{aligned} &\|(\boldsymbol{\sigma},\mathbf{u}) - (\boldsymbol{\sigma}_h,\mathbf{u}_h)\| + \sum_{j=1}^{2} \|(\boldsymbol{\rho}_j,\phi_j) - (\boldsymbol{\rho}_{j,h},\phi_{j,h})\| \\ &\qquad \leq\, C\left(\sup_{\mathbf{0}\neq(\boldsymbol{\tau},\mathbf{v})\in\mathbb{H}_{\mathtt{BF}}} \frac{|\mathcal{R}^{\mathtt{BF}}(\boldsymbol{\tau},\mathbf{v})|}{\|(\boldsymbol{\tau},\mathbf{v})\|} + \sum_{j=1}^{2} \sup_{\mathbf{0}\neq(\boldsymbol{\eta}_j,\psi_j)\in\mathbf{H}_{\mathtt{D}}} \frac{|\mathcal{R}^{\mathtt{D}}_j(\boldsymbol{\eta}_j,\psi_j)|}{\|(\boldsymbol{\eta}_j,\psi_j)\|}\right), \end{aligned} \tag{4.7}$$

where $\mathcal{R}^{\mathtt{BF}} : \mathbb{H}_{\mathtt{BF}} \to \mathrm{R}$ and $\mathcal{R}^{\mathtt{D}}_j : \mathbf{H}_{\mathtt{D}} \to \mathrm{R}$ are the residual functionals given by

$$\mathcal{R}^{\mathtt{BF}}(\boldsymbol{\tau},\mathbf{v}) = F_{\mathrm{D}}(\boldsymbol{\tau},\mathbf{v}) + F_{\boldsymbol{\phi}_h}(\boldsymbol{\tau},\mathbf{v}) - A((\boldsymbol{\sigma}_h,\mathbf{u}_h),(\boldsymbol{\tau},\mathbf{v})) - B_{\mathbf{u}_h}((\boldsymbol{\sigma}_h,\mathbf{u}_h),(\boldsymbol{\tau},\mathbf{v}))$$

for all $(\boldsymbol{\tau},\mathbf{v}) \in \mathbb{H}_{\mathtt{BF}}$, and

$$\mathcal{R}^{\mathtt{D}}_j(\boldsymbol{\eta}_j,\psi_j) = G_j(\boldsymbol{\eta}_j) - a_j(\boldsymbol{\rho}_{j,h},\boldsymbol{\eta}_j) - b(\boldsymbol{\eta}_j,\phi_{j,h}) - b(\boldsymbol{\rho}_{j,h},\psi_j) - c_j(\mathbf{u}_h;\phi_{j,h},\boldsymbol{\eta}_j)$$

for all $(\boldsymbol{\eta}_j,\psi_j) \in \mathbf{H}_{\mathtt{D}}$.

Proof. First, applying the inf-sup condition (2.16) to the error $(\boldsymbol{\zeta},\mathbf{z}) = (\boldsymbol{\sigma}-\boldsymbol{\sigma}_h, \mathbf{u}-\mathbf{u}_h)$, adding and substracting $B_{\mathbf{u}_h}((\boldsymbol{\sigma}_h,\mathbf{u}_h),(\boldsymbol{\tau},\mathbf{v}))$ and $F_{\boldsymbol{\phi}_h}(\boldsymbol{\tau},\mathbf{v})$, and using the first equation of (2.7), we deduce that

$$\begin{aligned}\frac{\alpha_A}{2}\,\|(\boldsymbol{\sigma}-\boldsymbol{\sigma}_h,\mathbf{u}-\mathbf{u}_h)\| \,\leq\, &\sup_{\mathbf{0}\neq(\boldsymbol{\tau},\mathbf{v})\in\mathbb{H}_{\mathtt{BF}}}\frac{\big|\mathcal{R}^{\mathtt{BF}}(\boldsymbol{\tau},\mathbf{v})\big|}{\|(\boldsymbol{\tau},\mathbf{v})\|}\\ &+\sup_{\mathbf{0}\neq(\boldsymbol{\tau},\mathbf{v})\in\mathbb{H}_{\mathtt{BF}}}\frac{\big|B_{\mathbf{u}-\mathbf{u}_h}((\boldsymbol{\sigma}_h,\mathbf{u}_h),(\boldsymbol{\tau},\mathbf{v}))\big|}{\|(\boldsymbol{\tau},\mathbf{v})\|}+\sup_{\mathbf{0}\neq(\boldsymbol{\tau},\mathbf{v})\in\mathbb{H}_{\mathtt{BF}}}\frac{\big|F_{\boldsymbol{\phi}-\boldsymbol{\phi}_h}(\boldsymbol{\tau},\mathbf{v})\big|}{\|(\boldsymbol{\tau},\mathbf{v})\|}\,.\end{aligned}\tag{4.8}$$

In turn, the continuities of $B_{\mathbf{w}}$ (cf. (2.9)) and $F_{\boldsymbol{\varphi}}$ (cf. (2.12)) establish (cf. [8, eqns. (3.4), (3.9)])

$$\begin{aligned}&\big|B_{\mathbf{u}-\mathbf{u}_h}((\boldsymbol{\sigma}_h,\mathbf{u}_h),(\boldsymbol{\tau},\mathbf{v}))\big|\leq \mathtt{F}\,\|\mathbf{K}\|_\infty\,\|\mathbf{i}_4\|^2\,\|\mathbf{u}_h\|_{1,\Omega}\,\|\mathbf{u}-\mathbf{u}_h\|_{1,\Omega}\,\|\boldsymbol{\tau}\|_{\mathbf{div};\Omega}\,,\\ &\big|F_{\boldsymbol{\phi}-\boldsymbol{\phi}_h}(\boldsymbol{\tau},\mathbf{v})\big|\leq \|\mathbf{K}\|_\infty\,\|\mathbf{g}\|_{0,4;\Omega}\,\|\boldsymbol{\phi}-\boldsymbol{\phi}_h\|_{0,4;\Omega}\,\|\boldsymbol{\tau}\|_{\mathbf{div};\Omega}\,,\end{aligned}$$

which, replaced back into (4.8), yields

$$\begin{aligned}&\|(\boldsymbol{\sigma}-\boldsymbol{\sigma}_h,\mathbf{u}-\mathbf{u}_h)\|\\ &\leq\frac{2}{\alpha_A}\sup_{\mathbf{0}\neq(\boldsymbol{\tau},\mathbf{v})\in\mathbb{H}_{\mathtt{BF}}}\frac{\big|\mathcal{R}^{\mathtt{BF}}(\boldsymbol{\tau},\mathbf{v})\big|}{\|(\boldsymbol{\tau},\mathbf{v})\|}+\frac{1}{r_1}\,\|\mathbf{u}_h\|_{1,\Omega}\|\mathbf{u}-\mathbf{u}_h\|_{1,\Omega}+C_{\mathbf{S}}\,\|\mathbf{g}\|_{0,4;\Omega}\|\boldsymbol{\phi}-\boldsymbol{\phi}_h\|_{0,4;\Omega}\,,\end{aligned}\tag{4.9}$$

where $C_{\mathbf{S}} := 2\,\|\mathbf{K}\|_\infty/\alpha_A$ (cf. [8, eq. (3.40)]) and r_1 is defined in (2.15). Similarly, applying the inf-sup condition (2.17) to $(\boldsymbol{\chi}_j,\varphi_j) = (\boldsymbol{\rho}_j-\boldsymbol{\rho}_{j,h},\phi_j-\phi_{j,h})$, making use of the second and third equations of (2.7), adding and substracting $c_j(\mathbf{u}_h;\phi_{j,h},\boldsymbol{\eta}_j)$, and using the continuity of c_j, which states that (cf. [8, eq. (3.7)])

$$\big|c_j(\mathbf{w};\psi,\boldsymbol{\eta})\big|\,\leq\,\mathtt{R}_j\,\|\mathbf{Q}_j^{-1}\|\,\|\mathbf{i}_4\|\,\|\mathbf{w}\|_{1,\Omega}\|\psi\|_{0,4;\Omega}\,\|\boldsymbol{\eta}\|_{\mathrm{div}_{4/3};\Omega}\,,$$

we deduce that

$$\begin{aligned}\frac{\gamma_j}{2}\,\|(\boldsymbol{\rho}_j-\boldsymbol{\rho}_{j,h},\phi_j-\phi_{j,h})\|\,&\leq\,\sup_{\mathbf{0}\neq(\boldsymbol{\eta}_j,\psi_j)\in\mathbf{H}_{\mathtt{D}}}\frac{\big|\mathcal{R}_j^{\mathtt{D}}(\boldsymbol{\eta}_j,\psi_j)\big|}{\|(\boldsymbol{\eta}_j,\psi_j)\|}+\sup_{\mathbf{0}\neq(\boldsymbol{\eta}_j,\psi_j)\in\mathbf{H}_{\mathtt{D}}}\frac{\big|c_j(\mathbf{u}-\mathbf{u}_h;\phi_{j,h},\boldsymbol{\eta}_j)\big|}{\|\boldsymbol{\eta}_j\|_{\mathrm{div}_{4/3};\Omega}}\\ &\leq\,\sup_{\mathbf{0}\neq(\boldsymbol{\eta}_j,\psi_j)\in\mathbf{H}_{\mathtt{D}}}\frac{\big|\mathcal{R}_j^{\mathtt{D}}(\boldsymbol{\eta}_j,\psi_j)\big|}{\|(\boldsymbol{\eta}_j,\psi_j)\|}+\mathtt{R}_j\,\|\mathbf{Q}_j^{-1}\|\,\|\mathbf{i}_4\|\,\|\phi_{j,h}\|_{0,4;\Omega}\,\|\mathbf{u}-\mathbf{u}_h\|_{1,\Omega}\,.\end{aligned}$$

Thus, summing up over $j\in\{1,2\}$, recalling the definition of r_2 in (2.15) and using (2.23) to bound $\|\boldsymbol{\phi}_h\|_{0,4;\Omega} := \|\phi_{1,h}\|_{0,4;\Omega}+\|\phi_{2,h}\|_{0,4;\Omega}$, we obtain

$$\sum_{j=1}^{2}\|(\boldsymbol{\rho}_j-\boldsymbol{\rho}_{j,h},\phi_j-\phi_{j,h})\|\,\leq\,\sum_{j=1}^{2}\frac{2}{\gamma_j}\sup_{\mathbf{0}\neq(\boldsymbol{\eta}_j,\psi_j)\in\mathbf{H}_{\mathtt{D}}}\frac{\big|\mathcal{R}_j^{\mathtt{D}}(\boldsymbol{\eta}_j,\psi_j)\big|}{\|(\boldsymbol{\eta}_j,\psi_j)\|}+\frac{c_{\widetilde{\mathbf{S}}_h}}{r_2}\|\boldsymbol{\phi}_{\mathrm{D}}\|_{1/2,\Gamma}\|\mathbf{u}-\mathbf{u}_h\|_{1,\Omega}\,,\tag{4.10}$$

with $c_{\widetilde{\mathbf{S}}_h}>0$ defined in [8, eq. (4.15)]. Then, using the estimate (4.10) to bound the last term in (4.9), recalling the definition of r_0 in (2.15), using (2.22) to bound $\|\mathbf{u}_h\|_{1,\Omega}$, and recalling that $C_{\mathbf{S}}$ and $c_{\widetilde{\mathbf{S}}_h}$, as well as $1/r_1$ and $1/r_2$, are bounded by $c_{\mathbf{T}_h}$ and $1/r_0$ (cf. [8, eq. (3.43)]), respectively, we deduce that

$$\begin{aligned}&\|(\boldsymbol{\sigma}-\boldsymbol{\sigma}_h,\mathbf{u}-\mathbf{u}_h)\|\\ &\leq\,C_1\sup_{\mathbf{0}\neq(\boldsymbol{\tau},\mathbf{v})\in\mathbb{H}_{\mathtt{BF}}}\frac{|\mathcal{R}^{\mathtt{BF}}(\boldsymbol{\tau},\mathbf{v})|}{\|(\boldsymbol{\tau},\mathbf{v})\|}\,+\,C_2\sum_{j=1}^{2}\sup_{\mathbf{0}\neq(\boldsymbol{\eta}_j,\psi_j)\in\mathbf{H}_{\mathtt{D}}}\frac{|\mathcal{R}_j^{\mathtt{D}}(\boldsymbol{\eta}_j,\psi_j)|}{\|(\boldsymbol{\eta}_j,\psi_j)\|}\\ &+\frac{c_{\mathbf{T}_h}}{r_0}\Big\{\|\mathbf{u}_{\mathrm{D}}\|_{0,\Gamma}+\|\mathbf{u}_{\mathrm{D}}\|_{1/2,\Gamma}+\|\mathbf{g}\|_{0,4;\Omega}\left(2\,\|\boldsymbol{\phi}_{\mathrm{D}}\|_{1/2,\Gamma}+\|\boldsymbol{\phi}_{\mathbf{r}}\|_{0,4;\Omega}\right)\Big\}\,\|\mathbf{u}-\mathbf{u}_h\|_{1,\Omega}\,,\end{aligned}\tag{4.11}$$

with $C_1, C_2 > 0$, independent of h. Thus, according to the assumption (4.5), (4.11) yields

$$\|(\boldsymbol{\sigma}-\boldsymbol{\sigma}_h, \mathbf{u}-\mathbf{u}_h)\| \leq \widehat{C}_1 \sup_{\mathbf{0}\neq(\boldsymbol{\tau},\mathbf{v})\in\mathbb{H}_{\mathtt{BF}}} \frac{|\mathcal{R}^{\mathtt{BF}}(\boldsymbol{\tau},\mathbf{v})|}{\|(\boldsymbol{\tau},\mathbf{v})\|} + \widehat{C}_2 \sum_{j=1}^{2} \sup_{\mathbf{0}\neq(\boldsymbol{\eta}_j,\psi_j)\in\mathbf{H}_{\mathtt{D}}} \frac{|\mathcal{R}^{\mathtt{D}}_j(\boldsymbol{\eta}_j,\psi_j)|}{\|(\boldsymbol{\eta}_j,\psi_j)\|}\,, \tag{4.12}$$

with $\widehat{C}_1, \widehat{C}_2 > 0$, independent of h. Next, using (4.12) to bound the last term in (4.10), we easily find that

$$\sum_{j=1}^{2} \|(\boldsymbol{\rho}_j-\boldsymbol{\rho}_{j,h}, \phi_j-\phi_{j,h})\| \leq \widehat{C}_3 \sup_{\mathbf{0}\neq(\boldsymbol{\tau},\mathbf{v})\in\mathbb{H}_{\mathtt{BF}}} \frac{|\mathcal{R}^{\mathtt{BF}}(\boldsymbol{\tau},\mathbf{v})|}{\|(\boldsymbol{\tau},\mathbf{v})\|} + \widehat{C}_4 \sum_{j=1}^{2} \sup_{\mathbf{0}\neq(\boldsymbol{\eta}_j,\psi_j)\in\mathbf{H}_{\mathtt{D}}} \frac{|\mathcal{R}^{\mathtt{D}}_j(\boldsymbol{\eta}_j,\psi_j)|}{\|(\boldsymbol{\eta}_j,\psi_j)\|}, \tag{4.13}$$

with $\widehat{C}_3, \widehat{C}_4 > 0$, independent of h. In this way, estimate (4.7) follows from (4.12) and (4.13). □

We now aim to bound the suprema in (4.7). Indeed, in virtue of the definitions of the forms A, $B_{\mathbf{w}}$, a_j, b and c_j (cf. (2.8)–(2.11)), we find that, for any $(\boldsymbol{\tau},\mathbf{v}) \in \mathbb{H}_0(\mathbf{div};\Omega) \times \mathbf{H}^1(\Omega)$ and $(\boldsymbol{\eta}_j,\psi_j) \in \mathbf{H}(\mathrm{div}_{4/3};\Omega) \times \mathrm{L}^4(\Omega)$, $j \in \{1,2\}$, there holds

$$\mathcal{R}^{\mathtt{BF}}(\boldsymbol{\tau},\mathbf{v}) = \mathcal{R}^{\mathtt{BF}}_1(\boldsymbol{\tau}) + \mathcal{R}^{\mathtt{BF}}_2(\mathbf{v}) \quad \text{and} \quad \mathcal{R}^{\mathtt{D}}_j(\boldsymbol{\eta}_j,\psi_j) = \mathcal{R}^{\mathtt{D}}_{j,1}(\boldsymbol{\eta}_j) + \mathcal{R}^{\mathtt{D}}_{j,2}(\psi_j)\,,$$

where

$$\begin{aligned} \mathcal{R}^{\mathtt{BF}}_1(\boldsymbol{\tau}) \;&=\; \langle \boldsymbol{\tau}\mathbf{n}, \mathbf{u}_{\mathrm{D}}\rangle_{\Gamma} - \frac{1}{\nu}\int_{\Omega} \boldsymbol{\sigma}^{\mathrm{d}}_h : \boldsymbol{\tau}^{\mathrm{d}} - \int_{\Omega} \mathbf{u}_h \cdot \mathbf{div}(\boldsymbol{\tau}) \\ &\quad - \int_{\Omega} \mathbf{K}\,\big(\mathbf{f}(\boldsymbol{\phi}_h) + \mathbf{div}(\boldsymbol{\sigma}_h) - \mathbf{K}^{-1}\mathbf{u}_h - \mathtt{F}\,|\mathbf{u}_h|\mathbf{u}_h\big)\cdot\mathbf{div}(\boldsymbol{\tau})\,, \end{aligned} \tag{4.14}$$

$$\mathcal{R}^{\mathtt{BF}}_2(\mathbf{v}) \;=\; \kappa_2 \int_{\Gamma} (\mathbf{u}_{\mathrm{D}} - \mathbf{u}_h)\cdot\mathbf{v} - \kappa_1 \int_{\Omega} \Big(\nabla\mathbf{u}_h - \frac{1}{\nu}\,\boldsymbol{\sigma}^{\mathrm{d}}_h\Big) : \nabla\mathbf{v}\,, \tag{4.15}$$

$$\mathcal{R}^{\mathtt{D}}_{j,1}(\boldsymbol{\eta}_j) \;=\; \big\langle \boldsymbol{\eta}_j\cdot\mathbf{n}, \phi_{j,\mathrm{D}}\big\rangle_{\Gamma} - \int_{\Omega} \mathbf{Q}_j^{-1}\,\big(\boldsymbol{\rho}_{j,h} + \mathtt{R}_j\,\phi_{j,h}\,\mathbf{u}_h\big)\cdot\boldsymbol{\eta}_j - \int_{\Omega} \phi_{j,h}\,\mathrm{div}(\boldsymbol{\eta}_j)\,, \tag{4.16}$$

and

$$\mathcal{R}^{\mathtt{D}}_{j,2}(\psi_j) \;=\; -\int_{\Omega} \psi_j\,\mathrm{div}(\boldsymbol{\rho}_{j,h})\,. \tag{4.17}$$

Notice that for convenience of the subsequent analysis we have added and subtracted the term given by $\int_\Omega \mathbf{u}_h\cdot\mathbf{div}(\boldsymbol{\tau})$ in (4.14). Then, the supremum in (4.7) can be bounded in terms of $\mathcal{R}^{\mathtt{BF}}_1$, $\mathcal{R}^{\mathtt{BF}}_2$, $\mathcal{R}^{\mathtt{D}}_{j,1}$, and $\mathcal{R}^{\mathtt{D}}_{j,2}$ as follows

$$\begin{aligned} &\|(\boldsymbol{\sigma},\mathbf{u}) - (\boldsymbol{\sigma}_h,\mathbf{u}_h)\| + \sum_{j=1}^{2} \|(\boldsymbol{\rho}_j,\phi_j) - (\boldsymbol{\rho}_{j,h},\phi_{j,h})\| \\ &\leq\; C\,\Big\{ \|\mathcal{R}^{\mathtt{BF}}_1\|_{\mathbb{H}_0(\mathbf{div};\Omega)'} + \|\mathcal{R}^{\mathtt{BF}}_2\|_{\mathbf{H}^1(\Omega)'} + \sum_{j=1}^{2} \Big(\|\mathcal{R}^{\mathtt{D}}_{j,1}\|_{\mathbf{H}(\mathrm{div}_{4/3};\Omega)'} + \|\mathcal{R}^{\mathtt{D}}_{j,2}\|_{\mathrm{L}^4(\Omega)'} \Big) \Big\}\,, \end{aligned} \tag{4.18}$$

and hence our next purpose is to derive suitable upper bounds for each one of the terms on the right hand side of (4.18). We begin by establishing the corresponding estimates for $\mathcal{R}^{\mathtt{BF}}_2$ and $\mathcal{R}^{\mathtt{D}}_{j,2}$ (cf. (4.15) and (4.17)), which follow from a straightforward application of the Cauchy–Schwarz and Hölder inequalities.

Lemma 4.3 *There exist positive constants C_1, C_2, independent of h, such that*

$$\|\mathcal{R}_2^{\mathtt{BF}}\|_{\mathbf{H}^1(\Omega)'} \,\leq\, C_1 \left\{ \sum_{T\in\mathcal{T}_h} \left(\left\| \nabla \mathbf{u}_h - \frac{1}{\nu}\,\boldsymbol{\sigma}_h^{\mathrm{d}} \right\|_{0,T}^2 + \sum_{e\in\mathcal{E}_{h,T}(\Gamma)} \|\mathbf{u}_{\mathrm{D}} - \mathbf{u}_h\|_{0,e}^2 \right) \right\}^{1/2}$$

and

$$\sum_{j=1}^{2} \|\mathcal{R}_{j,2}^{\mathtt{D}}\|_{\mathrm{L}^4(\Omega)'} \,\leq\, C_2 \left\{ \sum_{T\in\mathcal{T}_h} \sum_{j=1}^{2} \|\mathbf{div}(\boldsymbol{\rho}_{j,h})\|_{0,4/3;T}^{4/3} \right\}^{3/4} .$$

We now bound the term $\|\mathcal{R}_1^{\mathtt{BF}}\|_{\mathbb{H}_0(\mathbf{div};\Omega)'}$. To this end, we first observe that integrating by parts the expression $\int_\Omega \mathbf{u}_h \cdot \mathbf{div}(\boldsymbol{\tau})$ in (4.14), the functional $\mathcal{R}_1^{\mathtt{BF}}$ can be rewritten as follows

$$\begin{aligned} \mathcal{R}_1^{\mathtt{BF}}(\boldsymbol{\tau}) &= \langle \boldsymbol{\tau}\mathbf{n}, \mathbf{u}_{\mathrm{D}} - \mathbf{u}_h \rangle_\Gamma + \int_\Omega \left(\nabla \mathbf{u}_h - \frac{1}{\nu}\,\boldsymbol{\sigma}_h^{\mathrm{d}} \right) : \boldsymbol{\tau} \\ &\quad - \int_\Omega \mathbf{K}\, \left(\mathbf{f}(\boldsymbol{\phi}_h) + \mathbf{div}(\boldsymbol{\sigma}_h) - \mathbf{K}^{-1}\mathbf{u}_h - \mathtt{F}\,|\mathbf{u}_h|\mathbf{u}_h \right) \cdot \mathbf{div}(\boldsymbol{\tau}) \,. \end{aligned} \tag{4.19}$$

For simplicity, we prove the aforementioned result for the two-dimensional case. The three dimensional one proceeds analogously. Given $\boldsymbol{\tau} \in \mathbb{H}_0(\mathbf{div};\Omega)$, it follows from Lemma 3.3 that there exist $\mathbf{z} \in \mathbf{H}^2(\Omega)$ and $\boldsymbol{\chi} \in \mathbf{H}^1(\Omega)$, such that $\boldsymbol{\tau} = \nabla \mathbf{z} + \mathbf{curl}(\boldsymbol{\chi})$ in Ω, and

$$\|\mathbf{z}\|_{2,\Omega} + \|\boldsymbol{\chi}\|_{1,\Omega} \,\leq\, C_{Hel}\, \|\boldsymbol{\tau}\|_{\mathbf{div};\Omega} \,. \tag{4.20}$$

Then, we set $\boldsymbol{\tau}_h := \boldsymbol{\Pi}_h^k(\nabla \mathbf{z}) + \mathbf{curl}\,(\mathbf{I}_h(\boldsymbol{\chi})) + c_0\,\mathbb{I}$, where $c_0 \in \mathrm{R}$ is chosen so that $\int_\Omega \mathrm{tr}(\boldsymbol{\tau}_h) = 0$. In addition, bearing in mind the definition of $\mathcal{R}_1^{\mathtt{BF}}$ (cf. (4.14)), and employing the first equation of the Galerkin scheme (2.21) and the compatibility condition (2.2), we deduce that $\mathcal{R}_1^{\mathtt{BF}}(\boldsymbol{\tau}_h) = 0$, whence

$$\mathcal{R}_1^{\mathtt{BF}}(\boldsymbol{\tau}) \,=\, \mathcal{R}_1^{\mathtt{BF}}(\boldsymbol{\tau} - \boldsymbol{\tau}_h) \,=\, \mathcal{R}_1^{\mathtt{BF}}(\nabla \mathbf{z} - \boldsymbol{\Pi}_h^k(\nabla \mathbf{z})) + \mathcal{R}_1^{\mathtt{BF}}(\mathbf{curl}(\boldsymbol{\chi} - \mathbf{I}_h(\boldsymbol{\chi}))) \,. \tag{4.21}$$

The following lemma establishes the estimate for $\mathcal{R}_1^{\mathtt{BF}}$.

Lemma 4.4 *Assume that $\mathbf{u}_{\mathrm{D}} \in \mathbf{H}^1(\Gamma)$. Then, there exists a positive constant C, independent of h, such that*

$$\|\mathcal{R}_1^{\mathtt{BF}}\|_{\mathbb{H}_0(\mathbf{div};\Omega)'} \,\leq\, C \left\{ \sum_{T\in\mathcal{T}_h} \overline{\Theta}_{\mathtt{BF},T}^2 \right\}^{1/2} ,$$

where

$$\begin{aligned} \overline{\Theta}_{\mathtt{BF},T}^2 \,:=\, & \left\| \mathbf{f}(\boldsymbol{\phi}_h) + \mathbf{div}(\boldsymbol{\sigma}_h) - \mathbf{K}^{-1}\mathbf{u}_h - \mathtt{F}\,|\mathbf{u}_h|\mathbf{u}_h \right\|_{0,T}^2 \,+\, h_T^2 \left\| \nabla \mathbf{u}_h - \frac{1}{\nu}\,\boldsymbol{\sigma}_h^{\mathrm{d}} \right\|_{0,T}^2 \\ & + h_T^2 \left\| \underline{\mathbf{curl}} \left(\frac{1}{\nu}\,\boldsymbol{\sigma}_h^{\mathrm{d}} \right) \right\|_{0,T}^2 + \sum_{e\in\mathcal{E}_{h,T}(\Omega)} h_e \left\| \left[\!\left[\underline{\boldsymbol{\gamma}}_* \left(\frac{1}{\nu}\,\boldsymbol{\sigma}_h^{\mathrm{d}} \right) \right]\!\right] \right\|_{0,e}^2 \\ & + \sum_{e\in\mathcal{E}_{h,T}(\Gamma)} h_e \left\| \underline{\boldsymbol{\gamma}}_* \left(\frac{1}{\nu}\,\boldsymbol{\sigma}_h^{\mathrm{d}} - \nabla \mathbf{u}_{\mathrm{D}} \right) \right\|_{0,e}^2 + \sum_{e\in\mathcal{E}_{h,T}(\Gamma)} h_e\, \|\mathbf{u}_{\mathrm{D}} - \mathbf{u}_h\|_{0,e}^2 \,. \end{aligned} \tag{4.22}$$

Proof. We begin by considering the expression for $\mathcal{R}_1^{\mathtt{BF}}$ given by (4.19)). Thus, proceeding analogously as in the proof of [26, Lemma 4.4], that is, applying the Cauchy–Schwarz inequality, and using the approximation properties of $\boldsymbol{\Pi}_h$ (cf. Lemma 3.1), we find that

$$\begin{aligned}\left|\mathcal{R}_1^{\mathtt{BF}}(\nabla\mathbf{z}-\boldsymbol{\Pi}_h^k(\nabla\mathbf{z}))\right| \,\leq\, C_1\,\Bigg\{ & \sum_{T\in\mathcal{T}_h}\left\|\mathbf{f}(\boldsymbol{\phi}_h)+\mathbf{div}(\boldsymbol{\sigma}_h)-\mathbf{K}^{-1}\mathbf{u}_h-\mathtt{F}\,|\mathbf{u}_h|\mathbf{u}_h\right\|_{0,T}^2 \\ & +\sum_{T\in\mathcal{T}_h} h_T^2\left\|\nabla\mathbf{u}_h-\frac{1}{\nu}\,\boldsymbol{\sigma}_h^{\mathrm{d}}\right\|_{0,T}^2+\sum_{e\in\mathcal{E}_h(\Gamma)} h_e\,\|\mathbf{u}_{\mathrm{D}}-\mathbf{u}_h\|_{0,e}^2\Bigg\}^{1/2}\|\mathbf{z}\|_{2,\Omega}\,,\end{aligned} \tag{4.23}$$

with $C_1>0$, independent of h. In turn, in order to bound $\mathcal{R}_1^{\mathtt{BF}}(\mathbf{curl}(\boldsymbol{\chi}-\mathbf{I}_h(\boldsymbol{\chi})))$, we appeal to the original definition of $\mathcal{R}_1^{\mathtt{BF}}$ in (4.14), and proceed as in [26, Lemma 4.3] by using the integration by parts formula on the boundary Γ (cf. [17, Lemma 3.5, eq. (3.34)]):

$$\langle\mathbf{curl}(\boldsymbol{\chi}-\mathbf{I}_h(\boldsymbol{\chi}))\,\mathbf{n},\mathbf{u}_{\mathrm{D}}\rangle_\Gamma \,=\, -\,\langle\nabla\mathbf{u}_{\mathrm{D}}\,\mathbf{s},\boldsymbol{\chi}-\mathbf{I}_h(\boldsymbol{\chi})\rangle_\Gamma \,=\, -\left\langle\underline{\gamma}_*(\nabla\mathbf{u}_{\mathrm{D}}),\boldsymbol{\chi}-\mathbf{I}_h(\boldsymbol{\chi})\right\rangle_\Gamma\,, \tag{4.24}$$

so that applying local integration by parts, the Cauchy–Schwarz inequality, and the approximation properties of $\mathbf{I}_h$ (cf. Lemma 3.2), we obtain

$$\begin{aligned}\left|\mathcal{R}_1^{\mathtt{BF}}(\mathbf{curl}(\boldsymbol{\chi}-\mathbf{I}_h(\boldsymbol{\chi})))\right| \,\leq\, C_2\,\Bigg\{ & \sum_{T\in\mathcal{T}_h} h_T^2\left\|\underline{\mathbf{curl}}\left(\frac{1}{\nu}\,\boldsymbol{\sigma}_h^{\mathrm{d}}\right)\right\|_{0,T}^2 \\ & +\sum_{e\in\mathcal{E}_h(\Omega)} h_e\left\|\left[\left[\underline{\gamma}_*\left(\frac{1}{\nu}\,\boldsymbol{\sigma}_h^{\mathrm{d}}\right)\right]\right]\right\|_{0,e}^2+\sum_{e\in\mathcal{E}_h(\Gamma)} h_e\left\|\underline{\gamma}_*\left(\frac{1}{\nu}\,\boldsymbol{\sigma}_h^{\mathrm{d}}-\nabla\mathbf{u}_{\mathrm{D}}\right)\right\|_{0,e}^2\Bigg\}^{1/2}\|\boldsymbol{\chi}\|_{1,\Omega}\,,\end{aligned} \tag{4.25}$$

where the terms involving the set $\mathcal{E}_h(\Gamma)$ remain valid if $\mathbf{u}_{\mathrm{D}}\in\mathbf{H}^1(\Gamma)$. The conclusion follows directly from (4.21), (4.23), (4.25), and the stability of the Helmholtz decomposition (cf. (4.20)). □

Finally, we bound the residual term $\|\mathcal{R}_{j,1}^{\mathtt{D}}\|_{\mathbf{H}(\mathrm{div}_{4/3};\Omega)'}$ by following similar steps to those in [4, Lemma 5.6]. For the sake of simplicity, and similarly to Lemma 4.4, we focus on $d=2$. The three dimensional case proceeds analogously. Indeed, given $\boldsymbol{\eta}_j\in\mathbf{H}(\mathrm{div}_{4/3};\Omega)$, with $j\in\{1,2\}$, we know from Lemma 3.4 that there exist $\boldsymbol{\xi}_j\in\mathbf{W}^{1,4/3}(\Omega)$ and $w_j\in\mathrm{H}^1(\Omega)$, such that $\boldsymbol{\eta}_j=\boldsymbol{\xi}_j+\mathrm{curl}(w_j)$ in Ω, and

$$\|\boldsymbol{\xi}_j\|_{1,4/3;\Omega}+\|w_j\|_{1,\Omega}\,\leq\,C_{Hel}\,\|\boldsymbol{\eta}_j\|_{\mathrm{div}_{4/3};\Omega}\,. \tag{4.26}$$

Next, by virtue of the second equation of the Galerkin scheme (2.21) and the definition of $\mathcal{R}_{j,1}^{\mathtt{D}}$ (cf. (4.16)), we deduce that $\mathcal{R}_{j,1}^{\mathtt{D}}(\boldsymbol{\eta}_{j,h})=0$ for all $\boldsymbol{\eta}_{j,h}\in\mathbf{H}_h^{\boldsymbol{\rho}}$. Then, we set $\boldsymbol{\eta}_{j,h}:=\Pi_h^k(\boldsymbol{\xi}_j)+\mathrm{curl}(I_h(w_j))$, and deduce that

$$\mathcal{R}_{j,1}^{\mathtt{D}}(\boldsymbol{\eta}_j)=\mathcal{R}_{j,1}^{\mathtt{D}}(\boldsymbol{\eta}_j-\boldsymbol{\eta}_{j,h})\,=\,\mathcal{R}_{j,1}^{\mathtt{D}}\left(\boldsymbol{\xi}_j-\Pi_h^k(\boldsymbol{\xi}_j)\right)+\mathcal{R}_{j,1}^{\mathtt{D}}\left(\mathrm{curl}\left(w_j-I_h(w_j)\right)\right)\,. \tag{4.27}$$

The terms on the right-hand side of (4.27) are bounded as follows.

Lemma 4.5 *Assume that $\phi_{j,\mathrm{D}}\in\mathrm{H}^1(\Gamma)\cap\mathrm{L}^4(\Gamma)$ for each $j\in\{1,2\}$. Then, there exists a positive constant C, independent of h, such that for each $j\in\{1,2\}$ there holds*

$$\|\mathcal{R}_{j,1}^{\mathtt{D}}\|_{\mathbf{H}(\mathrm{div}_{4/3};\Omega)'}\,\leq\,C\left\{\sum_{T\in\mathcal{T}_h}\Theta_{\mathtt{D},j,T}^2\right\}^{1/2}\,, \tag{4.28}$$

where $\Theta_{\mathtt{D},j,T}$ is defined in (4.3).

Proof. First, employing similar arguments to the ones used in the proof of [4, Lemma 5.4], that is, local integration by parts, Hölder and Cauchy–Schwarz inequalities, Lemma 3.1 with $p = 4/3$, and the subadditivity inequality, we deduce that

$$\begin{aligned}\left|\mathcal{R}^{\mathtt{D}}_{j,1}(\boldsymbol{\xi}_j - \Pi^k_h(\boldsymbol{\xi}_j))\right| \,\leq\, \widehat{C}_1 \Bigg\{ & \sum_{e\in\mathcal{E}_h(\Gamma)} h_e^{1/2} \left\|\phi_{j,\mathrm{D}} - \phi_{j,h}\right\|^2_{0,4;e} \\ & + \sum_{T\in\mathcal{T}_h} h_T^{2-d/2} \left\|\nabla\phi_{j,h} - \mathbf{Q}_j^{-1}\left\{\boldsymbol{\rho}_{j,h} + \mathtt{R}_j\phi_{j,h}\mathbf{u}_h\right\}\right\|^2_{0,T} \Bigg\}^{1/2} \|\boldsymbol{\xi}_j\|_{1,4/3;\Omega}\,,\end{aligned} \tag{4.29}$$

with $\widehat{C}_1 > 0$ independent of h. On the other hand, proceeding as in [4, Lemma 5.5], i.e., recalling that $\phi_{j,\mathrm{D}} \in \mathrm{H}^1(\Gamma)\cap\mathrm{L}^4(\Gamma)$, using an integration by parts formula on the boundary Γ as in (4.24), applying local integration by parts, the Cauchy–Schwarz inequality, and the approximation properties of the Clément interpolant I_h (cf. Lemma 3.2), we arrive at

$$\begin{aligned}\left|\mathcal{R}^{\mathtt{D}}_{j,1}(\mathrm{curl}(w_j - I_h(w_j)))\right| \,\leq\, \widehat{C}_2 \Bigg\{ & \sum_{T\in\mathcal{T}_h} h_T^2 \left\|\underline{\mathrm{curl}}\left(\mathbf{Q}_j^{-1}\left(\boldsymbol{\rho}_{j,h} + \mathtt{R}_j\phi_{j,h}\mathbf{u}_h\right)\right)\right\|^2_{0,T} \\ & + \sum_{e\in\mathcal{E}_h(\Omega)} h_e \left\|\left[\!\left[\boldsymbol{\gamma}_*\left(\mathbf{Q}_j^{-1}\left(\boldsymbol{\rho}_{j,h} + \mathtt{R}_j\phi_{j,h}\mathbf{u}_h\right)\right)\right]\!\right]\right\|^2_{0,e} \\ & + \sum_{e\in\mathcal{E}_h(\Gamma)} h_e \left\|\boldsymbol{\gamma}_*\left(\mathbf{Q}_j^{-1}\left(\boldsymbol{\rho}_{j,h} + \mathtt{R}_j\phi_{j,h}\mathbf{u}_h\right) - \nabla\phi_{j,\mathrm{D}}\right)\right\|^2_{0,e} \Bigg\}^{1/2} \|w_j\|_{1,\Omega}\,,\end{aligned} \tag{4.30}$$

with $\widehat{C}_2 > 0$ independent of h. Finally, combining (4.29) and (4.30), and using the stability of the Helmholtz decomposition (cf. (4.26)), we get (4.28) and conclude the proof. □

We end this section by stressing that the estimate (4.6) is a straightforward consequence of Lemmas 4.2 and 4.3–4.5, the definition of the global estimator Θ_1 (cf. (4.1)), and the fact that the terms $h_T^2\left\|\nabla\mathbf{u}_h - \frac{1}{\nu}\boldsymbol{\sigma}_h^{\mathrm{d}}\right\|^2_{0,T}$ and $h_e\left\|\mathbf{u}_{\mathrm{D}} - \mathbf{u}_h\right\|^2_{0,e}$, which form part of $\overline{\Theta}_{\mathtt{BF},T}$ (cf. (4.22)), are dominated by $\left\|\nabla\mathbf{u}_h - \frac{1}{\nu}\boldsymbol{\sigma}_h^{\mathrm{d}}\right\|^2_{0,T}$ and $\left\|\mathbf{u}_{\mathrm{D}} - \mathbf{u}_h\right\|^2_{0,e}$, respectively.

4.2 Efficiency of the a posteriori error estimator

We now aim to establish the lower bound in (4.4). For this purpose, we will make extensive use of the original system of equations given by (2.6), which is recovered from the augmented-mixed continuous formulation (2.7) by choosing suitable test functions and integrating by parts backwardly the corresponding equations.

The following theorem is the main result of this section

Theorem 4.6 *Suppose that the data $\mathbf{u}_{\mathrm{D}}$, $\boldsymbol{\phi}_{\mathrm{D}}$ and $\boldsymbol{\phi}_{\mathtt{r}}$ satisfy* (4.5)*. Then, there exist a positive constant C_{eff}, independent of h, such that*

$$C_{\mathrm{eff}}\,\Theta_1 \,\leq\, \|(\boldsymbol{\sigma},\mathbf{u}) - (\boldsymbol{\sigma}_h,\mathbf{u}_h)\| + \sum_{j=1}^{2}\|(\boldsymbol{\rho}_j,\phi_j) - (\boldsymbol{\rho}_{j,h},\phi_{j,h})\| + \text{h.o.t.}\,, \tag{4.31}$$

where h.o.t. *stands for one or several terms of higher order.*

Throughout this section we assume, without loss of generality, that $\mathbf{u}_{\mathrm{D}}, \boldsymbol{\phi}_{\mathtt{r}}, \boldsymbol{\phi}_{\mathrm{D}}, \mathbf{K}^{-1}\mathbf{u}_h$, and $\mathbf{Q}_j^{-1}\boldsymbol{\rho}_{j,h}$, $j \in 1,2$, are all piecewise polynomials. Otherwise, if $\mathbf{u}_{\mathrm{D}}, \boldsymbol{\phi}_{\mathtt{r}}, \boldsymbol{\phi}_{\mathrm{D}}, \mathbf{K}$, and $\mathbf{Q}_j$ are sufficiently smooth, one proceeds similarly to [10, Section 6.2], so that higher order terms given by the errors arising from suitable polynomial approximation of these functions appear in (4.31), which explains the eventual h.o.t. in this inequality.

We begin the derivation of the efficiency estimates with the following result.

Lemma 4.7 *There exist positive constants C_1, C_2, C_3, independent of h, such that for each $T \in \mathcal{T}_h$ there hold*

$$\begin{aligned}
&\left\|\mathbf{f}(\boldsymbol{\phi}_h) + \mathbf{div}(\boldsymbol{\sigma}_h) - \mathbf{K}^{-1}\mathbf{u}_h - \mathtt{F}\,|\mathbf{u}_h|\mathbf{u}_h\right\|_{0,T} \\
&\quad \leq C_1 \left\{ \|\boldsymbol{\sigma} - \boldsymbol{\sigma}_h\|_{\mathbf{div},T} + \|\mathbf{u} - \mathbf{u}_h\|_{0,T} + \||\mathbf{u}|\mathbf{u} - |\mathbf{u}_h|\mathbf{u}_h\|_{0,T} + \|\boldsymbol{\phi} - \boldsymbol{\phi}_h\|_{0,4;T} \right\}, \\
&\left\| \nabla \mathbf{u}_h - \frac{1}{\nu}\,\boldsymbol{\sigma}_h^{\mathrm{d}} \right\|_{0,T} \leq C_2 \left\{ \|\mathbf{u} - \mathbf{u}_h\|_{1,T} + \|\boldsymbol{\sigma} - \boldsymbol{\sigma}_h\|_{0,T} \right\},
\end{aligned}$$

and

$$\|\mathrm{div}(\boldsymbol{\rho}_{j,h})\|_{0,4/3;T} \leq C_3 \, \|\boldsymbol{\rho}_j - \boldsymbol{\rho}_{j,h}\|_{\mathrm{div}_{4/3};T} \quad j \in \{1,2\}\,.$$

Proof. It suffices to recall that $\mathbf{f}(\boldsymbol{\phi}) = -\mathbf{div}(\boldsymbol{\sigma}) + \mathbf{K}^{-1}\mathbf{u} + \mathtt{F}\,|\mathbf{u}|\mathbf{u}$ in Ω, $\nabla \mathbf{u} = \frac{1}{\nu}\,\boldsymbol{\sigma}^{\mathrm{d}}$ in Ω, and $\mathrm{div}(\boldsymbol{\rho}_j) = 0$ in Ω (cf. (2.6)). Further details are omitted. □

Next, we provide the upper bound for the residual terms involving the Dirichlet datum $\mathbf{u}_{\mathrm{D}}$.

Lemma 4.8 *There exists a positive constant C_3, independent of h, such that*

$$\sum_{e \in \mathcal{E}_h(\Gamma)} \|\mathbf{u}_{\mathrm{D}} - \mathbf{u}_h\|_{0,e}^2 \leq C_3 \, \|\mathbf{u} - \mathbf{u}_h\|_{1,\Omega}^2\,.$$

Proof. It suffices to observe that

$$\sum_{e \in \mathcal{E}_h(\Gamma)} \|\mathbf{u}_{\mathrm{D}} - \mathbf{u}_h\|_{0,e}^2 = \sum_{e \in \mathcal{E}_h(\Gamma)} \|\mathbf{u} - \mathbf{u}_h\|_{0,e}^2 = \|\mathbf{u} - \mathbf{u}_h\|_{0,\Gamma}^2\,,$$

and then apply the trace inequality. □

In order to derive the upper bounds for the remaining terms defining the global *a posteriori* error estimator Θ_1 (cf. (4.1)), we use results from [5], inverse inequalities, and the localization technique based on element-bubble and edge-bubble functions. To this end, we now introduce further notations and preliminary results. Given $T \in \mathcal{T}_h$ and $e \in \mathcal{E}_{h,T}$, we let ψ_T and ψ_e be the usual element-bubble and edge-bubble functions, respectively (see [33] for details). In particular, $\psi_T \in \mathrm{P}_3(T)$, $\mathrm{supp}\,\psi_T \subseteq T$, $\psi_T = 0$ on ∂T, and $0 \leq \psi_T \leq 1$ in T. Similarly, $\psi_e|_T \in \mathrm{P}_2(T)$, $\mathrm{supp}\,\psi_e \subseteq \omega_e := \cup\{T' \in \mathcal{T}_h : e \in \mathcal{E}_{h,T'}\}$, $\psi_e = 0$ on $\partial T \setminus e$ and $0 \leq \psi_T \leq 1$ in ω_e. We also recall from [32] that, given $k \in \mathbb{N} \cup \{0\}$, there exists an extension operator $L : C(e) \to C(\omega_e)$ that satisfies $L(p) \in \mathrm{P}_k(T)$ and $L(p)|_e = p \;\forall\, p \in \mathrm{P}_k(e)$. Additional properties of ψ_T, ψ_e, and L are collected in the following lemma (though not all them will be employed in the rest of the paper).

Lemma 4.9 *Given $k \in \mathbb{N} \cup \{0\}$, there exist positive constants c_1, c_2, c_3 and c_4, depending only on k and the shape regularity of the triangulations (minimum angle condition), such that*

$$\|\psi_T q\|_{0,T}^2 \leq \|q\|_{0,T}^2 \leq c_1 \, \|\psi_T^{1/2} q\|_{0,T}^2 \quad \forall\, q \in \mathrm{P}_k(T) \qquad \forall\, T \in \mathcal{T}_h\,, \tag{4.32}$$

$$\|\psi_e L(p)\|_{0,e}^2 \,\leq\, \|p\|_{0,e}^2 \,\leq\, c_2\,\|\psi_e^{1/2} p\|_{0,e}^2 \quad \forall\, p \in \mathrm{P}_k(e) \qquad \forall\, e \in \mathcal{E}_h\,,$$

and

$$c_3\, h_e^{1/2} \|p\|_{0,e} \,\leq\, \|\psi_e^{1/2} L(p)\|_{0,T} \,\leq\, c_4\, h_e^{1/2} \|p\|_{0,e} \quad \forall\, p \in \mathrm{P}_k(e) \qquad \forall\, e \in \mathcal{E}_h\,.$$

Proof. See [32, Lemma 4.1] (see also [33, Lemma 3.3]). □

In addition, in what follows we will make use of suitable inverse inequalities. In fact, given $k \in \mathbb{N} \cup \{0\}$, there exist positive constants c_1, c_2, independent of h, such that (cf. [18, Lemma 1.138]):

$$\|v\|_{1,4/3;T} \,\leq\, c_1\, h_T^{-1+d/4}\, \|v\|_{0;T} \quad \forall\, v \in \mathrm{P}_k(T) \qquad \forall\, T \in \mathcal{T}_h\,, \tag{4.33}$$

and

$$\|v\|_{0,4;e} \,\leq\, c_2\, h_e^{(1-d)/4}\, \|v\|_{0;e} \quad \forall\, v \in \mathrm{P}_k(e) \qquad \forall\, e \in \mathcal{E}_h\,. \tag{4.34}$$

Finally, we recall a discrete trace inequality, which establishes the existence of a positive constant C, depending only on the shape regularity of the triangulations, such that for each $T \in \mathcal{T}_h$ and $e \in \mathcal{E}_{h,T}$, there holds

$$\|v\|_{0,e} \,\leq\, C \left\{ h_e^{-1/2}\, \|v\|_{0,T_e} + h_e^{1/2}\, |v|_{1,T_e} \right\} \quad \forall\, v \in \mathrm{H}^1(T_e)\,. \tag{4.35}$$

For the proof of inequality (4.35) we refer to [1, Theorem 3.10].

The corresponding bounds for the remaining terms defining $\Theta_{\mathtt{BF},T}$ (cf. (4.2)) are stated in the following lemma.

Lemma 4.10 *There exist positive constants C_4, C_5, independent of h, such that*

$$h_T \left\| \underline{\mathbf{curl}} \left(\frac{1}{\nu}\, \boldsymbol{\sigma}_h^{\mathrm{d}} \right) \right\|_{0,T} \,\leq\, C_4\, \|\boldsymbol{\sigma} - \boldsymbol{\sigma}_h\|_{0,T} \quad \forall\, T \in \mathcal{T}_h\,, \tag{4.36}$$

and

$$h_e^{1/2} \left\| \left[\!\!\left[\underline{\boldsymbol{\gamma}}_* \left(\frac{1}{\nu}\, \boldsymbol{\sigma}_h^{\mathrm{d}} \right) \right]\!\!\right] \right\|_{0,e} \,\leq\, C_5\, \|\boldsymbol{\sigma} - \boldsymbol{\sigma}_h\|_{0,\omega_e} \quad \forall\, e \in \mathcal{E}_h(\Omega)\,. \tag{4.37}$$

Furthermore, assuming $\mathbf{u}_{\mathrm{D}} \in \mathbf{H}^1(\Gamma)$, there exists a positive constant C_6, independent of h, such that

$$h_e^{1/2} \left\| \underline{\boldsymbol{\gamma}}_* \left(\frac{1}{\nu}\, \boldsymbol{\sigma}_h^{\mathrm{d}} - \nabla \mathbf{u}_{\mathrm{D}} \right) \right\|_{0,e} \,\leq\, C_6\, \|\boldsymbol{\sigma} - \boldsymbol{\sigma}_h\|_{0,\omega_e} \quad \forall\, e \in \mathcal{E}_h(\Gamma)\,. \tag{4.38}$$

Proof. First, noting that $\mathbf{curl}\left(\frac{1}{\nu}\boldsymbol{\sigma}^{\mathrm{d}}\right) = \mathbf{curl}(\nabla \mathbf{u}) = \mathbf{0}$, we find that (4.36)–(4.37) follows from a slight adaptation of [26, Lemma 4.11], whereas for the proof of (4.38) we refer the reader to [26, Lemma 4.15]. □

We now provide the upper bounds for the terms defining $\Theta_{\mathtt{D},j,T}$ (cf. (4.3)). Indeed, under the assumption that $\mathbf{Q}_1$ and $\mathbf{Q}_2$ are piecewise polynomial tensors, our strategy consists of mimicking the proofs of Lemmas 5.10, 5.11 and 5.12 in [4], which are not applicable as such here, but need to be modified as detailed in the proofs of the following three lemmas.

Lemma 4.11 *There exists a positive constant C_7, independent of h, such that for each $T \in \mathcal{T}_h$ and each $j \in \{1, 2\}$, there holds*

$$\begin{aligned} & h_T^{1-d/4} \left\| \nabla \phi_{j,h} - \mathbf{Q}_j^{-1} \left(\boldsymbol{\rho}_{j,h} + \mathtt{R}_j \phi_{j,h}\, \mathbf{u}_h \right) \right\|_{0,T} \\ & \quad \leq\, C_7 \left\{ h_T^{1-d/4} \left(\|\boldsymbol{\rho}_j - \boldsymbol{\rho}_{j,h}\|_{0,T} + \|\phi_j\, \mathbf{u} - \phi_{j,h}\, \mathbf{u}_h\|_{0,T} \right) + \|\phi_j - \phi_{j,h}\|_{0,4;T} \right\}\,. \end{aligned} \tag{4.39}$$

Proof. Given $T \in \mathcal{T}_h$ and $j \in \{1,2\}$, we define $\boldsymbol{\xi}_{j,T} := \nabla\phi_{j,h} - \mathbf{Q}_j^{-1}\left(\boldsymbol{\rho}_{j,h} + \mathtt{R}_j\phi_{j,h}\mathbf{u}_h\right)$ in T. Then, applying (4.32) to $\|\boldsymbol{\xi}_{j,T}\|_{0,T}$, using the identity $\nabla\phi_j = \mathbf{Q}_j^{-1}\left(\boldsymbol{\rho}_j + \mathtt{R}_j\phi_j\mathbf{u}\right)$ in Ω (cf. (2.6)), and integrating by parts, we find that

$$\begin{aligned}\|\boldsymbol{\xi}_{j,T}\|_{0,T}^2 &\leq c_1\|\psi_T^{1/2}\boldsymbol{\xi}_{j,T}\|_{0,T}^2 \\ &= c_1\int_T \psi_T\boldsymbol{\xi}_{j,T}\cdot\mathbf{Q}_j^{-1}\Big((\boldsymbol{\rho}_{j,h}-\boldsymbol{\rho}_j) + \mathtt{R}_j\left(\phi_{j,h}\,\mathbf{u}_h - \phi_j\,\mathbf{u}\right)\Big) + c_1\int_T(\phi_{j,h}-\phi_j)\,\mathrm{div}\left(\psi_T\boldsymbol{\xi}_{j,T}\right).\end{aligned}$$

In this way, applying Cauchy–Schwarz and Hölder's inequalities, we obtain

$$\begin{aligned}\|\boldsymbol{\xi}_{j,T}\|_{0,T}^2 \leq C\Big\{&\|\psi_T\boldsymbol{\xi}_{j,T}\|_{0,T}\left(\|\boldsymbol{\rho}_j-\boldsymbol{\rho}_{j,h}\|_{0,T} + \|\phi_j\,\mathbf{u}-\phi_{j,h}\,\mathbf{u}_h\|_{0,T}\right)\\ &+ \|\psi_T\boldsymbol{\xi}_{j,T}\|_{1,4/3;T}\,\|\phi_j-\phi_{j,h}\|_{0,4;T}\Big\},\end{aligned}$$

and combining (4.33) with (4.32) to bound $\|\psi_T\boldsymbol{\xi}_{j,T}\|_{1,4/3;T}$ by $h_T^{-1+d/4}\,\|\boldsymbol{\xi}_{j,T}\|_{0,T}$, we deduce

$$\|\boldsymbol{\xi}_{j,T}\|_{0,T} \leq C\left\{\|\boldsymbol{\rho}_j-\boldsymbol{\rho}_{j,h}\|_{0,T} + \|\phi_j\,\mathbf{u}-\phi_{j,h}\,\mathbf{u}_h\|_{0,T} + h_T^{-1+d/4}\,\|\phi_j-\phi_{j,h}\|_{0,4;T}\right\}, \tag{4.40}$$

which yields (4.39) with a positive constant C independent of h. □

Lemma 4.12 *Suppose that $\phi_{j,\mathrm{D}}$, $j \in \{1,2\}$, are piecewise polynomial functions. Then, there exists a positive constant C_8, independent of h, such that*

$$\begin{aligned}&h_e^{1/4}\|\phi_{j,\mathrm{D}}-\phi_{j,h}\|_{0,4;e}\\ &\quad\leq C_8\left\{h_T^{1-d/4}\Big(\|\boldsymbol{\rho}_j-\boldsymbol{\rho}_{j,h}\|_{0,T} + \|\phi_j\mathbf{u}-\phi_{j,h}\mathbf{u}_h\|_{0,T}\Big) + \|\phi_j-\phi_{j,h}\|_{0,4;T}\right\}\end{aligned} \tag{4.41}$$

for all $e \in \mathcal{E}_{h,T}(\Gamma)$.

Proof. We proceed as in [4, Lemma 5.11]. In fact, given $e \in \mathcal{E}_h(\Gamma)$ an edge or face of an element, depending on whether $d=2$ or $d=3$, respectively, it follows from (4.34) that

$$\|\phi_{j,\mathrm{D}}-\phi_{j,h}\|_{0,4;e} \leq C\,h_e^{(1-d)/4}\,\|\phi_{j,\mathrm{D}}-\phi_{j,h}\|_{0,e}\,, \tag{4.42}$$

which, along with (4.35), yields

$$\|\phi_{j,\mathrm{D}}-\phi_{j,h}\|_{0,4;e} \leq C\left\{h_e^{(-1-d)/4}\,\|\phi_j-\phi_{j,h}\|_{0,T} + h_e^{(3-d)/4}\,|\phi_j-\phi_{j,h}|_{1,T}\right\}. \tag{4.43}$$

Next, in order to estimate the right-hand side of (4.43), we use first the Cauchy-Schwarz inequality and the fact that $|T| \cong h_T^d$, to deduce that there exists a positive constant $c>0$, independent of h, such that

$$\|\phi_j-\phi_{j,h}\|_{0,T} \leq c\,h_T^{d/4}\,\|\phi_j-\phi_{j,h}\|_{0,4;T}\,. \tag{4.44}$$

In turn, using the identity $\nabla\phi_j = \mathbf{Q}^{-1}(\boldsymbol{\rho}_j + \mathtt{R}_j\phi_j\,\mathbf{u})$ in Ω (cf. (2.6)) and the boundedness of $\mathbf{Q}^{-1}$, which follows from (2.3), and performing some algebraic manipulations, we obtain

$$\begin{aligned}|\phi_j-\phi_{j,h}|_{1,T} &= \left\|\mathbf{Q}^{-1}(\boldsymbol{\rho}_j-\boldsymbol{\rho}_{j,h}) + \mathtt{R}_j\mathbf{Q}^{-1}(\phi_j\,\mathbf{u}-\phi_{j,h}\,\mathbf{u}_h) + \mathbf{Q}^{-1}(\boldsymbol{\rho}_{j,h}+\mathtt{R}_j\phi_{j,h}\,\mathbf{u}_h) - \nabla\phi_{j,h}\right\|_{0,T}\\ &\leq C\left(\|\boldsymbol{\rho}_j-\boldsymbol{\rho}_{j,h}\|_{0,T} + \left\|\phi_j\,\mathbf{u}-\phi_{j,h}\,\mathbf{u}_h\right\|_{0,T}\right) + \left\|\nabla\phi_{j,h} - \mathbf{Q}^{-1}\left(\boldsymbol{\rho}_{j,h}+\mathtt{R}_j\phi_{j,h}\,\mathbf{u}_h\right)\right\|_{0,T},\end{aligned}$$

which, together with (4.40), implies

$$|\phi_j - \phi_{j,h}|_{1,T} \leq C \left\{ \|\boldsymbol{\rho}_j - \boldsymbol{\rho}_{j,h}\|_{0,T} + \|\phi_j \, \mathbf{u} - \phi_{j,h} \, \mathbf{u}_h\|_{0,T} + h_T^{-1+d/4} \, \|\phi_j - \phi_{j,h}\|_{0,4;T} \right\}. \tag{4.45}$$

Finally, it is easy to see that (4.41) follows from estimates (4.43), (4.44), and (4.45), and the fact that $h_e \cong h_T$. □

Lemma 4.13 *There exist positive constant C_9, C_{10}, independent of h, such that*

$$h_T \left\| \underline{\mathrm{curl}} \left(\mathbf{Q}_j^{-1} \left(\boldsymbol{\rho}_{j,h} + \mathtt{R}_j \phi_{j,h} \, \mathbf{u}_h \right) \right) \right\|_{0,T} \leq C_9 \left\{ \|\boldsymbol{\rho}_j - \boldsymbol{\rho}_{j,h}\|_{0,T} + \|\phi_j \, \mathbf{u} - \phi_{j,h} \, \mathbf{u}_h\|_{0,T} \right\} \tag{4.46}$$

for all $T \in \mathcal{T}_h$, and

$$h_e^{1/2} \left\| \left[\left[\boldsymbol{\gamma}_* \left(\mathbf{Q}_j^{-1} \left(\boldsymbol{\rho}_{j,h} + \mathtt{R}_j \phi_{j,h} \, \mathbf{u}_h \right) \right) \right] \right] \right\|_{0,e} \leq C_{10} \left\{ \|\boldsymbol{\rho}_j - \boldsymbol{\rho}_{j,h}\|_{0,\omega_e} + \|\phi_j \, \mathbf{u} - \phi_{j,h} \, \mathbf{u}_h\|_{0,\omega_e} \right\} \tag{4.47}$$

for all $e \in \mathcal{E}_h(\Omega)$. Additionally, if $\phi_{j,\mathrm{D}}$, $j \in \{1,2\}$, is a piecewise polynomial function, there exists a positive constant C_{11}, independent of h, such that

$$h_e^{1/2} \left\| \boldsymbol{\gamma}_* \left(\mathbf{Q}_j^{-1} \left(\boldsymbol{\rho}_{j,h} + \mathtt{R}_j \phi_{j,h} \mathbf{u}_h \right) - \nabla \phi_{j,\mathrm{D}} \right) \right\|_{0,e} \leq C_{11} \left\{ \|\boldsymbol{\rho}_j - \boldsymbol{\rho}_{j,h}\|_{0,T_e} + \|\phi_j \mathbf{u} - \phi_{j,h} \mathbf{u}_h\|_{0,T_e} \right\} \tag{4.48}$$

for all $e \in \mathcal{E}_h(\Gamma)$, where T_e is the element to which e belongs.

Proof. For the two-dimensional case, the derivation of the first two inequalities proceeds as in [15, Lemma 3.11] by applying Lemmas 6.1 and 6.2 in [5]. Indeed, from these results we know that there exists a positive constant C, independent of h, such for each piecewise polynomial function $\boldsymbol{\eta}_h$ in $\mathcal{T}_h$, and for each $\boldsymbol{\eta} \in \mathbf{L}^2(\Omega)$ satisfying $\underline{\mathrm{curl}}(\boldsymbol{\eta}) = 0$ in Ω, there hold

$$h_T \, \|\underline{\mathrm{curl}}(\boldsymbol{\eta}_h)\|_{0,T} \leq C \, \|\boldsymbol{\eta} - \boldsymbol{\eta}_h\|_{0,T} \quad \text{and} \quad h_e^{1/2} \, \|[\![\boldsymbol{\gamma}_*(\boldsymbol{\eta}_h)]\!]\|_{0,e} \leq C \, \|\boldsymbol{\eta} - \boldsymbol{\eta}_h\|_{0,\omega_e} .$$

Thus, taking $\boldsymbol{\eta} := \mathbf{Q}_j^{-1} \left(\boldsymbol{\rho}_j + \mathtt{R}_j \phi_j \mathbf{u} \right) = \nabla \phi_j$ and $\boldsymbol{\eta}_h := \mathbf{Q}_j^{-1} \left(\boldsymbol{\rho}_{j,h} + \mathtt{R}_j \phi_{j,h} \mathbf{u}_h \right)$, we obtain (4.46) and (4.47). In turn, these same arguments combined with [23, Lemma 21] allow us to deduce the inequality (4.48). Further details are omitted. On the other hand, the proof for the three-dimensional case follows from a slight modification of those of Lemmas 4.9, 4.10, and 4.13 in [22]. □

In order to complete the global efficiency given by (4.31) (cf. Theorem 4.6), we now need to estimate the terms $\||\mathbf{u}|\mathbf{u} - |\mathbf{u}_h|\mathbf{u}_h\|_{0,T}^2$ and $\|\phi_j \mathbf{u} - \phi_{j,h} \mathbf{u}_h\|_{0,T}^2$ appearing in the upper bounds provided by Lemmas 4.7 and 4.11–4.13. To this end, we first make use of the Hölder inequality to obtain

$$\||\mathbf{u}|\mathbf{u} - |\mathbf{u}_h|\mathbf{u}_h\|_{0,T}^2 \leq 2 \left(\|\mathbf{u}\|_{0,4;T}^2 + \|\mathbf{u}_h\|_{0,4;T}^2 \right) \|\mathbf{u} - \mathbf{u}_h\|_{0,4;T}^2 ,$$

from which, applying Cauchy-Schwarz's inequality and simple algebraic estimates, we find that

$$\begin{aligned} \sum_{T \in \mathcal{T}_h} \||\mathbf{u}|\mathbf{u} - |\mathbf{u}_h|\mathbf{u}_h\|_{0,T}^2 &\leq 2 \left\{ \sum_{T \in \mathcal{T}_h} \left(\|\mathbf{u}\|_{0,4;T}^2 + \|\mathbf{u}_h\|_{0,4;T}^2 \right)^2 \right\}^{1/2} \left\{ \sum_{T \in \mathcal{T}_h} \|\mathbf{u} - \mathbf{u}_h\|_{0,4;T}^4 \right\}^{1/2} \\ &\leq 2\sqrt{2} \left(\|\mathbf{u}\|_{0,4;\Omega}^4 + \|\mathbf{u}_h\|_{0,4;\Omega}^4 \right)^{1/2} \|\mathbf{u} - \mathbf{u}_h\|_{0,4;\Omega}^2 \leq 2\sqrt{2} \left(\|\mathbf{u}\|_{0,4;\Omega}^2 + \|\mathbf{u}_h\|_{0,4;\Omega}^2 \right) \|\mathbf{u} - \mathbf{u}_h\|_{0,4;\Omega}^2 . \end{aligned}$$

In this way, employing the continuous injection $\mathbf{i}_4 : \mathbf{H}^1(\Omega) \to \mathbf{L}^4(\Omega)$, and the *a priori* bounds of $\|\mathbf{u}\|_{1,\Omega}$ and $\|\mathbf{u}_h\|_{1,\Omega}$ (cf. (2.18), (2.22)), we deduce from the foregoing inequality that there exists a positive constant C, depending only on data, and hence independent of h, such that

$$\sum_{T \in \mathcal{T}_h} \||\mathbf{u}|\mathbf{u} - |\mathbf{u}_h|\mathbf{u}_h\|_{0,T}^2 \leq C \, \|\mathbf{u} - \mathbf{u}_h\|_{1,\Omega}^2 . \tag{4.49}$$

Similarly, adding and subtracting $\phi_j\,\mathbf{u}_h$ (it also works with $\phi_{j,h}\,\mathbf{u}$), and applying Hölder's inequality, we deduce that

$$\|\phi_j\mathbf{u}-\phi_{j,h}\mathbf{u}_h\|^2_{0,T}\,\leq\,2\,\left(\|\phi_j\|^2_{0,4;T}+\|\mathbf{u}_h\|^2_{0,4,T}\right)\left(\|\mathbf{u}-\mathbf{u}_h\|^2_{0,4;T}+\|\phi_j-\phi_{j,h}\|^2_{0,4;T}\right)\,,$$

so that proceeding analogously to the first part of the derivation of (4.49), and then using the continuous injection $\mathbf{i}_4:\mathbf{H}^1(\Omega)\to\mathbf{L}^4(\Omega)$, and the a priori bounds of $\|\phi_j\|_{0,4;\Omega}$ and $\|\mathbf{u}_h\|_{1,\Omega}$ (cf. (2.19), (2.22)), we are able to show that there exists a positive constant $\widetilde{C}$, depending only on data, and hence independent of h, such that

$$\sum_{T\in\mathcal{T}_h}\|\phi_j\,\mathbf{u}-\phi_{j,h}\,\mathbf{u}_h\|^2_{0,T}\,\leq\,\widetilde{C}\left\{\|\mathbf{u}-\mathbf{u}_h\|^2_{1,\Omega}+\|\phi_j-\phi_{j,h}\|^2_{0,4;\Omega}\right\}.\tag{4.50}$$

Consequently, it is not difficult to see that (4.31) follows from the definition of Θ_1 (cf. (4.1)), Lemmas 4.7–4.13, and the estimates (4.49) and (4.50).

5 A second a posteriori error estimator

In this section we introduce and analyze another *a posteriori* error estimator for our augmented fully-mixed finite element scheme (2.21), which is not based on the Helmholtz decomposition for $\boldsymbol{\tau}\in\mathbb{H}(\mathbf{div};\Omega)$. More precisely, this second estimator arises simply from a different way of bounding $\|\mathcal{R}_1^{\mathtt{BF}}\|_{\mathbb{H}_0(\mathbf{div};\Omega)'}$ (cf. (4.14)) in the preliminary estimate for the total error given by (4.18). Then, with the same notations and discrete spaces from Sections 2.3 and 3, we now introduce for each $T\in\mathcal{T}_h$ the local error indicator

$$\begin{aligned}\widetilde{\Theta}^2_{\mathtt{BF},T}\,:=\,&\left\|\mathbf{f}(\boldsymbol{\phi}_h)+\mathbf{div}(\boldsymbol{\sigma}_h)-\mathbf{K}^{-1}\mathbf{u}_h-\mathtt{F}\,|\mathbf{u}_h|\mathbf{u}_h\right\|^2_{0,T}\\&+\left\|\nabla\mathbf{u}_h-\frac{1}{\nu}\,\boldsymbol{\sigma}_h\right\|^2_{0,T}+\sum_{e\in\mathcal{E}_{h,T}(\Gamma)}\|\mathbf{u}_{\mathrm{D}}-\mathbf{u}_h\|^2_{0,e}\,,\end{aligned}$$

and define the following global residual error estimator

$$\Theta_2\,:=\,\left\{\sum_{T\in\mathcal{T}_h}\left(\widetilde{\Theta}^2_{\mathtt{BF},T}+\sum_{j=1}^{2}\Theta^2_{\mathtt{D},j,T}\right)+\|\mathbf{u}_{\mathrm{D}}-\mathbf{u}_h\|^2_{1/2,\Gamma}\right\}^{1/2}\,+\,\left\{\sum_{T\in\mathcal{T}_h}\sum_{j=1}^{2}\|\mathrm{div}(\boldsymbol{\rho}_{j,h})\|^{4/3}_{0,4/3;T}\right\}^{3/4}\tag{5.1}$$

where $\Theta_{\mathtt{D},j,T}$ is defined in (4.3).

The reliability and efficiency of the *a posteriori* error estimator Θ_2 are stated next.

Theorem 5.1 *Assume that the data $\mathbf{u}_{\mathrm{D}}$, $\boldsymbol{\phi}_{\mathrm{D}}$ and $\boldsymbol{\phi}_{\mathtt{r}}$ satisfy* (4.5)*. Then, there exist positive constants $\widetilde{C}_{\mathrm{rel}}$, $\widetilde{C}_{\mathrm{eff}}$, independent of h, such that*

$$\widetilde{C}_{\mathrm{eff}}\,\Theta_2+\text{h.o.t.}\,\leq\,\|(\boldsymbol{\sigma},\mathbf{u})-(\boldsymbol{\sigma}_h,\mathbf{u}_h)\|+\sum_{j=1}^{2}\|(\boldsymbol{\rho}_j,\phi_j)-(\boldsymbol{\rho}_{j,h},\phi_{j,h})\|\,\leq\,\widetilde{C}_{\mathrm{rel}}\,\Theta_2\,.\tag{5.2}$$

Proof. As announced, the proof of reliability reduces basically to derive another upper bound for $\|\mathcal{R}_1^{\mathtt{BF}}\|_{\mathbb{H}_0(\mathbf{div};\Omega)'}$. Indeed, applying the Cauchy–Schwarz and trace inequalities in (4.19), we readily deduce that

$$\begin{aligned}\|\mathcal{R}_1^{\mathtt{BF}}\|_{\mathbb{H}_0(\mathbf{div};\Omega)'}\,\leq\,C\,\Big\{&\left\|\mathbf{f}(\boldsymbol{\phi}_h)+\mathbf{div}(\boldsymbol{\sigma}_h)-\mathbf{K}^{-1}\mathbf{u}_h-\mathtt{F}|\mathbf{u}_h|\mathbf{u}_h\right\|_{0,\Omega}\\&+\left\|\nabla\mathbf{u}_h-\frac{1}{\nu}\,\boldsymbol{\sigma}^{\mathrm{d}}_h\right\|_{0,\Omega}+\|\mathbf{u}_{\mathrm{D}}-\mathbf{u}_h\|_{1/2,\Gamma}\Big\}\,,\end{aligned}\tag{5.3}$$

where C is a positive constant independent of h. In this way, replacing (5.3) back into (4.18), we obtain the upper bound in (5.2) concluding the required estimate. On the other hand, for the efficiency estimate we simply observe, thanks to the trace theorem in $\mathbf{H}^1(\Omega)$, that there exists a positive constant c, depending on Γ and Ω, such that

$$\|\mathbf{u}_{\mathrm{D}} - \mathbf{u}_h\|^2_{1/2,\Gamma} \,\leq\, c\,\|\mathbf{u} - \mathbf{u}_h\|^2_{1,\Omega}\,.$$

The rest of the arguments are contained in the proof of Theorem 4.6, and hence we omit further details. □

At this point we remark that the eventual use of Θ_2 (cf. (5.1)) in an adaptive algorithm solving (2.21) would be discouraged by the non-local character of the expression $\|\mathbf{u}_{\mathrm{D}} - \mathbf{u}_h\|^2_{1/2,\Gamma}$. In order to circumvent this situation, we now replace this term by a suitable upper bound, which yields a reliable and fully local *a posteriori* error estimator.

Theorem 5.2 *Assume that the data* $\mathbf{u}_{\mathrm{D}}$, $\boldsymbol{\phi}_{\mathrm{D}}$ *and* $\boldsymbol{\phi}_{\mathtt{r}}$ *satisfy* (4.5), *and let*

$$\widehat{\Theta}_2 \,:=\, \left\{ \sum_{T\in\mathcal{T}_h} \left(\widehat{\Theta}^2_{\mathtt{BF},T} + \sum_{j=1}^{2} \Theta^2_{\mathtt{D},j,T} \right) \right\}^{1/2} + \sum_{j=1}^{2} \left\{ \sum_{T\in\mathcal{T}_h} \|\mathrm{div}(\boldsymbol{\rho}_{j,h})\|^{4/3}_{0,4/3;T} \right\}^{3/4}, \tag{5.4}$$

where

$$\begin{aligned} \widehat{\Theta}^2_{\mathtt{BF},T} \,:=\, & \left\| \mathbf{f}(\boldsymbol{\phi}_h) + \mathbf{div}(\boldsymbol{\sigma}_h) - \mathbf{K}^{-1}\mathbf{u}_h - \mathtt{F}\,|\mathbf{u}_h|\mathbf{u}_h \right\|^2_{0,T} \\ & + \left\| \nabla\mathbf{u}_h - \frac{1}{\nu}\,\boldsymbol{\sigma}_h \right\|^2_{0,T} + \sum_{e\in\mathcal{E}_{h,T}(\Gamma)} \|\mathbf{u}_{\mathrm{D}} - \mathbf{u}_h\|^2_{1,e}\,. \end{aligned} \tag{5.5}$$

Then, there exists a positive constant $\widehat{C}_{\mathrm{rel}}$, *independent of* h, *such that*

$$\|(\boldsymbol{\sigma},\mathbf{u}) - (\boldsymbol{\sigma}_h,\mathbf{u}_h)\| + \sum_{j=1}^{2} \|(\boldsymbol{\rho}_j,\phi_j) - (\boldsymbol{\rho}_{j,h},\phi_{j,h})\| \,\leq\, \widehat{C}_{\mathrm{rel}}\,\widehat{\Theta}_2\,. \tag{5.6}$$

Proof. It reduces to bound $\|\mathbf{u}_{\mathrm{D}} - \mathbf{u}_h\|_{1/2,\Gamma}$. In fact, since $\mathrm{H}^1(\Gamma)$ is continuously embedded in $\mathrm{H}^{1/2}(\Gamma)$, there exists a positive constant C, depending on Γ, such that

$$\|\mathbf{u}_{\mathrm{D}} - \mathbf{u}_h\|^2_{1/2,\Gamma} \,\leq\, C\,\|\mathbf{u}_{\mathrm{D}} - \mathbf{u}_h\|^2_{1,\Gamma} \,=\, C \sum_{e\in\mathcal{E}_h(\Gamma)} \|\mathbf{u}_{\mathrm{D}} - \mathbf{u}_h\|^2_{1,e}\,,$$

which, together with the upper bound of (5.2), implies (5.6) and finishes the proof. □

6 Numerical results

This section serves to illustrate the performance and accuracy of the proposed augmented fully-mixed finite element scheme (2.21) along with the reliability and efficiency properties of the *a posteriori* error estimators Θ_1 (cf. (4.1)) and $\widehat{\Theta}_2$ (cf. (5.4)), in 2D and 3D domains. Regarding $\widehat{\Theta}_2$, it was established in Section 5 that it is reliable, but efficient only up to all its terms, except the last one in (5.5), which is associated with the boundary Γ. Indeed, while the numerical results to be displayed below suggest that $\widehat{\Theta}_2$ could actually verify both properties, the eventual efficiency is just a conjecture by now. All simulations were implemented using the FEniCS library [2]. A Newton–Raphson method with a fixed

tolerance tol = 1E-06 was used for the resolution of the nonlinear problem (2.21). In what follows, we refer to the corresponding sets of finite element subspaces generated by $k = 0$ and $k = 1$, as simply $\mathbb{RT}_0 - \mathbf{P}_1 - \mathbf{RT}_0 - \mathrm{P}_0 - \mathbf{RT}_0 - \mathrm{P}_0$ and $\mathbb{RT}_1 - \mathbf{P}_2 - \mathbf{RT}_1 - \mathrm{P}_1 - \mathbf{RT}_1 - \mathrm{P}_1$, respectively.

Next, we denote by N the total number of degrees of freedom. The global error and the effectivity indexes associated to the global estimators Θ_1 and $\widehat{\Theta}_2$ are denoted, respectively, by

$$\mathrm{e}(\vec{\mathbf{t}}) := \mathrm{e}(\boldsymbol{\sigma}) + \mathrm{e}(\mathbf{u}) + \sum_{j=1}^{2} \big(\mathrm{e}(\boldsymbol{\rho}_j) + \mathrm{e}(\phi_j)\big), \quad \mathrm{eff}(\Theta_1) := \frac{\mathrm{e}(\vec{\mathbf{t}})}{\Theta_1}, \quad \text{and} \quad \mathrm{eff}(\widehat{\Theta}_2) := \frac{\mathrm{e}(\vec{\mathbf{t}})}{\widehat{\Theta}_2},$$

where

$$\mathrm{e}(\boldsymbol{\sigma}) := \|\boldsymbol{\sigma} - \boldsymbol{\sigma}_h\|_{\mathbf{div};\Omega}, \quad \mathrm{e}(\mathbf{u}) := \|\mathbf{u} - \mathbf{u}_h\|_{1,\Omega},$$

$$\mathrm{e}(\boldsymbol{\rho}_j) := \|\boldsymbol{\rho}_j - \boldsymbol{\rho}_{j,h}\|_{\mathrm{div}_{4/3};\Omega}, \quad \mathrm{e}(\phi_j) := \|\phi_j - \phi_{j,h}\|_{0,4;\Omega}, \quad j \in \{1,2\}.$$

We emphasize that other variables of physical interest such as the velocity gradient and heat vector can be computed using the postproccessing formulae detailed in [8, Section 5]. However, for sake of simplicity, we only present results for the error of the pressure (cf. (2.5)), namely

$$\mathrm{e}(p) := \|p - p_h\|_{0,\Omega}, \quad \text{with } p_h := -\frac{1}{d}\mathrm{tr}(\boldsymbol{\sigma}_h)\,.$$

Moreover, using the fact that $N^{-1/d} \cong h$, the respective experimental rates of convergence are computed as

$$r(\diamond) := -\,d\,\frac{\log\left(\mathrm{e}(\diamond)/\mathrm{e}'(\diamond)\right)}{\log\left(N/N'\right)} \quad \text{for each } \diamond \in \Big\{\boldsymbol{\sigma}, \mathbf{u}, p, \boldsymbol{\rho}_1, \boldsymbol{\rho}_2, \phi_1, \phi_2, \vec{\mathbf{t}}\Big\},$$

where N and N' denote the total degrees of freedom associated to two consecutive triangulations with errors $\mathrm{e}(\diamond)$ and $\mathrm{e}'(\diamond)$, respectively.

The examples to be considered in this section are described next. In all of them, for sake of simplicity, we take $\nu = 1$, $\varrho = 1$, $\mathtt{R}_1 = 1$, $\mathtt{R}_2 = 1$, $\underline{\boldsymbol{\phi}}_{\mathtt{r}} = \mathbf{0}$, $\mathbf{g} = (0,-1)^{\mathrm{t}}$ when $d = 2$ and $\mathbf{g} = (0,0,-1)^{\mathrm{t}}$ when $d = 3$, and similarly to [8, Section 6], we choose the parameters κ_1, κ_2 as in (2.14), that is, $\kappa_1 = \nu$ and $\kappa_2 = \nu/2$. In turn, in the first three examples we consider $\mathtt{F} = 10$ and the tensors $\mathbf{K}$, $\mathbf{Q}_1$, and $\mathbf{Q}_2$ are taken as the identity matrix $\mathbb{I}$, which satisfy (2.3).

Example 1 is used to show the accuracy of the method and the behaviour of the effectivity indexes of the *a posteriori* error estimators Θ_1 and $\widehat{\Theta}_2$, whereas Examples 2–3 and 4–5 are utilized to illustrate the associated adaptive algorithms, with and without manufactured solution, respectively, in both 2D and 3D domains. The corresponding adaptivity procedure, taken from [33], is described as follows:

(1) Start with a coarse mesh $\mathcal{T}_h$ of $\overline{\Omega}$.

(2) Solve the Newton iterative method associated with (2.21) on the current mesh.

(3) Compute the local indicator $\Theta_{1,T}$ (respectively $\widehat{\Theta}_{2,T}$) for each $T \in \mathcal{T}_h$, where

$$\Theta_{1,T} := \left\{\Theta^2_{\mathtt{BF},T} + \sum_{j=1}^{2} \Theta^2_{\mathrm{D},j,T}\right\}^{1/2} + \sum_{j=1}^{2} \|\mathrm{div}(\boldsymbol{\rho}_{j,h})\|_{0,4/3;T}\,, \qquad \text{(cf. (4.2), (4.3))}$$

$$\widehat{\Theta}_{2,T} := \left\{\widehat{\Theta}^2_{\mathtt{BF},T} + \sum_{j=1}^{2} \Theta^2_{\mathrm{D},j,T}\right\}^{1/2} + \sum_{j=1}^{2} \|\mathrm{div}(\boldsymbol{\rho}_{j,h})\|_{0,4/3;T}\,. \qquad \text{(cf. (5.5), (4.3))}$$

(4) Check the stopping criterion and decide whether to finish or go to the next step.

(5) Use Plaza and Carey's algorithm [30] to refine each $T' \in \mathcal{T}_h$ satisfying

$$\Theta_{1,T'} \geq C_{\rm per} \max\left\{\Theta_{1,T} : \quad T \in \mathcal{T}_h\right\} \text{ for some } C_{\rm per} \in (0,1)\,. \tag{6.1}$$

(6) Define the resulting mesh as the current mesh, and go to step (2).

In particular, in Examples 2–5 below we take $C_{\rm per} = 0.5$. Certainly, if the refinement is with respect to the local indicator $\widehat{\Theta}_{2,T}$, we simply replace $\Theta_{1,T'}$ and $\Theta_{1,T}$ by $\widehat{\Theta}_{2,T'}$ and $\widehat{\Theta}_{2,T}$, respectively, in the criterion (6.1).

Example 1: Accuracy assessment with a smooth solution in a square domain.

In this first example, we concentrate on the accuracy of the mixed method as well as the properties of the *a posteriori* error estimators through the effectivity indexes $\mathsf{eff}(\Theta_1)$ and $\mathsf{eff}(\widehat{\Theta}_2)$, under a quasi-uniform refinement strategy. We consider the square domain $\Omega := (0,1)^2$, and adjust the data in (2.6) so that the exact solution is given by the smooth functions

$$\mathbf{u}(x_1,x_2) := \begin{pmatrix} \sin(\pi x_1)\cos(\pi x_2) \\ -\cos(\pi x_1)\sin(\pi x_2) \end{pmatrix}, \quad p(x_1,x_2) := \sin(x_1 - 0.5)\,,$$
$$\phi_1(x_1,x_2) := 0.5 + 0.5\cos(x_1 x_2)\,, \quad \text{and} \quad \phi_2(x_1,x_2) := 0.1 + 0.3\exp(x_1 x_2)\,.$$

The errors and associated rates of convergence are reported in Tables 6.1 and 6.2, which are in accordance with the theoretical bounds established in [8, Theorem 5.6 and Lemma 5.7]. In addition, the global *a posteriori* error indicators $\Theta_1, \widehat{\Theta}_2$, and their respective effectivity indexes are also displayed there, from where we highlight that the latter remain always bounded.

Example 2: Adaptivity in a 2D L-shaped domain.

The second example is aimed at testing the features of adaptive mesh refinement after both *a posteriori* error estimators Θ_1 and $\widehat{\Theta}_2$ (cf. (4.1), (5.4)). We consider an L-shaped domain $\Omega := (-1,1)^2 \setminus (0,1)^2$. The manufactured solution is given by

$$\mathbf{u}(x_1,x_2) := \begin{pmatrix} -\pi\cos(\pi x_2)\sin(\pi x_1) \\ \pi\cos(\pi x_1)\sin(\pi x_2) \end{pmatrix}, \quad p(x_1,x_2) := \frac{10(1-x_1)}{(x_1-0.09)^2 + (x_2-0.09)^2} - p_0\,,$$
$$\phi_1(x_1,x_2) := \frac{1}{x_2 + 1.055}\,, \quad \text{and} \quad \phi_2(x_1,x_2) := \frac{2}{x_2 + 1.07}\,,$$

where $p_0 \in \mathrm{R}$ is chosen so that $\int_\Omega p = 0$. Note that the pressure, temperature and concentration fields exhibit high gradients near the origin and the lines $x_2 = -1.055$ and $x_2 = -1.07$, respectively. Figure 6.1 summarizes the convergence history of the method when applied to quasi-uniform and adaptive (via Θ_1 and $\widehat{\Theta}_2$) refinements of the domain, which yield sub-optimal and optimal rates of convergence, respectively. Further corresponding details can be observed in Tables 6.3 - 6.4 and Tables 6.5 - 6.6, where the errors, rates of convergence, efficiency indexes, and Newton iterations are displayed for both refinements. We stress that the adaptive algorithm improves the efficiency of the method by delivering quality solutions at a lower computational cost, in particular to the point that it is possible

to get a better one (in terms of $\mathrm{e}(\vec{\mathbf{t}})$) with approximately only the 10% of the degrees of freedom of the last quasi-uniform mesh for the mixed scheme with both $k = 0$ and $k = 1$. Furthermore, the initial mesh and approximate solutions builded using the adaptive $\mathbb{RT}_1 - \mathbf{P}_2 - \mathbf{RT}_1 - \mathrm{P}_1 - \mathbf{RT}_1 - \mathrm{P}_1$ scheme (via Θ_1) with 663,663 degree of freedom are shown in Figure 6.2. We observe there that the pressure and temperature exhibit high gradients in the contraction region and at the bottom of the domain, respectively. In turn, examples of some adapted meshes generated using Θ_1 and $\widehat{\Theta}_2$, with $k = 1$, are collected in Figure 6.3. We notice a clear clustering of elements near the corner region of the contraction and the bottom of the L-shape domain as we expected.

Example 3: Adaptivity in a 3D L-shape domain.

Here we replicate the Example 2 in a three-dimensional setting by considering the 3D L-shape domain $\Omega := (0,2) \times (0,1) \times (0,2) \setminus (0,1)^3$, and the manufactured exact solution

$$\mathbf{u}(x_1,x_2,x_3) := \begin{pmatrix} \sin(\pi x_1)\cos(\pi x_2)\cos(\pi x_3) \\ -2\cos(\pi x_1)\sin(\pi x_2)\cos(\pi x_3) \\ \cos(\pi x_1)\cos(\pi x_2)\sin(\pi x_3) \end{pmatrix}, \quad \phi_1(x_1,x_2,x_3) := 0.5 + 0.5\cos(x_1x_2x_3)\,,$$

$$p(x_1,x_2,x_3) := \frac{1}{(x_1-1.07)^2 + (x_3-1.07)^2} - p_0\,, \quad \text{and} \quad \phi_2(x_1,x_2,x_3) := 0.1 + 0.3\exp(x_1x_2x_3)\,.$$

Tables 6.7 and 6.8 along with Figure 6.4 confirm a disturbed convergence under quasi-uniform refinement, whereas optimal convergence rates are obtained when adaptive refinements guided by the *a posteriori* error estimators Θ_1 and $\widehat{\Theta}_2$, with $k = 0$, are used. In addition, it is also observed in Figure 6.4 that the results for $\widehat{\Theta}_2$ are similar to those obtained for Θ_1, reason why the corresponding table of numerical results is omitted. In turn, the initial mesh and some approximated solutions after seven refinement steps (via Θ_1) are collected in Figure 6.5. In particular, we see there that the pressure presents high values and hence, most likely, high gradients as well near the contraction region of the 3D L-shape domain, as we expected. The latter is complemented with Figure 6.6, where snapshots of three meshes via Θ_1 show a clustering of elements in the same region.

Example 4: Flow through a 2D porous media with channel network.

Inspired by [8, Example 3, Section 6], we now focus on a flow through a porous medium with a channel network considering strong jump discontinuities of the parameters $\mathtt{F}$ and $\mathbf{K}$ accross the two regions. We consider the square domain $\Omega := (-1,1)^2$ with an internal channel network denoted as Ω_{c} (see the first plot of Figure 6.7 below), and boundary Γ, whose left, right, upper and lower parts are given by $\Gamma_{\mathrm{left}} = \{-1\} \times (-1,1)$, $\Gamma_{\mathrm{right}} = \{1\} \times (-1,1)$, $\Gamma_{\mathrm{top}} = (-1,1) \times \{1\}$, and $\Gamma_{\mathrm{bottom}} = (-1,1) \times \{-1\}$, respectively. We consider the coupling of the Brinkman–Forchheimer and double-diffusion equations (2.6) in the whole domain Ω with $\mathbf{Q}_1 = 0.5\mathbb{I}$, $\mathbf{Q}_2 = 0.125\mathbb{I}$, but with different values of the parameters $\mathtt{F}$ and $\mathbf{K} = \alpha\,\mathbb{I}$ for the interior and the exterior of the channel, namely

$$\mathtt{F} = \begin{cases} 10 & \text{in } \Omega_{\mathrm{c}} \\ 1 & \text{in } \overline{\Omega} \setminus \Omega_{\mathrm{c}} \end{cases} \quad \text{and} \quad \alpha = \begin{cases} 1 & \text{in } \Omega_{\mathrm{c}} \\ 0.001 & \text{in } \overline{\Omega} \setminus \Omega_{\mathrm{c}} \end{cases}. \tag{6.2}$$

This choice corresponds to increased inertial effect ($\mathtt{F} = 10$) in the channel and a high permeability ($\alpha = 1$), compared to reduced inertial effect ($\mathtt{F} = 1$) in the porous media and low permeability

($\alpha = 0.001$). In addition, the boundaries conditions are

$$\mathbf{u} = (0.2, 0)^{\mathrm{t}} \quad \text{on} \quad \Gamma_{\text{left}}\,, \quad \boldsymbol{\sigma}\mathbf{n} = \mathbf{0} \quad \text{on} \quad \Gamma \backslash \Gamma_{\text{left}}\,,$$

$$\phi_1 = 0.3 \quad \text{on} \quad \Gamma_{\text{left}}\,, \quad \phi_1 = 0 \quad \text{on} \quad \Gamma_{\text{right}}\,, \quad \boldsymbol{\rho}_1 \cdot \mathbf{n} = 0 \quad \text{on} \quad \Gamma_{\text{bottom}} \cup \Gamma_{\text{top}}\,,$$

$$\phi_2 = 0.2 \quad \text{on} \quad \Gamma_{\text{left}}\,, \quad \phi_1 = 0 \quad \text{on} \quad \Gamma_{\text{right}}\,, \quad \boldsymbol{\rho}_1 \cdot \mathbf{n} = 0 \quad \text{on} \quad \Gamma_{\text{bottom}} \cup \Gamma_{\text{top}}\,.$$

In particular, the first row of boundary equations corresponds to inflow on the left boundary and zero stress outflow on the rest of the boundary. In Figure 6.7, for the sake of simplicity, we only display the computed magnitude of the velocity and a velocity gradient component, which were built using the $\mathbb{RT}_0 - \mathbf{P}_1 - \mathbf{RT}_0 - \mathrm{P}_0 - \mathbf{RT}_0 - \mathrm{P}_0$ scheme on a mesh with $83,034$ triangle elements obtained via Θ_1. Similarly to [8, Example 3, Section 6], faster flow through the channel network, with a significant velocity gradient across the interface between the porous medium and the channel, are observed. These results are in agreement with those obtained in [8] but now taking into account that the mesh employed was obtained through an adaptive refinement process guided by the *a posteriori* error indicator Θ_1. In turn, snapshots of some adapted meshes generated using Θ_1 and $\widehat{\Theta}_2$, are depicted in Figure 6.8. Notice that the meshes obtained via the indicator Θ_1 are slightly more refined in the interior of the domain than the meshes obtained via the indicator $\widehat{\Theta}_2$. This fact is justified by the terms that capture the jumps between triangles, which arise from the Helmoltz decomposition applied to the Brinkman–Forchheimer equations and the consequent local integration by parts procedures. We conclude that the estimator Θ_1 is more sensible than $\widehat{\Theta}_2$ to detect the strong jump discontinuities of the model parameters along the interface between the channel and porous media.

Example 5: Flow through a 3D porous media with channel network.

In the final example we replicate the Example 4 in a three-dimensional setting. To that end, we consider a 3D porous media with channel network as is described in the first plot of the Figure 6.9. The model parameters $\mathtt{F}$ and $\mathbf{K} = \alpha\,\mathbb{I}$ are taken as in (6.2) but now considering $\alpha = 0.0001$ in $\Omega \setminus \overline{\Omega}_c$. In addition, the boundaries conditions are

$$\mathbf{u} = (0.2, 0, 0)^{\mathrm{t}} \quad \text{on} \quad \Gamma_{\text{left}}, \quad \mathbf{u} = \mathbf{0} \quad \text{on} \quad \Gamma_{\text{bottom}} \cup \Gamma_{\text{top}}, \quad \boldsymbol{\sigma}\mathbf{n} = \mathbf{0} \quad \text{on} \quad \Gamma_{\text{back}} \cup \Gamma_{\text{front}} \cup \Gamma_{\text{right}},$$

$$\phi_1 = 0.3 \quad \text{on} \quad \Gamma_{\text{left}}, \quad \phi_1 = 0 \quad \text{on} \quad \Gamma_{\text{right}}, \quad \boldsymbol{\rho}_1 \cdot \mathbf{n} = 0 \quad \text{on} \quad \Gamma_{\text{bottom}} \cup \Gamma_{\text{top}} \cup \Gamma_{\text{back}} \cup \Gamma_{\text{front}},$$

$$\phi_2 = 0.2 \quad \text{on} \quad \Gamma_{\text{left}}, \quad \phi_1 = 0 \quad \text{on} \quad \Gamma_{\text{right}}, \quad \boldsymbol{\rho}_1 \cdot \mathbf{n} = 0 \quad \text{on} \quad \Gamma_{\text{bottom}} \cup \Gamma_{\text{top}} \cup \Gamma_{\text{back}} \cup \Gamma_{\text{front}}.$$

In Figure 6.9 we display the computed magnitude of the velocity and concentration field builded using the $\mathbb{RT}_0 - \mathbf{P}_1 - \mathbf{RT}_0 - \mathrm{P}_0 - \mathbf{RT}_0 - \mathrm{P}_0$ scheme via the indicator Θ_1. We observe faster flow through the channel network as in its 2D counterpart. In addition, the concentration is higher on the left of the boundary and goes decaying to the right of the domain as we expected. Finally, snapshots of the initial mesh and two meshes via the *a posteriori* error estimator Θ_1 are shown in Figure 6.10, where again, as in Example 4, a suitable refinement around the interface that couples the porous medium with the channel network as well as the region near the inflow boundary, are obtained.

References

[1] S. Agmon, Lectures on Elliptic Boundary Value Problems. Prepared for publication by B. Frank Jones, Jr. with the assistance of George W. Batten, Jr. Revised edition of the 1965 original. AMS Chelsea Publishing, Providence, RI, 2010.

N	$\mathrm{e}(\boldsymbol{\sigma})$	$r(\boldsymbol{\sigma})$	$\mathrm{e}(\mathbf{u})$	$r(\mathbf{u})$	$\mathrm{e}(p)$	$r(p)$	$\mathrm{e}(\boldsymbol{\rho}_1)$	$r(\boldsymbol{\rho}_1)$	$\mathrm{e}(\boldsymbol{\rho}_2)$	$r(\boldsymbol{\rho}_2)$
1251	1.88e+00	–	6.07e-01	–	1.30e-01	–	1.53e-01	–	1.10e-01	–
4803	9.33e-01	1.04	3.07e-01	1.01	6.43e-02	1.05	7.82e-02	1.00	5.61e-02	1.01
18819	4.66e-01	1.02	1.54e-01	1.01	3.20e-02	1.02	3.94e-02	1.00	2.82e-02	1.01
74499	2.33e-01	1.01	7.71e-02	1.01	1.60e-02	1.01	1.98e-02	1.00	1.41e-02	1.00
296451	1.16e-01	1.00	3.86e-02	1.00	7.98e-03	1.00	9.88e-03	1.00	7.07e-03	1.00

$\mathrm{e}(\phi_1)$	$r(\phi_1)$	$\mathrm{e}(\phi_2)$	$r(\phi_2)$	$\mathrm{e}(\vec{\mathbf{t}})$	$r(\vec{\mathbf{t}})$	Θ_1	$\mathsf{eff}(\Theta_1)$	$\widehat{\Theta}_2$	$\mathsf{eff}(\widehat{\Theta}_2)$	iter
1.10e-02	–	2.12e-02	–	2.78e+00	–	2.67e+00	1.040	2.62e+00	1.058	5
5.49e-03	1.04	1.06e-02	1.03	1.39e+00	1.03	1.36e+00	1.026	1.32e+00	1.057	5
2.74e-03	1.02	5.31e-03	1.01	6.96e-01	1.02	6.85e-01	1.015	6.62e-01	1.051	5
1.37e-03	1.01	2.66e-03	1.01	3.48e-01	1.01	3.46e-01	1.004	3.34e-01	1.041	5
6.84e-04	1.00	1.33e-03	1.00	1.74e-01	1.00	1.76e-01	0.987	1.70e-01	1.023	5

Table 6.1: Example 1: $\mathbb{RT}_0 - \mathbf{P}_1 - \mathbf{RT}_0 - \mathrm{P}_0 - \mathbf{RT}_0 - \mathrm{P}_0$ scheme with quasi-uniform refinement.

N	$\mathrm{e}(\boldsymbol{\sigma})$	$r(\boldsymbol{\sigma})$	$\mathrm{e}(\mathbf{u})$	$r(\mathbf{u})$	$\mathrm{e}(p)$	$r(p)$	$\mathrm{e}(\boldsymbol{\rho}_1)$	$r(\boldsymbol{\rho}_1)$	$\mathrm{e}(\boldsymbol{\rho}_2)$	$r(\boldsymbol{\rho}_2)$
4035	1.40e-01	–	4.59e-02	–	7.41e-03	–	1.10e-02	–	7.27e-03	–
15747	3.51e-02	2.03	1.17e-02	2.00	1.82e-03	2.06	2.84e-03	1.99	1.86e-03	2.00
62211	8.77e-03	2.02	2.96e-03	2.00	4.53e-04	2.03	7.19e-04	2.00	4.71e-04	2.00
247299	2.19e-03	2.01	7.43e-04	2.00	1.13e-04	2.01	1.81e-04	2.00	1.18e-04	2.00
986115	5.48e-04	2.00	1.86e-04	2.00	2.82e-05	2.01	4.53e-05	2.00	2.97e-05	2.00

$\mathrm{e}(\phi_1)$	$r(\phi_1)$	$\mathrm{e}(\phi_2)$	$r(\phi_2)$	$\mathrm{e}(\vec{\mathbf{t}})$	$r(\vec{\mathbf{t}})$	Θ_1	$\mathsf{eff}(\Theta_1)$	$\widehat{\Theta}_2$	$\mathsf{eff}(\widehat{\Theta}_2)$	iter
5.44e-04	–	9.05e-04	–	2.06e-01	–	2.50e-01	0.821	2.27e-01	0.904	5
1.35e-04	2.05	2.27e-04	2.00	5.19e-02	2.02	6.33e-02	0.819	5.73e-02	0.905	5
3.36e-05	2.02	5.68e-05	2.02	1.30e-02	2.01	1.60e-02	0.815	1.44e-02	0.902	5
8.38e-06	2.01	1.42e-05	2.01	3.26e-03	2.01	4.03e-03	0.808	3.64e-03	0.895	5
2.10e-06	2.00	3.55e-06	2.00	8.15e-04	2.00	1.02e-03	0.795	9.28e-04	0.878	5

Table 6.2: Example 1: $\mathbb{RT}_1 - \mathbf{P}_2 - \mathbf{RT}_1 - \mathrm{P}_1 - \mathbf{RT}_1 - \mathrm{P}_1$ scheme with quasi-uniform refinement.

[2] M. S. Alnæs, J. Blechta, J. Hake, A. Johansson, B. Kehlet, A. Logg, C. Richardson, J. Ring, M. E. Rognes, and G. N. Wells, *The fenics project version 1.5.* Archive of Numerical Software 3 (2015), 9–23.

[3] F. Brezzi and M. Fortin, Mixed and Hybrid Finite Element Methods. Springer Series in Computational Mathematics, 15. Springer-Verlag, New York, 1991.

[4] J. Camaño, S. Caucao, R. Oyarzúa, and S. Villa-Fuentes, *A posteriori error analysis of a momentum conservative Banach spaces based mixed-FEM for the Navier–Stokes problem.* Appl. Numer. Math. 176 (2022), 134–158.

[5] C. Carstensen, *A posteriori error estimate for the mixed finite element method.* Math. Comp. 66 (1997), no. 218, 465–476.

[6] S. Caucao, M. Discacciati, G.N. Gatica, and R. Oyarzúa, *A conforming mixed finite element method for the Navier–Stokes/Darcy–Forchheimer coupled problem.* ESAIM Math. Model. Numer. Anal. 54 (2020), no. 5, 1689–1723.

N	e($\boldsymbol{\sigma}$)	$r(\boldsymbol{\sigma})$	e($\mathbf{u}$)	$r(\mathbf{u})$	e(p)	$r(p)$	e($\boldsymbol{\rho}_1$)	$r(\boldsymbol{\rho}_1)$	e($\boldsymbol{\rho}_2$)	$r(\boldsymbol{\rho}_2)$
1725	9.74e+02	–	1.64e+01	–	4.58e+01	–	9.81e+02	–	1.00e+03	–
6729	7.01e+02	0.48	1.25e+01	0.39	2.76e+01	0.75	5.80e+02	0.77	5.79e+02	0.81
27255	4.53e+02	0.62	6.38e+00	0.97	1.46e+01	0.91	3.44e+02	0.74	3.34e+02	0.79
108045	2.40e+02	0.92	2.30e+00	1.48	7.20e+00	1.03	1.87e+02	0.89	1.77e+02	0.92
431997	1.21e+02	0.99	7.63e-01	1.59	3.51e+00	1.04	1.00e+02	0.90	9.31e+01	0.93

e(ϕ_1)	$r(\phi_1)$	e(ϕ_2)	$r(\phi_2)$	e($\vec{\mathbf{t}}$)	$r(\vec{\mathbf{t}})$	Θ_1	eff(Θ_1)	$\widehat{\Theta}_2$	eff($\widehat{\Theta}_2$)	iter
1.07e+01	–	1.23e+01	–	3.00e+03	–	2.66e+03	1.122	2.63e+03	1.135	6
3.63e+00	1.59	4.48e+00	1.48	1.88e+03	0.69	1.71e+03	1.099	1.69e+03	1.113	6
1.61e+00	1.17	2.07e+00	1.11	1.14e+03	0.71	1.04e+03	1.101	1.02e+03	1.119	6
7.62e-01	1.08	1.00e+00	1.05	6.08e+02	0.92	5.51e+02	1.103	5.40e+02	1.126	6
3.96e-01	0.94	5.21e-01	0.94	3.16e+02	0.95	2.85e+02	1.106	2.79e+02	1.131	6

Table 6.3: Example 2: $\mathbb{RT}_0 - \mathbf{P}_1 - \mathbf{RT}_0 - \mathrm{P}_0 - \mathbf{RT}_0 - \mathrm{P}_0$ scheme with quasi-uniform refinement.

N	e($\boldsymbol{\sigma}$)	$r(\boldsymbol{\sigma})$	e($\mathbf{u}$)	$r(\mathbf{u})$	e(p)	$r(p)$	e($\boldsymbol{\rho}_1$)	$r(\boldsymbol{\rho}_1)$	e($\boldsymbol{\rho}_2$)	$r(\boldsymbol{\rho}_2)$
5583	6.47e+02	–	6.69e+00	–	2.30e+01	–	6.17e+02	–	5.75e+02	–
22143	2.54e+02	1.36	2.95e+00	1.19	8.85e+00	1.39	2.49e+02	1.32	2.16e+02	1.42
90267	9.06e+01	1.47	6.29e-01	2.20	2.69e+00	1.69	9.35e+01	1.40	7.48e+01	1.51
358971	2.59e+01	1.81	1.19e-01	2.42	7.05e-01	1.94	2.78e+01	1.76	2.11e+01	1.84
1437603	6.57e+00	1.98	2.74e-02	2.11	1.72e-01	2.03	8.06e+00	1.79	5.90e+00	1.83

e(ϕ_1)	$r(\phi_1)$	e(ϕ_2)	$r(\phi_2)$	e($\vec{\mathbf{t}}$)	$r(\vec{\mathbf{t}})$	Θ_1	eff(Θ_1)	$\widehat{\Theta}_2$	eff($\widehat{\Theta}_2$)	iter
2.66e+00	–	2.98e+00	–	1.85e+03	–	1.61e+03	1.144	1.59e+03	1.160	6
7.22e-01	1.89	8.46e-01	1.83	7.23e+02	1.36	6.59e+02	1.098	6.48e+02	1.116	6
2.49e-01	1.52	2.84e-01	1.55	2.60e+02	1.46	2.39e+02	1.087	2.34e+02	1.109	6
7.45e-02	1.75	8.12e-02	1.81	7.51e+01	1.80	6.83e+01	1.099	6.69e+01	1.122	6
2.27e-02	1.71	2.39e-02	1.76	2.06e+01	1.86	1.87e+01	1.100	1.83e+01	1.125	6

Table 6.4: Example 2: $\mathbb{RT}_1 - \mathbf{P}_2 - \mathbf{RT}_1 - \mathrm{P}_1 - \mathbf{RT}_1 - \mathrm{P}_1$ scheme with quasi-uniform refinement.

[7] S. Caucao, G.N. Gatica, and R. Oyarzúa, *A posteriori error analysis of an augmented fully mixed formulation for the nonisothermal Oldroyd-Stokes problem.* Numer. Methods Partial Differential Equations 35 (2019), no. 1, 295–324.

[8] S. Caucao, G.N. Gatica, R. Oyarzúa, and N. Sánchez, *A fully-mixed formulation for the steady double-diffusive convection system based upon Brinkman–Forchheimer equations.* J. Sci. Comput. 85 (2020), no. 2, Paper No. 44, 37 pp.

[9] S. Caucao, G.N. Gatica, R. Oyarzúa, and F. Sandoval, *Residual-based a posteriori error analysis for the coupling of the Navier-Stokes and Darcy-Forchheimer equations.* ESAIM: Math. Model. Numer. Anal. 55 (2021), no. 2, 659–687.

[10] S. Caucao, D. Mora, and R. Oyarzúa, *A priori and a posteriori error analysis of a pseudostress-based mixed formulation of the Stokes problem with varying density.* IMA J. Numer. Anal. 36 (2016), no. 2, 947–983.

[11] S. Caucao, R. Oyarzúa, and S. Villa-Fuentes, *A posteriori error analysis of a momentum and thermal energy conservative mixed-FEM for the Boussinesq equations.* Preprint 2020-29, Cen-

N	$\mathrm{e}(\boldsymbol{\sigma})$	$r(\boldsymbol{\sigma})$	$\mathrm{e}(\mathbf{u})$	$r(\mathbf{u})$	$\mathrm{e}(p)$	$r(p)$	$\mathrm{e}(\boldsymbol{\rho}_1)$	$r(\boldsymbol{\rho}_1)$	$\mathrm{e}(\boldsymbol{\rho}_2)$	$r(\boldsymbol{\rho}_2)$
1725	9.74e+02	–	1.64e+01	–	4.93e+01	–	9.81e+02	–	1.00e+03	–
2247	7.67e+02	1.81	1.28e+01	1.86	4.06e+01	1.47	6.99e+02	2.56	7.07e+02	2.64
2679	4.80e+02	5.34	8.37e+00	4.85	2.63e+01	4.92	6.55e+02	0.73	6.61e+02	0.78
4317	3.10e+02	1.83	6.17e+00	1.28	1.97e+01	1.22	4.13e+02	1.93	4.09e+02	2.01
8487	2.18e+02	1.05	4.74e+00	0.78	1.42e+01	0.96	2.49e+02	1.50	2.46e+02	1.50
12675	1.57e+02	1.64	4.13e+00	0.68	1.04e+01	1.58	2.02e+02	1.03	2.04e+02	0.93
21243	1.14e+02	1.23	3.66e+00	0.47	7.92e+00	1.04	1.54e+02	1.06	1.60e+02	0.94
41571	8.08e+01	1.03	3.10e+00	0.50	5.74e+00	0.96	1.15e+02	0.88	1.17e+02	0.94
77343	5.76e+01	1.09	2.17e+00	1.14	4.01e+00	1.16	8.48e+01	0.97	8.75e+01	0.92
155535	4.04e+01	1.02	1.59e+00	0.89	2.84e+00	0.99	6.09e+01	0.95	6.22e+01	0.98
289359	2.90e+01	1.07	1.09e+00	1.22	2.00e+00	1.13	4.55e+01	0.94	4.70e+01	0.90
574851	2.04e+01	1.02	8.18e-01	0.84	1.42e+00	0.99	3.30e+01	0.93	3.37e+01	0.98

$\mathrm{e}(\phi_1)$	$r(\phi_1)$	$\mathrm{e}(\phi_2)$	$r(\phi_2)$	$\mathrm{e}(\vec{\mathbf{t}})$	$r(\vec{\mathbf{t}})$	Θ_1	$\mathsf{eff}(\Theta_1)$	iter
1.07e+01	–	1.23e+01	–	3.00e+03	–	2.66e+03	1.122	6
4.87e+00	5.99	5.96e+00	5.49	2.20e+03	2.35	1.93e+03	1.135	6
4.54e+00	0.79	5.53e+00	0.85	1.81e+03	2.18	1.58e+03	1.147	6
2.09e+00	3.26	2.68e+00	3.03	1.14e+03	1.94	1.01e+03	1.131	6
1.09e+00	1.93	1.48e+00	1.77	7.20e+02	1.37	6.37e+02	1.129	6
8.70e-01	1.12	1.24e+00	0.87	5.69e+02	1.17	5.03e+02	1.132	6
6.66e-01	1.03	1.01e+00	0.81	4.33e+02	1.05	3.81e+02	1.137	6
4.68e-01	1.05	6.93e-01	1.12	3.16e+02	0.94	2.78e+02	1.138	6
3.43e-01	1.00	5.20e-01	0.92	2.33e+02	0.99	2.05e+02	1.138	6
2.42e-01	1.00	3.65e-01	1.01	1.66e+02	0.98	1.46e+02	1.136	6
1.82e-01	0.91	2.78e-01	0.88	1.23e+02	0.96	1.08e+02	1.134	6
1.30e-01	0.98	1.95e-01	1.04	8.83e+01	0.97	7.82e+01	1.129	6

Table 6.5: EXAMPLE 2: $\mathbb{RT}_0 - \mathbf{P}_1 - \mathbf{RT}_0 - \mathrm{P}_0 - \mathbf{RT}_0 - \mathrm{P}_0$ scheme with adaptive refinement via Θ_1.

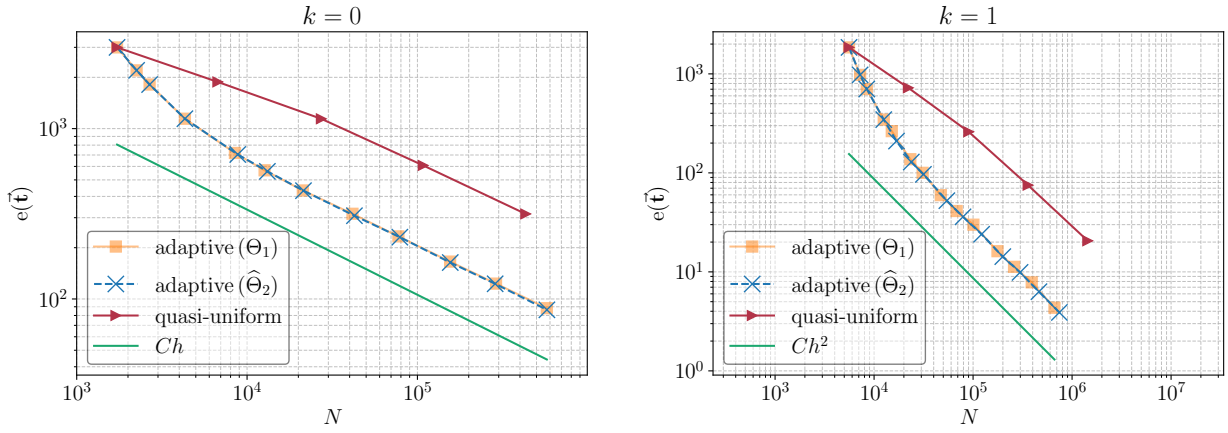

Figure 6.1: EXAMPLE 2: Log-log plots of $\mathrm{e}(\vec{\mathbf{t}})$ vs N for quasi-uniform/adaptive schemes via Θ_1 and $\widehat{\Theta}_2$ for $k = 0$ and $k = 1$ (left and right plots, respectively).

N	e($\boldsymbol{\sigma}$)	$r(\boldsymbol{\sigma})$	e($\mathbf{u}$)	$r(\mathbf{u})$	e(p)	$r(p)$	e($\boldsymbol{\rho}_1$)	$r(\boldsymbol{\rho}_1)$	e($\boldsymbol{\rho}_2$)	$r(\boldsymbol{\rho}_2)$
5583	6.47e+02	–	6.69e+00	–	2.30e+01	–	6.17e+02	–	5.75e+02	–
7227	2.52e+02	7.32	2.63e+00	7.24	8.91e+00	7.36	3.78e+02	3.79	3.42e+02	4.04
8439	1.58e+02	6.02	1.75e+00	5.27	6.09e+00	4.91	2.88e+02	3.49	2.54e+02	3.82
12519	8.95e+01	2.87	1.08e+00	2.43	3.45e+00	2.89	1.38e+02	3.73	1.15e+02	4.00
16851	4.26e+01	4.99	6.43e-01	3.51	1.95e+00	3.83	9.08e+01	2.82	7.49e+01	2.91
23775	3.75e+01	0.75	6.04e-01	0.36	1.76e+00	0.59	4.94e+01	3.54	4.10e+01	3.50
31515	2.09e+01	4.15	4.67e-01	1.82	1.14e+00	3.07	4.09e+01	1.34	3.42e+01	1.29
54339	1.31e+01	1.72	4.07e-01	0.51	7.59e-01	1.50	2.03e+01	2.57	1.84e+01	2.27
79119	8.65e+00	2.20	3.47e-01	0.85	5.35e-01	1.86	1.42e+01	1.89	1.26e+01	2.01
122007	5.24e+00	2.32	2.65e-01	1.25	3.27e-01	2.28	9.76e+00	1.75	8.68e+00	1.74
199647	3.36e+00	1.80	1.63e-01	1.97	2.16e-01	1.68	5.62e+00	2.24	5.08e+00	2.17
298251	2.11e+00	2.30	9.99e-02	2.43	1.29e-01	2.56	4.07e+00	1.61	3.57e+00	1.75
462903	1.36e+00	2.01	7.22e-02	1.48	8.60e-02	1.85	2.58e+00	2.07	2.28e+00	2.05
744255	8.56e-01	1.95	4.10e-02	2.39	5.42e-02	1.94	1.58e+00	2.07	1.40e+00	2.04

e(ϕ_1)	$r(\phi_1)$	e(ϕ_2)	$r(\phi_2)$	e($\vec{\mathbf{t}}$)	$r(\vec{\mathbf{t}})$	$\widehat{\Theta}_2$	eff($\widehat{\Theta}_2$)	iter
2.66e+00	–	2.98e+00	–	1.85e+03	–	1.61e+03	1.144	6
1.47e+00	4.58	1.72e+00	4.23	9.77e+02	4.95	8.74e+02	1.117	6
8.90e-01	6.51	1.06e+00	6.29	7.04e+02	4.23	6.36e+02	1.106	6
3.91e-01	4.17	4.59e-01	4.24	3.45e+02	3.61	3.11e+02	1.108	6
2.68e-01	2.54	3.18e-01	2.48	2.10e+02	3.36	1.93e+02	1.088	6
1.41e-01	3.73	1.67e-01	3.72	1.29e+02	2.83	1.17e+02	1.098	6
1.08e-01	1.87	1.34e-01	1.60	9.66e+01	2.04	8.80e+01	1.097	6
6.56e-02	1.84	9.74e-02	1.16	5.24e+01	2.25	4.79e+01	1.093	6
4.20e-02	2.38	5.90e-02	2.66	3.60e+01	2.00	3.28e+01	1.095	6
2.96e-02	1.62	4.17e-02	1.60	2.40e+01	1.87	2.20e+01	1.091	6
1.76e-02	2.10	2.54e-02	2.01	1.43e+01	2.12	1.31e+01	1.085	6
1.18e-02	2.00	1.66e-02	2.13	9.88e+00	1.83	9.07e+00	1.089	6
7.63e-03	1.98	1.09e-02	1.91	6.31e+00	2.04	5.84e+00	1.080	6
4.80e-03	1.95	6.74e-03	2.03	3.89e+00	2.04	3.61e+00	1.077	6

Table 6.6: EXAMPLE 2: $\mathbb{RT}_1 - \mathbf{P}_2 - \mathbf{RT}_1 - \mathrm{P}_1 - \mathbf{RT}_1 - \mathrm{P}_1$ scheme with adaptive refinement via $\widehat{\Theta}_2$.

tro de Investigación en Ingeniería Matemática (CI^{2}MA), Universidad de Concepción, Concepción, Chile, (2020).

[12] P. CLÉMENT, *Approximation by finite element functions using local regularisation.* RAIRO Modélisation Mathématique et Analyse Numérique 9 (1975), 77–84.

[13] E. COLMENARES, G.N. GATICA, AND R. OYARZÚA, *Fixed point strategies for mixed variational formulations of the stationary Boussinesq problem.* C. R. Math. Acad. Sci. Paris 354 (2016), no. 1, 57–62.

[14] E. COLMENARES, G.N. GATICA, AND R. OYARZÚA, *A posteriori error analysis of an augmented mixed-primal formulation for the stationary Boussinesq model.* Calcolo 54 (2017), no. 3, 1055–1095.

N	e($\boldsymbol{\sigma}$)	$r(\boldsymbol{\sigma})$	e($\mathbf{u}$)	$r(\mathbf{u})$	e(p)	$r(p)$	e($\boldsymbol{\rho}_1$)	$r(\boldsymbol{\rho}_1)$	e($\boldsymbol{\rho}_2$)	$r(\boldsymbol{\rho}_2)$
14679	2.38e+02	–	4.96e+00	–	1.22e+01	–	8.04e-01	–	8.84e-01	–
40048	2.35e+02	0.03	3.87e+00	0.74	9.85e+00	0.64	5.69e-01	1.03	6.41e-01	0.96
96977	1.75e+02	0.99	2.99e+00	0.88	6.98e+00	1.17	4.09e-01	1.12	4.69e-01	1.06
265548	1.42e+02	0.63	2.17e+00	0.95	5.22e+00	0.87	2.77e-01	1.17	3.26e-01	1.09
670471	1.19e+02	0.57	1.64e+00	0.91	3.99e+00	0.87	1.96e-01	1.11	2.36e-01	1.04
1276920	1.03e+02	0.64	1.33e+00	0.98	3.30e+00	0.88	1.57e-01	1.04	1.93e-01	0.93

e(ϕ_1)	$r(\phi_1)$	e(ϕ_2)	$r(\phi_2)$	e($\vec{\mathbf{t}}$)	$r(\vec{\mathbf{t}})$	Θ_1	eff(Θ_1)	$\widehat{\Theta}_2$	eff($\widehat{\Theta}_2$)	iter
4.33e-02	–	9.48e-02	–	2.44e+02	–	2.53e+02	0.962	2.49e+02	0.979	5
3.21e-02	0.89	6.41e-01	0.96	2.40e+02	0.05	2.11e+02	1.136	2.07e+02	1.158	5
2.34e-02	1.07	4.69e-01	1.06	1.79e+02	0.99	1.74e+02	1.029	1.70e+02	1.052	5
1.69e-02	0.98	3.26e-01	1.09	1.44e+02	0.64	1.47e+02	0.985	1.44e+02	1.005	5
1.25e-02	0.97	2.36e-01	1.04	1.21e+02	0.58	1.22e+02	0.988	1.20e+02	1.008	5
1.04e-02	0.85	1.93e-01	0.93	1.05e+02	0.65	1.05e+02	1.000	1.03e+02	1.022	5

Table 6.7: Example 3: $\mathbb{RT}_0 - \mathbf{P}_1 - \mathbf{RT}_0 - \mathrm{P}_0 - \mathbf{RT}_0 - \mathrm{P}_0$ scheme with quasi-uniform refinement.

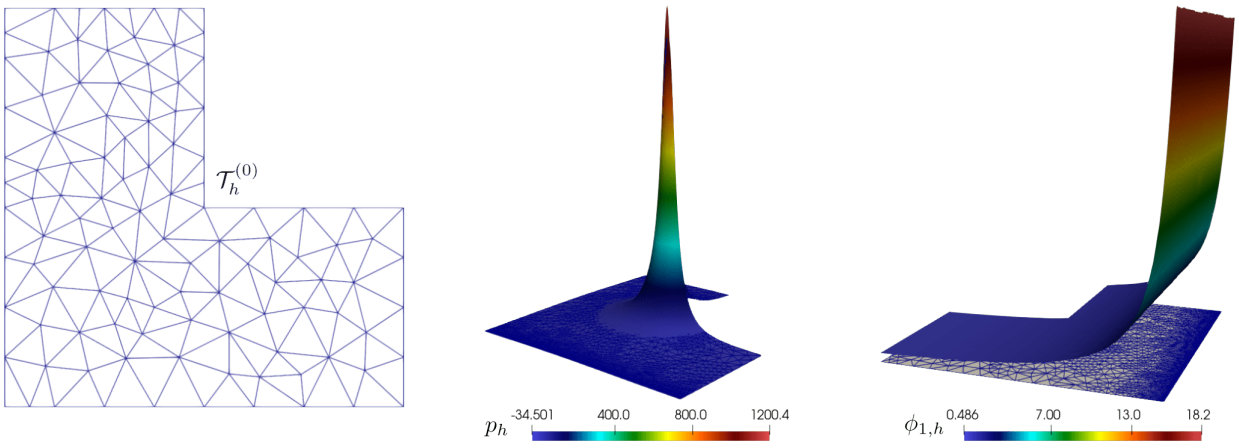

Figure 6.2: Example 2: Initial mesh, computed pressure and temperature fields.

[15] E. Colmenares, G.N. Gatica, and R. Oyarzúa, *A posteriori error analysis of an augmented fully-mixed formulation for the stationary Boussinesq model.* Comput. Math. Appl. 77 (2019), no. 3, 693–714.

[16] E. Creuse, M. Farhloul, and L. Paquet, *A posteriori error estimation for the dual mixed finite element method for the p-Laplacian in a polygonal domain.* Comput. Methods Appl. Mech. Engrg. 196 (2007), no. 25-28, 2570–2582.

[17] C. Domínguez, G. N. Gatica, and S. Meddahi, *A posteriori error analysis of a fully-mixed finite element method for a two-dimensional fluid-solid interaction problem.* J. Comput. Math. 33 (2015), no. 6, 606–641.

[18] A. Ern and J.-L. Guermond, Theory and Practice of Finite Elements. Applied Mathematical Sciences, 159. Springer-Verlag, New York, 2004.

N	e($\boldsymbol{\sigma}$)	$r(\boldsymbol{\sigma})$	e($\mathbf{u}$)	$r(\mathbf{u})$	e(p)	$r(p)$	e($\boldsymbol{\rho}_1$)	$r(\boldsymbol{\rho}_1)$	e($\boldsymbol{\rho}_2$)	$r(\boldsymbol{\rho}_2)$
14679	2.38e+02	–	4.96e+00	–	1.22e+01	–	8.04e-01	–	8.84e-01	–
24634	1.81e+02	1.56	4.26e+00	0.88	6.73e+00	3.44	6.79e-01	0.98	7.60e-01	0.88
47487	1.17e+02	2.02	3.69e+00	0.65	4.01e+00	2.37	6.26e-01	0.37	7.23e-01	0.23
115645	7.69e+01	1.40	3.30e+00	0.38	2.64e+00	1.41	5.76e-01	0.28	6.48e-01	0.37
195700	6.10e+01	1.32	3.21e+00	0.14	2.14e+00	1.20	5.71e-01	0.06	6.40e-01	0.07
405208	4.41e+01	1.33	3.16e+00	0.07	1.67e+00	1.01	5.65e-01	0.04	6.34e-01	0.04
821077	3.43e+01	1.07	2.21e+00	1.52	1.35e+00	0.89	3.79e-01	1.70	4.75e-01	1.23
1790290	2.58e+01	1.09	1.99e+00	0.42	1.03e+00	1.04	3.37e-01	0.46	3.85e-01	0.81

e(ϕ_1)	$r(\phi_1)$	e(ϕ_2)	$r(\phi_2)$	e($\vec{\mathbf{t}}$)	$r(\vec{\mathbf{t}})$	Θ_1	eff(Θ_1)	iter
4.33e-02	–	9.48e-02	–	2.44e+02	–	2.53e+02	0.962	5
4.19e-02	0.19	7.60e-01	0.88	1.87e+02	1.54	1.74e+02	1.073	5
4.17e-02	0.02	7.23e-01	0.23	1.22e+02	1.96	1.19e+02	1.022	5
3.85e-02	0.27	6.48e-01	0.37	8.15e+01	1.35	7.90e+01	1.032	5
3.84e-02	0.02	6.40e-01	0.07	6.55e+01	1.25	6.30e+01	1.039	5
3.83e-02	0.00	6.34e-01	0.04	4.86e+01	1.23	4.68e+01	1.038	5
3.00e-02	1.05	4.75e-01	1.23	3.75e+01	1.10	3.63e+01	1.032	5
2.26e-02	1.08	3.85e-01	0.81	2.86e+01	1.04	2.77e+01	1.034	5

Table 6.8: EXAMPLE 3: $\mathbb{RT}_0 - \mathbf{P}_1 - \mathbf{RT}_0 - \mathrm{P}_0 - \mathbf{RT}_0 - \mathrm{P}_0$ scheme with adaptive refinement via Θ_1.

[19] V.J. ERVIN AND T.N. PHILLIPS, *Residual a posteriori error estimator for a three-field model of a non-linear generalized Stokes problem*. Comput. Methods Appl. Mech. Engrg. 195 (2006), no. 19-22, 2599–2610.

[20] G.N. GATICA, A Simple Introduction to the Mixed Finite Element Method. Theory and Applications. SpringerBriefs in Mathematics. Springer, Cham, 2014.

[21] G.N. GATICA, *A note on stable Helmholtz decompositions in 3D*. Appl. Anal. 99 (2020), no. 7, 1110–1121.

[22] G.N. GATICA, L.F. GATICA, AND F.A. SEQUEIRA, *A priori and a posteriori error analyses of a pseudostress-based mixed formulation for linear elasticity*. Comput. Math. Appl. 71 (2016), no. 2, 585–614.

[23] G.N. GATICA, G.C. HSIAO, AND S. MEDDAHI, *A residual-based a posteriori error estimator for a two-dimensional fluid-solid interaction problem*. Numer. Math. 114 (2009), no. 1, 63–106.

[24] G.N. GATICA, C. INZUNZA, R. RUIZ-BAIER, AND F. SANDOVAL, *A posteriori error analysis of Banach spaces-based fully-mixed finite element methods for Boussinesq-type models*. J. Numer. Math., to appear.

[25] G.N. GATICA, A. MÁRQUEZ, AND W. RUDOLPH, *A priori and a posteriori error analyses of augmented twofold saddle point formulations for nonlinear elasticity problems*. Comput. Methods Appl. Mech. Engrg. 264 (2013), 23–48.

[26] G.N. GATICA, A. MÁRQUEZ, AND M.A. SÁNCHEZ, *Analysis of a velocity-pressure-pseudostress formulation for the stationary Stokes equations*. Comput. Methods Appl. Mech. Engrg. 199 (2010), no. 17-20, 1064–1079.

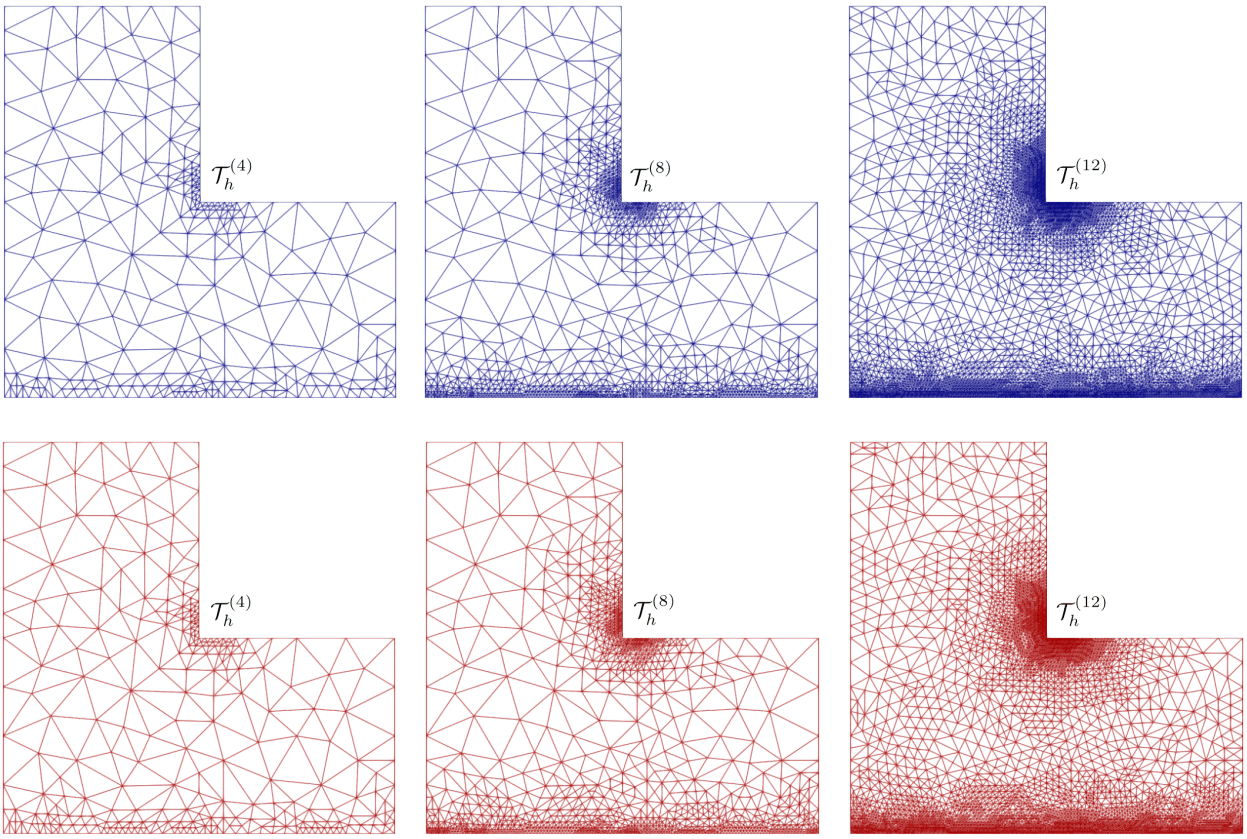

Figure 6.3: EXAMPLE 2: Three snapshots of adapted meshes according to the indicators Θ_1 and $\widehat{\Theta}_2$ for $k = 1$ (top and bottom plots, respectively).

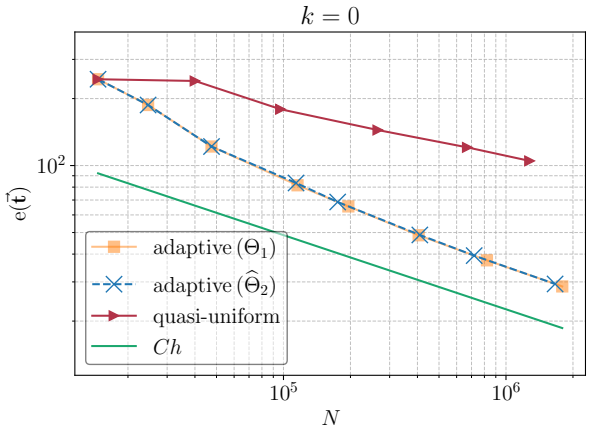

Figure 6.4: EXAMPLE 3: Log-log plot of $\mathrm{e}(\vec{\mathbf{t}})$ vs N for quasi-uniform/adaptive schemes via Θ_1 and $\widehat{\Theta}_2$ for $k = 0$.

[27] L. F. GATICA, R. OYARZÚA, AND N. SÁNCHEZ, *A priori and a posteriori error analysis of an augmented mixed-FEM for the Navier–Stokes-Brinkman problem.* Comput. Math. Appl. 75 (2018), no. 7, 2420–2444.

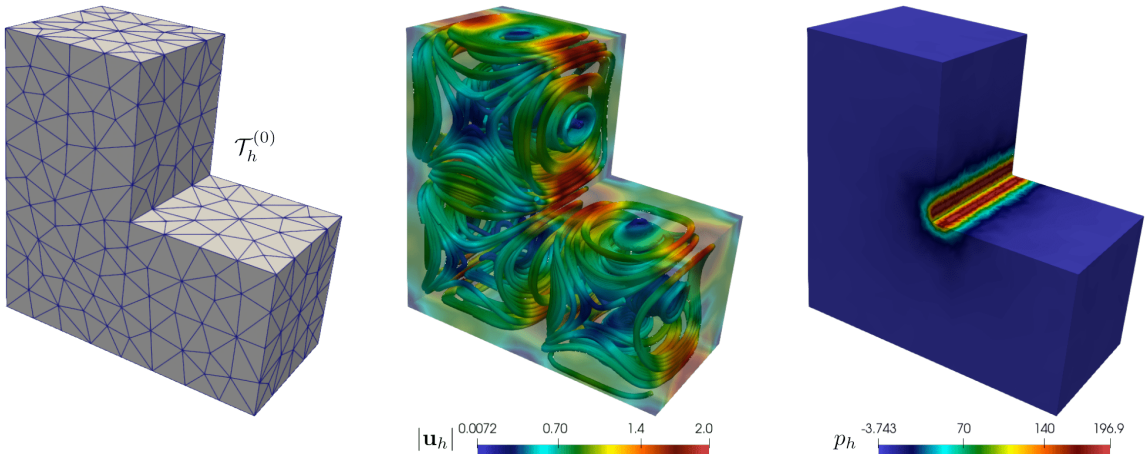

Figure 6.5: EXAMPLE 3: Initial mesh, computed velocity streamlines, and pressure field.

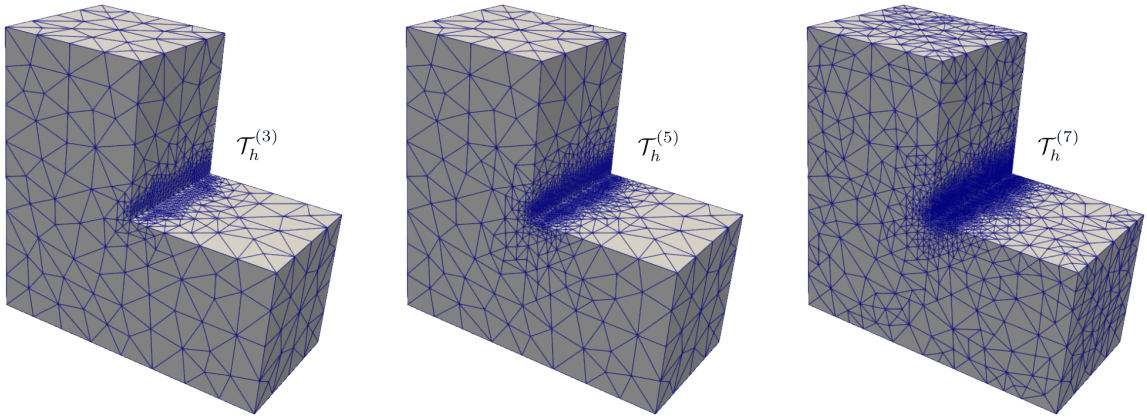

Figure 6.6: EXAMPLE 3: Three snapshots of adapted meshes according to the indicator Θ_1 for $k = 0$.

[28] G.N. GATICA, R. RUIZ-BAIER, AND G. TIERRA, *A posteriori error analysis of an augmented mixed method for the Navier–Stokes equations with nonlinear viscosity*. Comput. Math. Appl. 72 (2016), no. 9, 2289–2310.

[29] P.N. KALONI AND J. GUO, *Steady nonlinear double-diffusive convection in a porous medium based upon the Brinkman–Forchheimer model*. J. Math. Anal. Appl. 204 (1996), no. 1, 138–155.

[30] A. PLAZA AND G. F. CAREY, *Local refinement of simplicial grids based on the skeleton*. Appl. Numer. Math. 32 (2000), no. 2, 195–218.

[31] T. SAYAH, *A posteriori error estimates for the Brinkman-Darcy-Forchheimer problem*. Comput. Appl. Math. 40 (2021), no. 7, Paper No. 256, 38 pp.

[32] R. VERFÜRTH, *A posteriori error estimation and adaptive mesh-refinement techniques*. J. Comput. Appl. Math. 50 (1994), no. 1–3, 67–83.

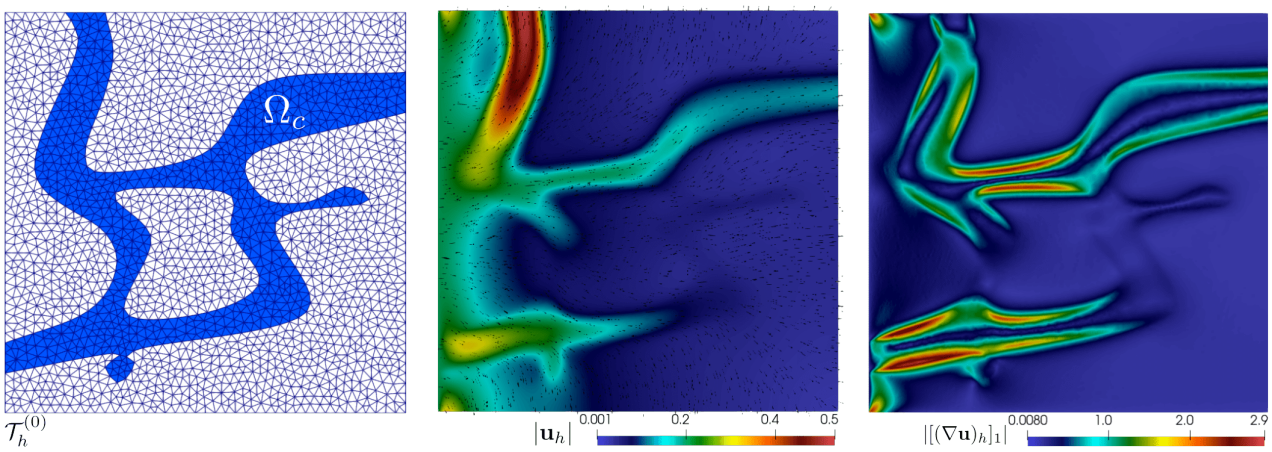

Figure 6.7: EXAMPLE 4: Initial mesh, computed magnitude of the velocity, and velocity gradient component.

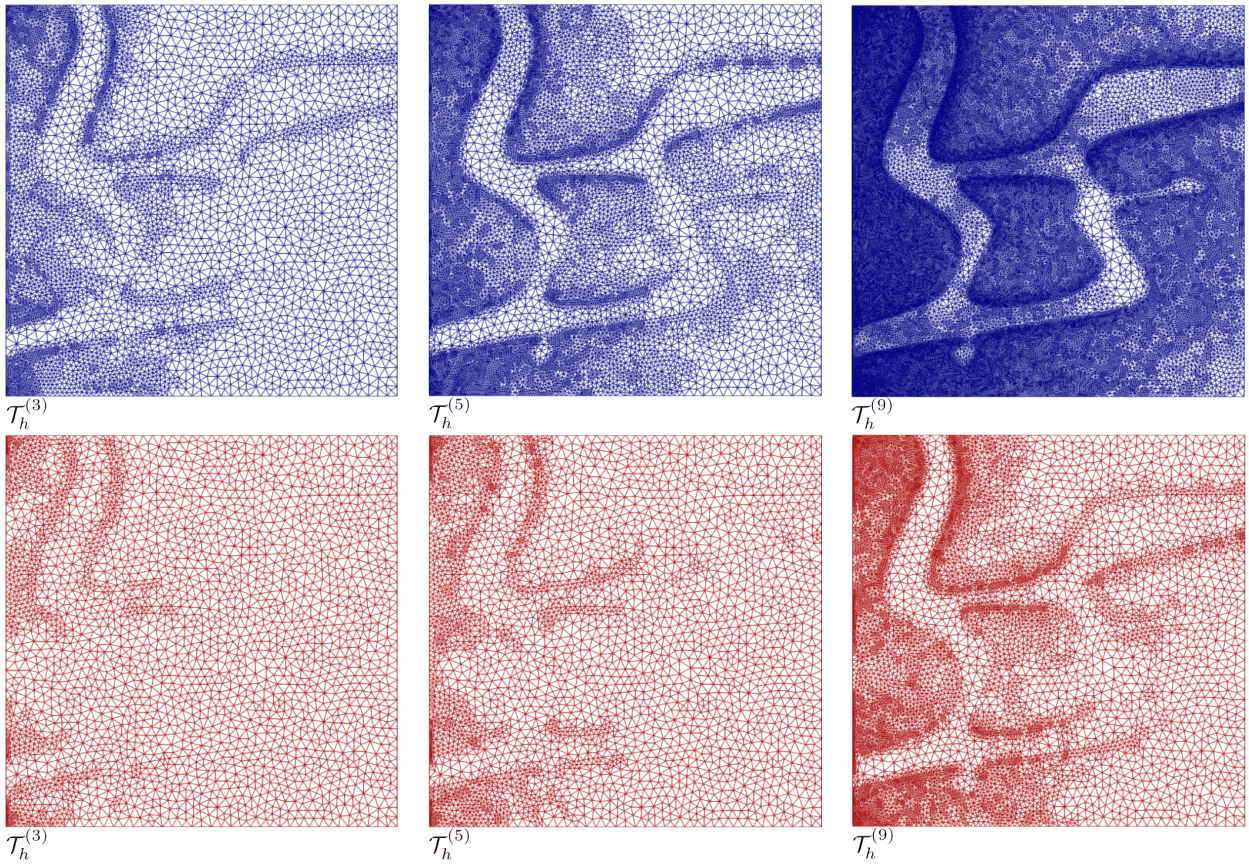

Figure 6.8: EXAMPLE 4: Three snapshots of adapted meshes according to the indicators Θ_1 and $\widehat{\Theta}_2$ for $k = 0$ (top and bottom plots, respectively).

[33] R. VERFÜRTH, *A Review of A-Posteriori Error Estimation and Adaptive Mesh-Refinement Techniques.* Wiley Teubner, Chichester, 1996.

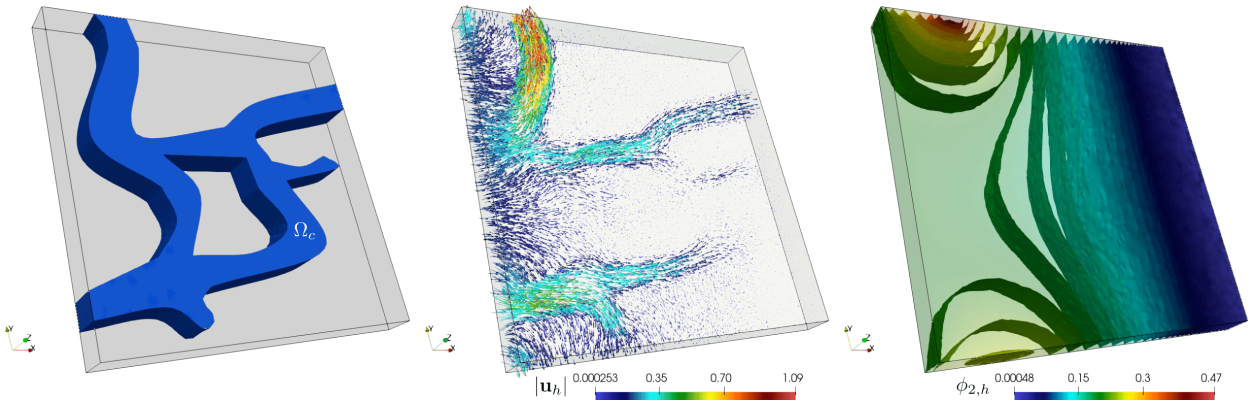

Figure 6.9: EXAMPLE 5: Domain configuration, computed magnitude of the velocity, and concentration field.

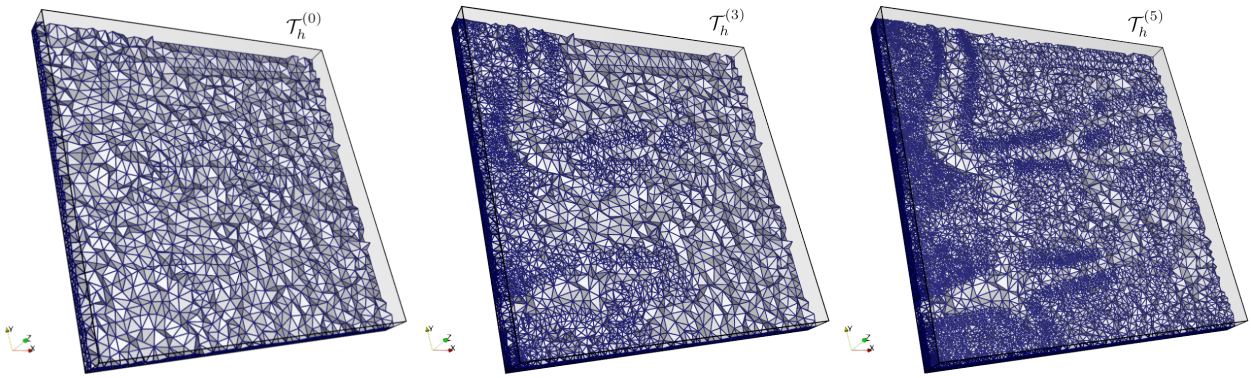

Figure 6.10: EXAMPLE 5: Initial mesh and two snapshots of adapted meshes according to the indicator Θ_1 for $k = 0$.